

1 **The responses to each referee have been concatenated into this document. Changes that have been made**
2 **the manuscript are in red.**

3

4 **Response to reviewer #1**

5 We thank the reviewer for their time in evaluating our paper and we thank the reviewer for their frank comments.

6 We respectfully disagree with their conclusions. However, the reviewer highlights some weaknesses which we
7 have addressed in the manuscript. The reviewers' criticisms are:

- 8 1. That the study only offers small advances over current literature;
- 9 2. That the model used is not state of the art;
- 10 3. That the experiment configuration is unrealistic.

11 In the following, we answer those points in turn to stress that:

- 12 1. Our study provides novel insights into semi-direct effect processes that suggest they are much more
13 subtle and more elusive than previously thought;
- 14 2. The model used in our study contains the appropriate amount of complexity to answer our scientific
15 objective, and that adding complexity would unnecessarily complicate the picture;
- 16 3. The experiments that we performed are relevant to understanding real semi-direct perturbations of
17 marine stratocumulus clouds.

18 These points are reflected in the changes we have made to the revised manuscript to address these arguments.

19

- 20 1. The first major criticism is that this study offers only small advances over previous studies. To date there
21 are only two high-profile reviews of black carbon (BC) semi-direct effect on clouds: Koch and Del Genio
22 (2010) and Bond et al. (2013), which addresses BC impacts on climate more generally. Both reviews rely
23 on just a single high resolution modelling study (Johnson et al., 2004) and a single case to support the
24 conclusion that the semi-direct effect is negative on a global average. More recent studies have focused
25 on stratocumulus-to-cumulus transition (Yamaguchi et al., 2015; Zhou et al., 2017), which makes
26 isolating semi-direct effects difficult. Given this paucity in model and observations, the role of BC over
27 marine stratocumulus is still a major uncertainty. Observations have shown that BC can occur at various
28 heights above marine stratocumulus and this study investigates how this variability translates into the
29 vertical profile of heating produced and the response of the underlying cloud.

30

31 Our results strongly suggest that semi-direct effects are much more subtle than previous literature
32 assessed. We find that the semi-direct effect strongly weakens with increasing gap between cloud and BC
33 layer – as soon as the gap is larger than about 100 m, semi-direct effects become unimportant. We also
34 find a strong diurnal cycle that means that, although semi-direct effects may be large instantaneously,
35 changes of signs with time provide a weak daily average. To our knowledge these conclusions are entirely
36 new and build upon the very small collection of high-resolution modelling studies that have studied the
37 semi-direct effect of elevated BC layers above stratocumulus. If the reviewer is aware of studies that we
38 have missed we would greatly welcome these references.

39
40
41
42
43
44
45
46
47
48
49
50
51
52
53
54
55
56
57
58
59
60
61
62
63
64
65
66
67
68
69
70
71
72
73
74
75

Considering the reviewer’s criticism, it is apparent that the importance of the main results was not made clear enough. We have therefore amended the abstract and conclusions in the revised manuscript to make this clearer and to highlight the new results.

In the abstract:

“Our results suggest that the daily mean semi-direct effect is more elusive than previously assessed. We find that the daily mean semi-direct effect is dominated by the distance between the cloud and absorbing aerosol layer. Within the first 24 hours the semi–direct effect is positive but remains under 2 Wm⁻² unless the aerosol layer is directly above the cloud. For longer durations, the daily mean semi–direct effect is consistently negative but weakens by 30 %, 60 %, and 95 % when the distance between cloud and aerosol layer is 100 m, 250 m, and 500 m, respectively. Both cloud response and semi–direct effect increase for thinner and denser layers of absorbing aerosol.”

In the conclusions:

“The aerosol-layer sensitivity experiments in section 3.3 suggest that the daily mean SDE strongly weakens as the distance of the gap between the cloud top and aerosol layer increases. Table 3 shows that on the second day of the simulation no gap results in a daily mean SDE of -7 Wm⁻² compared to -0.4 Wm⁻² for a 500 m gap. Additionally, even for a large perturbation (AOD of 0.5) the daily mean SDE in the initial 24 hours of the 50 m gap experiment is only 1 Wm⁻². These results are in general agreement with the stratocumulus–to–cumulus transition LES studies by Yamaguchi et al. (2015) and Zhou et al. (2017)...”

2. We agree that the model used in this work is microphysically simpler than other recent studies (e.g., Yamaguchi et al., 2015; Zhou et al., 2017). The microphysics in this work is single moment, while the other studies use double moment scheme with impacts on the cloud droplet distribution. While such a simplification would be problematic if we were investigating the interaction of BC aerosols with the cloud, in this work, we instead focus on BC above the cloud. We agree that the issue is simplified by not advecting / subsiding BC aerosols but this type of set-up matches the scientific objective of assessing the impact of aerosol layers above the cloud. The Large Eddy Model (LEM) has a long track record of being used to study cloud-precipitation-aerosol interactions for several cloud regimes and was included in several LES inter-comparisons. To cite only the studies published in the past 10 years: Hill et al., 2009, Hill et al., 2014, Efstathiou et al., 2015; Efstathiou et al., 2016; Ackerman et al., 2009; Dussen et al., 2013; Ovchinnikov et al., 2014; De Roode et al., 2016). We have added a sentence into the model description section to demonstrate the track record of the LEM.

As recognised by Reviewer #2 we designed our experiments to study the semi-direct effect from the bottom–up with a systematic approach that allowed us to investigate, for the first time, the sensitivity of the

76 thermodynamic response of the boundary layer to properties of the BC layer, as well as the meteorological
77 conditions and key model parameters. In that context, complexity needs to be added where it is useful.
78 The reviewer mentions two specific limitations of our model: the lack of representation of aerosol indirect
79 effects, and the Eulerian framework used by the model.

80

81 Our model does not consider indirect effects because they would quickly muddy the water. We however
82 agree that potential mitigating impacts of indirect effects need discussing and have expanded our current
83 discussion on possible impacts from indirect effects in Section 4 of the revised manuscript. As discussed
84 by Petters et al. (2012) some modelling studies focusing on stratocumulus find that LWP decreases with
85 cloud droplet number concentration (Nd), whereas others find that LWP increases. Some studies find
86 increases in entrainment rate, whereas others show decreases. The diversity in response was attributed
87 to differences in modelling frameworks and the profiles of state variables used to initialise the model. In
88 addition, in-situ observations routinely find that the BC over the Southeast Atlantic is transported in moist
89 layers. As the BC layer is entrained into the cloud layer the increased flux of water from the free-
90 troposphere could act to mitigate the changes in LWP and entrainment that occurs alongside an increased
91 Nd.

92

93 Our model uses a Eulerian framework where the BC layer remains at a constant height above the cloud
94 whereas the heat perturbation is allowed to subside into the cloud. Although we agree that in reality both
95 should subside, the sensitivity experiments that form the core of our study include changes to the gap
96 between cloud and BC layer. Therefore we learn from our model that if the BC layer could subside with the
97 heat, an enhancement of the inversion strengthening would be seen. We agree that this point should be
98 added to the discussion, and have included this in Section 4, but stress that it does not affect our
99 conclusions and the novelty of the study.

100

101 The new text reads:

102 *“Our model uses a Eulerian framework where the absorbing aerosol layer remains at a constant height*
103 *above the cloud whereas the heat perturbation is allowed to subside into the cloud. In reality the aerosol*
104 *layer may also subside. The sensitivity experiments in section 3.3 show that as the aerosol layer*
105 *approaches the cloud layer the SDE increases, therefore if we were to represent aerosol layer subsidence*
106 *we would expect an enhanced cloud response and SDE.”*

107

108

109 The reviewer believes there may be something wrong with our model due to the large impact that
110 precipitation has on our results. The cloud-base precipitation rate obtained in our model configuration
111 ranges from 0.2 mm day⁻¹ at night to 0.01 mm day⁻¹ during the day. For a cloud with a LWP of 60 g m⁻²
112 this is within the range of observations presented by Abel et al. (2010). As discussed in Ackerman et al.
113 (2009) and Wood et al. (2012), drizzle plays an important role in the dynamical processes throughout the
114 boundary layer, therefore we do not believe this aspect of our results is wrong. A brief evaluation of the
115 precipitation rate has been included in Section 3.1 of the revised manuscript.

116

117 The new text reads:

118 *“The precipitation rate at the surface (not shown) ranges from a maximum of 0.2 mm day⁻¹ at night to a*
119 *minimum of 0.01 mm day⁻¹ during the day. For a cloud with a LWP of 60 g m⁻² this is within the range of*
120 *observations presented by Abel et al. (2010). “*

121

122 3. We agree with the reviewer that the steady state stage of our simulations is not realistic. Indeed, that is
123 acknowledged in the text. But the core of the paper, which provides the novel results, focuses on the
124 initial response, which is realistic. The steady state response is not analysed at all for the sensitivity
125 experiments. We have added text to Section 3.2 to clarify the reason for the simulations.

126

127 As well as the current sentence in 3.2:

128 *“This study focuses on the initial response because it is more relevant for real–world understanding as the*
129 *aerosol perturbation is unlikely to remain constant for several days, and the lifetime of stratocumulus decks*
130 *is generally on the order of a few days only. However, the steady–state response provides insight into the*
131 *key drivers behind the BL modifications.”*

132

133 We also add the following to section 3.2.1

134 *“The final three days of the 15–day base experiment provide a mean diurnal cycle of the cloud response.*
135 *Although aerosol layers do not persist above stratocumulus decks for so long in reality, the steady-state*
136 *response provides insight into the key drivers behind the BL modifications.”*

137

138 In summary, we stand by our model, its setup, and the range of experiments that we performed. Our bottom–up
139 approach allows us to robustly study the semi–direct effect and test considerably more parameter space than
140 previous studies. Our results build upon a very small collection of modelling studies and provide the community
141 with much needed insight into the subtleties of semi-direct responses of stratocumulus clouds. But we thank the
142 reviewer for highlighting shortcomings in the description of our work, which we have addressed in the revised
143 version.

144 **Response to reviewer #2**

145

146 We thank the reviewer for their helpful comments and the suggested changes / clarifications. We address each
147 comment in turn below. Reviewer comments are in bold, and changes made to the manuscript in italics.

148

149 **Page 4, line 74: Plural “extend of cloud-aerosol gaps”**

150 The manuscript has been amended to read “*extent of cloud-aerosol gaps*”.

151

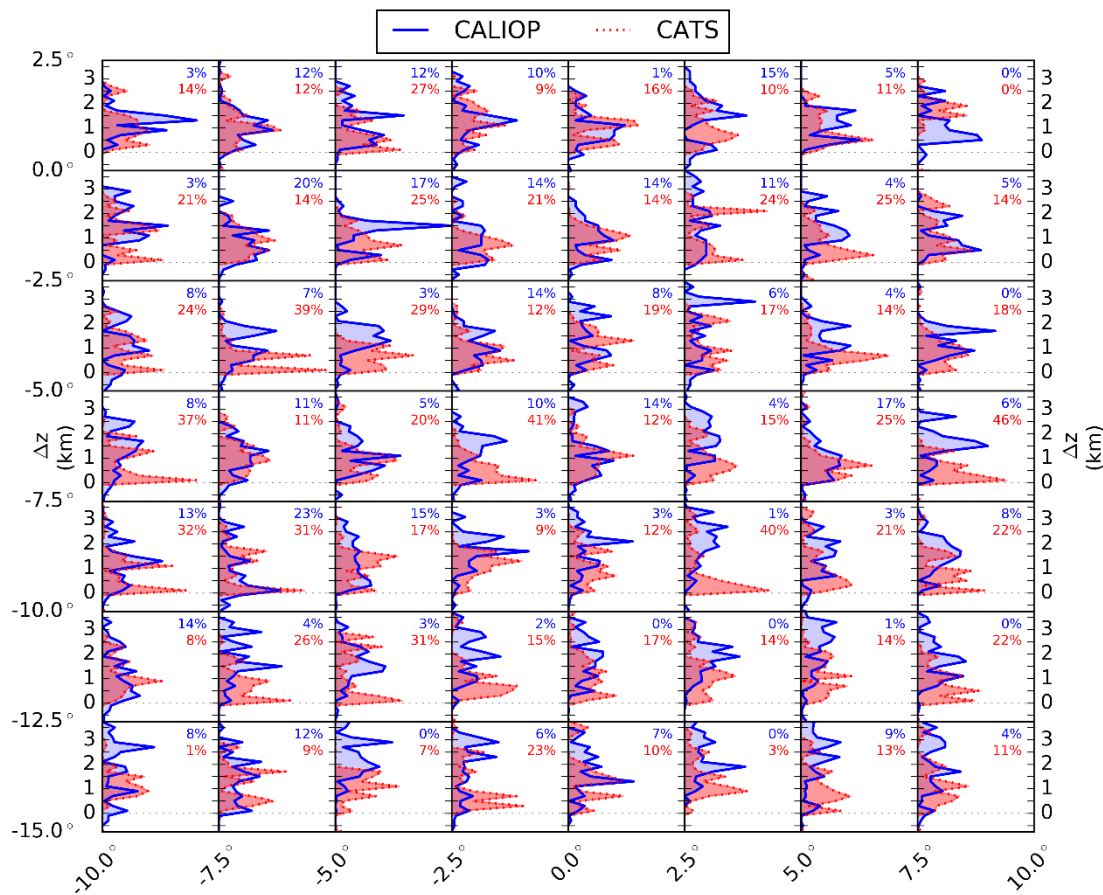
152 **Page 5, Model setup: Maybe add a sentence to the lateral boundary conditions. In assume they are
153 periodic?**

154 The reviewer is correct; the lateral boundary conditions are periodic. *This has been included in the model setup
155 section.*

156

157 **Page 6 and 7, Setup of elevated-aerosol experiments: Unfortunately, the CALIOP measurements are not
158 that reliable, which makes this paragraph less significant. For cloud measurements it is often a trade-off
159 between accuracy and representativeness of different datasets. Aren’t there other data available, like
160 aircraft measurements that could complement the used data?**

161 We have complemented the CALIOP (532 nm channel) analysis with the Cloud-Aerosol Transport System (CATS)
162 1064-nm lidar dataset on-board the International Space Station (CATS-ISS_L2O_D-M7.2-V3-00_05kmLay). The
163 CATS lidar retrieves feature altitudes using the 1064 nm wavelength channel, which is better able to retrieve the
164 lower extent of the aerosol layer than the 532 nm channel used by CALIOP as it is not fully attenuated (Rajapakshe
165 et al., 2017). The CATS dataset is only available for 3 years, compared to the 10 years of CALIOP data used for
166 the current climatology, hence we present both datasets. Figure R1 below shows that the aerosol layer is closer to
167 the cloud top in the CATS dataset than in the CALIOP dataset. Both datasets display considerably variability in the
168 cloud-aerosol gap but provide evidence that the gap is most likely less than 1000 m. Therefore our experimental
169 design remains appropriate. The corresponding figure in the manuscript (*Figure 1*) *has been updated* with Figure
170 R1 and the text has been updated to reflect these changes.



171

172 **Figure R1. Normalised frequency of occurrence of gap distance between cloud layer top and aerosol base heights from CALIOP**
 173 **(blue solid line) and CATS (red dotted line) for single layer coincidences of aerosol and cloud in the months of July, August, and**
 174 **September (2007–2016 for CALIOP; 2015–2017 for CATS) over the southeast Atlantic (15°S to 2.5°N, 10°W to 10°E). Gaps are**
 175 **binned from -1.5 to 5.5 km in 200 m increments and data in each grid has been normalised to the maximum frequency across the**
 176 **whole study area. The percentage of scenes where the aerosol layer base is less than 360 m above the cloud top height is shown in**
 177 **the top right of each subplot, in blue for CALIOP and red for CATS.**

178

179 **Page 7, line 195: I refer to “This type of experiment is analogous to a satellite retrieval that estimates the**
 180 **AOD and aerosol layer top but does not detect the lower extend of the aerosol layer.” How can this be**
 181 **analogous, if you cannot infer the geometric thickness? Do you assume an extinction profile?**

182 Our explanation was confusing and has been clarified. The situation we are describing is when column-integrated
 183 total AOD, as retrieved for example by MODIS, is combined with partial knowledge of the layer geometric thickness,
 184 as retrieved for example by CALIOP. This combination occurs for example in the CCCM product. We have rewritten
 185 the paragraph to clarify the point we are making as follows:

186 “This type of experiment aims to understand the importance of correctly retrieving the full extent of the aerosol layer
187 from a satellite retrieval when only the AOD is known. Those variables are for example provided in the combined
188 CCCM satellite product (Kato et al., 2010; 2011).”

189

190 **Page 7, end of line 185: “absorbing aerosol” instead of “layer”.**

191 This has been amended as suggested.

192

193 **Page 8, Eq.1: The ordering of the flux terms in the formula is wrong. It must be:**

$$194 \quad SDE = F_{TOA,aerosol} - F_{TOA,no-aerosol} - DRE$$

195 Agreed. We have corrected the formula in the manuscript.

196

197 **Page 14, Fig. 5: Is below-cloud RH the vertical mean for the distance from ocean surface to the cloud base?**

198 **Otherwise, at which height is the value taken?**

199 The below-cloud RH is the vertical mean from above the ocean surface to the cloud base. We have clarified this in
200 the manuscript and updated Figure 5 and Figure 6. While amending the figures, a mistake in plotting RH at the
201 surface layer has been detected. This has been fixed and the mistake does not affect any of the text as the same
202 response is observed in all figures.

203

204 **Page 15, line 340: Based on Fig. 6e the total water path (TWP) (units kgm-2), and not the total water content**
205 **(TWC) (kgm-3) is compared. The reduction in total water path is in-line with the reduced BL height (which**
206 **also decreases by about 15**

207 We have amended the manuscript to read ‘total water path’ and have changed the variable ‘Total BL qt’ to ‘TWP
208 of BL’ throughout the manuscript. The reviewer’s comment seems to have been truncated, so we cannot respond
209 to the missing part.

210

211 **Page 17, Eq. 3: This equation is confusing. The following formulation should be equivalent:**

$$212 \quad Z_{lower} = Z_{max} \cdot (1 - 0.025)$$
$$213 \quad Z_{upper} = Z_{max} \cdot (1 + 0.25)$$

212

213 **If not, please rewrite it in a more understandable way.**

214 Agreed. We have removed the equation and provided a more accurate description.

215 *“Figure 7 shows timeseries for the aerosol layer–sensitivity experiments. In this analysis the inversion strength $\Delta\theta$*
216 *is determined between altitudes Z_{upper} and Z_{lower} . The value of Z_{upper} is the topmost altitude where the absolute*
217 *gradient $\left|\frac{d\theta_l}{dz}\right|$ is 25% of its maximum, and Z_{lower} is the lowermost altitude where $\left|\frac{d\theta_l}{dz}\right|$ is 2.5% of its maximum. The*
218 *upper threshold is determined at a higher percentage of $\left|\frac{d\theta_l}{dz}\right|$ than the lower threshold to limit spurious values*
219 *occurring from aerosol layers close to the inversion layer that impact θ_l .”*

220

221 **Page 17, line 374: The explanation provided is not very convincing. Isn't the initial peak of positive SDE**
222 **occurring before or around midday? Anyway, at the time it occurs, the clout top height and entrainment**
223 **rate seem not to be significantly affected by the aerosol layer (look at Fig. 5 or Fig. 7 red line of the 500m-**
224 **gap experiment). How much does the elevated aerosol layer affect radiative cooling of the cloud tops at**
225 **night? Does the initial positive spike in SDE could be related to this?**

226 **Page 19, lines 415 - 417: See comment above**

227

228 As the reviewer rightly suggests, the positive SDE occurs before midday rather than after midday as we erroneously
229 wrote. This has been corrected.

230

231 The reviewer is not convinced by our explanation and suggests the positive SDE may be influenced by changes to
232 the cloud-top longwave cooling. *We have addressed this comment by including a new figure (Figure R2 in this*
233 *document, Figure S1 in the revised manuscript)* in the supplementary information and improving our explanation in
234 the manuscript. The new figure focuses on the cloud response in the first day (from 0230 to 1600) and includes the
235 changes to cloud properties, buoyancy flux, advected total water content tendency, cloud-top longwave cooling,
236 and LW fluxes for three of the experiments with a variable cloud-aerosol gap (with AOD=0.2 and layer geometric
237 thickness of 250m).

238

239 The new figure shows that the positive SDE is driven by the decrease in LWP (Figure R2b) that is most evident at
240 0830 and 1000 for the experiments with gaps of 0 and 100 m. This response is caused by an increase in cloud
241 base height (Figure R2a) without a corresponding change in cloud top height, which thins the cloud and reduces
242 the LWP. Cloud base height increases because of weaker mixing within the boundary layer which reduces the
243 transport of moisture within and beneath the cloud (Figure R2d). That reduced transport occurs because at 0830
244 the buoyancy flux throughout the profile weakens (Figure R2c), at the time at which entrainment starts to sharply
245 decrease (Figure 5b). Note that below-cloud RH (Figure 5d) does not increase until after midday which indeed
246 suggests that the increasing cloud base height is driven by in-cloud changes or the flux of moisture to the cloud
247 base. As the day progresses the continued reduction in entrainment rate results in a moister boundary layer and

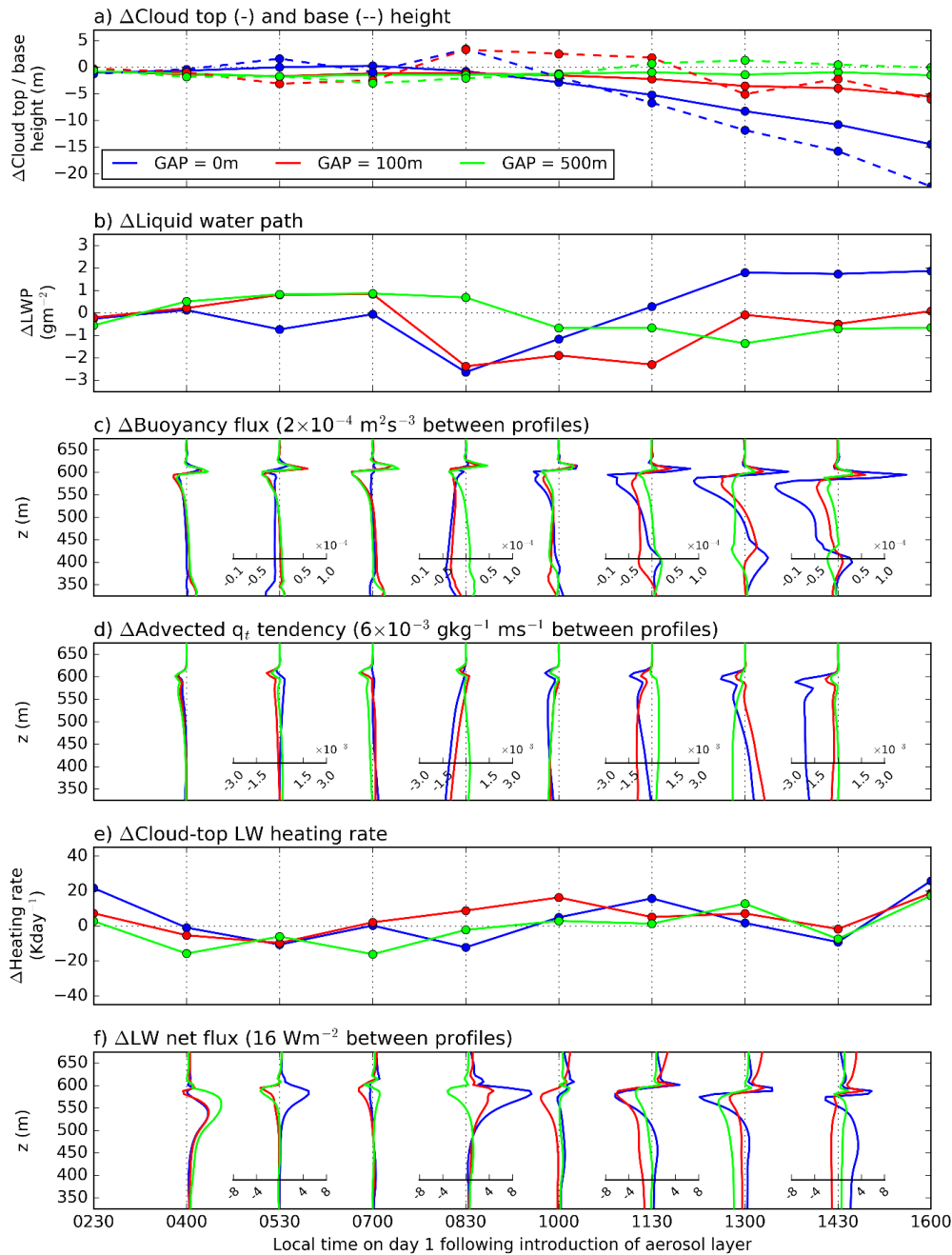
248 an increase in RH below the cloud, which allows the cloud base to decrease and LWP to increase. This explains
249 why stronger perturbations to the entrainment rate on the first day (such as when the layer is close to the cloud)
250 results in a quicker recovery of the LWP (see Figure 7). This improved explanation has been included in Section
251 3.3.1.

252

253 With regards to the cloud-top LW cooling, we would expect the cooling rate to be weakened by the presence of the
254 elevated aerosol layer and any additional heating of the layer, both of which would increase downwelling LW. Figure
255 R2e shows that there are instantaneous differences in LW cooling up to a magnitude of 20 K day^{-1} , however the
256 sign changes throughout the day. The response of the net LW flux shown in Figure R2f confirms that there is little
257 impact to the fluxes above cloud before sunrise. The buoyancy flux profiles in Figure R2c do show a limited
258 response to the aerosol layer before sunrise (at 0400 hours) in all experiments but there is little simultaneous LWP
259 response. The dominant cloud response appears to occur after sunrise, which suggests the decrease in LWP is
260 driven by an enhanced inversion strength rather than weakened cloud-top LW cooling. We have included a brief
261 discussion of this additional effect in Section 3.2.1. as:

262

263 “There is little response of the cloud before sunrise, which suggests a weak insulating effect of the aerosol layer
264 on longwave fluxes at the cloud top. This is supported by a lack of systematically weakened cloud-top longwave
265 cooling (Fig. S1 in the supporting information), which would be expected for an increased downwelling longwave
266 flux from the aerosol layer.”



267

268 **Figure R2. Response to the presence of an aerosol layer above the cloud (gap of 0 m in blue, 100 m in red, and 500 m in green) of a)**
 269 **the cloud top (solid line) and cloud base (dashed line) heights, b) the cloud liquid water path (LWP), c) profiles of the mean buoyancy**
 270 **flux, d) profiles of the mean advected total water content tendency, e) cloud-top longwave cooling, and f) profiles of mean longwave**
 271 **net flux (positive values indicate increased downward flux). The geometric thickness of the aerosol layer is 250 m and its optical**
 272 **depth is 0.2. Data is shown for the first day following the introduction of the aerosol layer. Mean instantaneous profiles (shown in**
 273 **panels c, d, and f) for each time are centred on a value of zero, depicted by the vertical dotted lines. Each profile is separated on the**
 274 **x-axis by a constant magnitude shown above each corresponding plot.**

275

276 **Page 27, Fig. 10 e,k,q: Please specify “BL mean” and “BL total”. I assume the dotted line is “BL total”? If**
277 **“BL total” refers to TWP and “BL mean” to TWC you can see how the moisture content of air increases**
278 **within the BL, despite an overall decrease in TWP due to the shrinking of the BL**

279 We have amended the figure and text as suggested to provide clarity.

280

281 **Page 29, line 633: This can only hold true if it is reasonable to neglect emission of longwave radiation of**
282 **the aerosol layer and ergo its insulating effect**

283 This relates to the comment about cloud-top LW cooling addressed above with Figure R2. Figure R2f shows the
284 response of the net LW flux profiles. Before sunrise the net fluxes above cloud are < 1.5 % greater when the aerosol
285 layer is present, suggesting a weak insulating effect. During the day this increases up to a maximum of ~ 5 % as
286 the temperature of the aerosol layer increases, but still indicates a weak insulating effect.

287 Section 3.2.1 already contains a discussion of the changes to LW fluxes and cloud-top cooling following the
288 comment above, and we have added the following sentence to the discussion and conclusions section:

289 *“The insulating effect of the aerosol layer only weakly influences the net longwave fluxes and divergence above*
290 *the cloud.”*

291

292 **Page 29, line 638: “, the magnitude of SDE is increased. . .”, or “, SDE is amplified. . .”is less ambiguous,**
293 **as the sign of SDE is negative.**

294 Agreed. The manuscript has been amended to read *“SDE is amplified”*.

295

296 **Page 31, line 719: missing “explain”**

297 The manuscript has been amended as suggested.

298

299

300 **Response to reviewer #3**

301 We thank the reviewer for their helpful comments. We begin by responding to the general comments, then we
302 address each detailed remark in turn below. Reviewer comments are in bold, and changes made to the manuscript
303 in italics.

304

305 General comments:

306 **The paper gives the impression that the general influence of absorbing aerosol on the cloud evolution has**
307 **been investigated. However, it is only the radiative effect of the absorbing aerosol layer that enters in the**
308 **discussion on the SDE, not the effect of aerosols “polluting” and thus modifying additionally the**
309 **thermodynamic and hydrological cycle of the cloud and the BL. This should be highlighted in abstract and**
310 **introduction, and should not only be mentioned at the end of the conclusion. The title of the paper should**
311 **already include the key parameter of this study, i.e. “ a persistent absorbing aerosol layer”.**

312

313 As suggested by the reviewer, we have highlighted the focus of our study in the title, abstract, and introduction.

314 The title has been changed to *“Diurnal cycle of the semi-direct effect from a persistent absorbing aerosol layer*
315 *over marine stratocumulus in large-eddy simulations”*

316

317 Our experiment description in the abstract has been extended and now reads: *“Here we use large eddy simulations*
318 *to investigate the sensitivity of stratocumulus clouds to the properties of an absorbing aerosol layer located above*
319 *the inversion layer, with a focus on the location, timing, and strength of the radiative heat perturbation”*

320

321 At the end of the introduction, when the outline of the study is summarised, we include the following: *“In this study*
322 *the UK Met Office Large Eddy Model (LEM) is used to investigate and quantify the impact that the properties of an*
323 *elevated absorbing aerosol layer have on the cloud and radiative response of marine stratocumulus, with a focus*
324 *on the role that the location, timing, and strength of the heat perturbation has on the underlying cloud and boundary*
325 *layer.”*

326

327 **It is the LES model and its turbulence closure, which primarily determine the simulation results. Also the**
328 **cloud description, even in simplified way, as it is in this study, affects the finding. Using other LES and**
329 **cloud models (as done by other studies) will lead to a different result for the semi direct effect. This should**
330 **be also highlighted in the conclusions of this paper.**

331

332 We agree that past literature has shown a large amount of diversity when different LES models are used to study
333 semi-direct effects, although we expect that the fundamental causal chain explaining the response in our model

334 would also be involved in the response simulated by other models. The following has been included in the
335 conclusions section:

336 *“Inconsistent responses between LES models can also arise through differences in the representation of*
337 *processes, including unresolved sub-grid scale turbulence (e.g., Stevens et al. 2005) and microphysics (van der*
338 *Dussen et al., 2013). Our results show that the heat perturbation above the cloud layer impacts all aspects of the*
339 *BL profile, therefore it would be beneficial to repeat this study using other LES models to test our conclusions.”*

340

341 **123 is the radiation code applied for all 130x130 columns individually or only for one mean profiles of T,**
342 **Qvap and Qliq?**

343 The radiation scheme is applied to all columns. We have clarified this in Section 2.2 with the following text:

344 *“Radiation calculations are performed for all grid points within the domain every 30 seconds.”*

345

346 **212-220 makes it almost impossible to understand the calculation of the SDE. A reference would be helpful**
347 **(Hill and Dobbie, 1980?). I guess DRE uses the results of the simulations with the aerosol layer, actually**
348 **not explained in the paper.**

349 As suggested, we have included a reference to Johnson et al. 2004 which provides a description of the SDE
350 calculation.

351 We state how the DRE is calculated in lines 250 to 251, but have added a sentence to clarify:

352 *“DRE is calculated as the difference between F_{TOA} and that obtained in a second, diagnostic, call to the radiation*
353 *scheme with the same profiles of liquid water, water vapour, and atmospheric gases, but without aerosol. This*
354 *second call is only performed for the simulations with aerosol present.”*

355

356 **233 in caption of Fig. 3: $w'w'w'$ is named the perturbation in mean vertical velocity. No, it is the perturbation**
357 **of w to the power of 3, but it has another physical meaning. Why was it selected to illustrate the BL**
358 **turbulence characteristics?**

359 We agree that a more appropriate variable to illustrate BL turbulence is the mean variance in vertical velocity
360 perturbation ($\overline{w'w'}$). We have updated figure 3 and relevant text in Section 3.1, which is the only instance of use
361 throughout the manuscript.

362

363 **239-240 “During the daytime, ... through weakened surface to atmosphere gradients”. The total water**
364 **profiles (which are dominated by the presence Q_{vap}) for $t = 13h$ and $t = 5.30h$ in Fig.3c illustrate the**
365 **contrary. Only the surface gradient in the first 10-20 m above the sea at 5.30h is stronger than the daytime**
366 **conditions. Also for THETA_liq in Fig. 3b a weak gradient exists during daytime but none at 5.30h. This**
367 **explanation of the decoupled state of the BL during daytime is not really convincing. Fig.3d and e better**

368 **indicate the daytime / nighttime differences in the BL which are controlled by the vertical turbulent**
369 **transport of tke and thus by the turbulence simulated in the LES model.**

370 We agree with the reviewer that our explanation did not provide a convincing description of the day / night
371 differences in BL turbulence. As suggested, we have used figures 3d and 3e to illustrate the different turbulent
372 structures and the decoupling during daytime. The sentence now reads:

373 *“During the daytime, solar heating reduces the buoyancy flux (Fig. 3d) through an offset in the longwave cooling*
374 *and reduces turbulence throughout the BL (Fig. 3e). This weakens the BL circulation and prevents mixing*
375 *throughout the BL and promotes a decoupled state in which the flux of moisture from the surface to the cloud is*
376 *insufficient to maintain the cloud base height, as evident from the non-constant BL profiles of θ_l (Fig. 3b) and q_t*
377 *(Fig. 3c) at 1300 hours.”*

378

379 **241 SST is kept constant, how are surface heat and moisture fluxes calculated? Give the key parameters.**

380 The surface fluxes are calculated using Monin–Obukhov similarity theory, which is reported in section 2.1
381 (Description of model; line 117). As suggested by the reviewer, we have expanded on this to provide more
382 information. The sentence now reads:

383 *“Surface fluxes of moisture and heat are calculated using Monin–Obukhov similarity theory (Monin and Obukhov,*
384 *1954) which predicts the surface frictional stresses and heat fluxes using the local gradients between the surface*
385 *and the overlying model level. For these experiments a prescribed constant sea surface temperature is used.”*

386

387 **274 Terminology in the caption of Fig.4: instead of “response” a more explicit description like “differences**
388 **between no-aerosol simulation and simulation with an elevated aerosol layer” would make the illustration**
389 **DCloud, DLWP and DAbedo and the reference to equation (1) more understandable.**

390 The figure caption has been amended as suggested.

391

392 **298 ... allows the cloud layer to maintain a higher RH. This is difficult to understand and to believe, as**
393 **explained in 2.2 the cloud model excess supersaturation is converted in liquid water.**

394 The reviewer is correct. We erroneously referred to the cloud layer, rather than the sub-cloud layer. This has been
395 corrected to read:

396 *“The increase in RH occurs due to the weakened w_e which reduces the amount of warm dry FT air that is mixed*
397 *into the BL and allows the sub-cloud layer to maintain a higher RH.”*

398

399 **301 -302 ... enhanced RH below cloud (caused by an increase in water vapour) ... by the decrease in latent**
400 **heat flux. This is not credible. Q_{total} , i.e. mainly Q_{vap} , continuously decreases; also LHF mainly**

401 **decreases but RH increases. RH is a function of two independent state variables T and Q_{vap}. What**
402 **happened to the temperature T during the “aerosol” simulations in the BL.**

403 The RH below cloud increases (Fig. 5f) due to the increase in qt (total water specific humidity) below cloud, which
404 occurs despite a decrease in the total water path (Fig. 5f). We believe we introduced some confusion with the
405 variable name ‘total BL qt’ which, as pointed out by reviewer #2, should be correctly termed total water path.

406 We chose not to show the qt below the cloud in these plots, and instead use the decrease in LHF from the surface
407 and increase in mean RH below cloud to demonstrate this response, which occurs alongside a small decrease in
408 BL liquid-water potential temperature of ~0.1 K (discussed in more detail below). The increase in mean qt can be
409 seen further on in the manuscript in Fig. 10e.

410 We have addressed this by replacing ‘total BL qt’ with total water path (TWP) throughout the manuscript, and as
411 discussed below we have introduced the mean BL liquid water potential temperature into Figures 5 and 6 to support
412 our analysis.

413

414 **The paper completely omits a discussion on changes of the T profile in the BL after section 3.1.**
415 **Temperature perturbations above the BL are the key parameter for the different SDE scenario in this study**
416 **but a discussion of subsequent temperature changes in the BL is completely ignored - why?**

417 In our simulations the temperature only plays a minor role in the BL response, yet as correctly pointed out by the
418 reviewer, we do not discuss this at any point. To address this, we now include the BL liquid-water potential
419 temperature (θ_l) response in Figures 5 and 6, which are shown below as Fig. R1 and R2, respectively.

420 The figures show that the mean θ_l decreases by ~0.1 K over the initial three days of the simulation (Fig. R1) and
421 ~0.2 K after 10 days (Fig. R2). The sources for changes to the θ_l occur through exchanges across the inversion
422 layer at the top of the BL, changes in LW and SW fluxes, surface fluxes, and precipitation. In our simulations the
423 enhanced inversion strength reduces the flux of warm air into the BL, however, this may be partially offset by the
424 heat perturbation produced by the absorbing aerosol layer. Small decreases in precipitation are offset by reduced
425 latent heat flux at the surface, and due to the high cloud fraction in the simulations, changes to LW and SW fluxes
426 within the BL are small. The pattern of the θ_l response in Fig. R1 is similar to the entrainment rate (Fig. 5b) which
427 makes it likely that the process controlling the simulated response in θ_l is the change to the entrainment rate.

428 The magnitude of the response in both the initial and the steady-state response is small (up to 0.2 K in the steady-
429 state) which demonstrates that the dominant driver of changes to RH below cloud is from the water vapour, rather
430 than the temperature.

431

432

433

434

435 In addition to the new subplots in figures 5 and 6, we have included text in section 3.2.1:

436 *“The increase in RH occurs due to the weakened w_e which reduces the amount of warm dry FT air that is mixed*
437 *into the BL and allows the sub-cloud layer to maintain a higher RH. The relatively small decrease in potential*
438 *temperature of ~ 0.1 K (Fig. 5g) suggests that the RH response is driven by an increase in water vapour.”*

439

440 in section 3.2.2:

441 *“The small response in mean BL potential temperature of -0.2 K (Fig. 6f) strengthens the hypothesis that the RH*
442 *response below-cloud is driven by changes in available water vapour, rather than the decrease in temperature,*
443 *although it is worth noting that this decrease in temperature will act to slightly increase the RH.”*

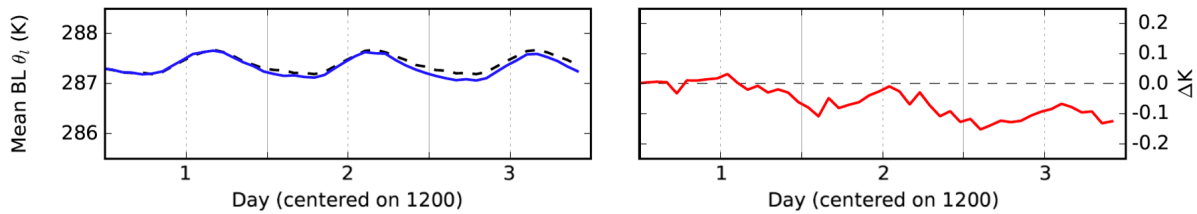
444

445 in section 4:

446 *“The reduction in the entrainment of warm and dry air from the FT reduces the amount of mixing, reducing the sink*
447 *of \bar{q}_t in the cloud layer and allowing the BL to maintain a greater RH. The result is an increase in \bar{q}_t , a small*
448 *decrease in BL temperature, and an increase in RH.”*

449

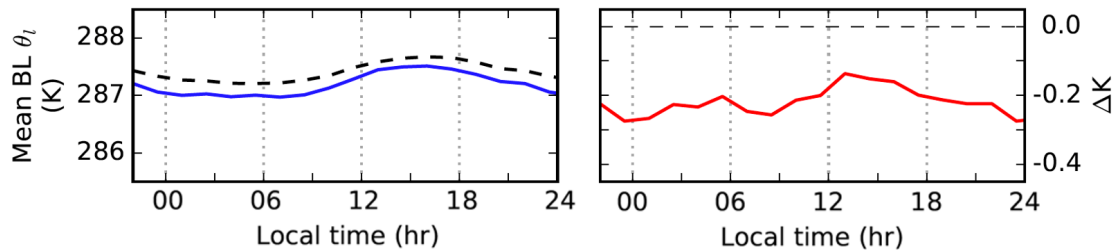
450



451

452 **Figure R1. ‘Initial’ domain averaged cloud response of BL liquid-water potential temperature –**
453 **subplot taken from Figure 5 in the revised manuscript.**

454



455

456 **Figure R2. Domain averaged ‘steady-state’ cloud response of BL liquid-water potential**
457 **temperature – subplot taken from Figure 6 in the revised manuscript.**

458

459 **308 where can we see thicker clouds in Fig.5a in the afternoon of day 3? I can't.**

460 The paragraph in question refers to the increase in LWP of $\sim 2 \text{ g kg}^{-1}$ that is evident in Fig. 5c from just before
461 midday and continuing through the afternoon on day 3. There is also a corresponding increase in the geometric
462 thickness of the cloud at midday evident in Fig. 5a which shows that the cloud base has decreased more than the
463 cloud top.

464
465 We have clarified the paragraph by starting the paragraph with the following:

466 *“The thicker cloud (enhanced LWP; Fig. 5a) on the afternoon of the third day...”*

467

468 A similar change has been made to the previous paragraph which discusses the thinner cloud on the morning of
469 the third day.

470

471 **335-336 “The decrease in cloud layer height allows better mixing beneath the cloud base, which enhances**
472 **the evaporation of moisture from the surface between 0900 and 1500 ”. This is in any case a speculation.**
473 **It is not coherent with the daytime turbulence profile of Fig. 3e for the non-aerosol simulation.**

474 A given eddy generated in the cloud layer will be able to penetrate a certain distance below the cloud. If the cloud
475 layer is reduced in altitude then the eddy will be able to influence layers closer to the surface. We see evidence of
476 this occurring in our simulations. Figure R3a shows that although the maximum turbulence in the cloud layer is
477 slightly weaker in the aerosol simulation, the decrease in cloud altitude by $\sim 200 \text{ m}$ systematically shifts the $w'w'$
478 profile downwards, so that turbulence below cloud is greater in the simulations with aerosol. The buoyancy flux
479 profile (Fig. R3b) shows that this results in positive buoyancy flux below cloud, as opposed to a negative value in
480 the no-aerosol simulation, resulting in the response that we observe in Figure 6.

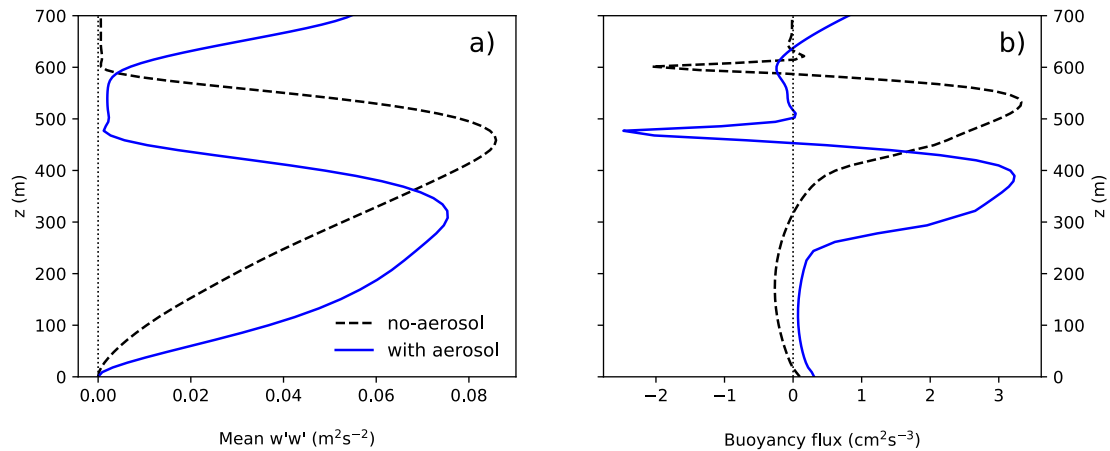
481

482 *Figure R3 has been included in the supplementary information* (as Figure S2) and is now referred to in the
483 manuscript in section 3.2.2:

484

485 *“This modification to the diurnal cycle of the cloud is driven by an increased coupling between surface moisture flux*
486 *and cloud base during the daytime (see Fig. S2 in the supplementary information) ...”*

487



488

489 **Figure R3. Domain-mean vertical profiles of a) variance in vertical velocity perturbation $w'w'$, and**
 490 **b) buoyancy flux on day 13 of the simulation at 1300 local time for the no-aerosol simulation**
 491 **(black dashed line) and following the introduction of a layer of absorbing aerosol (blue solid line)**
 492 **in the base experiment (0 m cloud–aerosol gap, 250 m thick layer, and AOD of 0.2).**

493

494 **346 rephrase “reduction in evaporation and associated cooling of entrained air”. What do you mean with**
 495 **cooling of entrained air?**

496 The air that is entrained into the cloud layer from the free troposphere is dry. The subsequent mixing of the dry and
 497 cloudy air results in net evaporation which acts to cool the parcel of air, generating (negative) buoyancy.

498 As suggested, we have rephrased the sentence, which now reads:

499 *“The weakened BL circulation is therefore due to a reduction in entrainment. The mixing of dry air into the cloud*
 500 *layer results in evaporation and a cooling which generates buoyancy; a reduction in entrainment therefore weakens*
 501 *cloud–top buoyancy production.”*

502

503 **347 the reduced vertical motions reduce surface evaporation. Same question as above for 241.**

504 As per the previous question the text concerning the surface fluxes in section 2.1 has been expanded to provide
 505 more information.

506

507 **394 Fig. caption 7: same remark as in 274.**

508 The caption has been changed as suggested.

509

510

511

512 **416 ... quicker than the cloud base. Where or how to detect?**

513 The current manuscript does not provide evidence of this, as also highlighted by Reviewer #2. We have therefore
514 included additional plots in the supplementary information and have rewritten the first paragraph of section 3.3.1 to
515 discuss this in more detail. The paragraph reads:

516

517 *“The majority of experiments show a positive spike in SDE (Fig. 7d, i and n) just before midday on the first day.*
518 *This occurs due to the lag–time in response between the direct impact to the cloud from changes to w_e , and the*
519 *increase in sub–cloud RH. Figure S1 in the supplementary information focuses on the response in the initial 24*
520 *hours. The positive SDE is driven by the decrease in LWP caused by an increase in cloud base height (Fig. 5a and*
521 *Fig. S1a) without a corresponding change in cloud top height. The decrease in w_e weakens buoyancy production*
522 *throughout the cloud layer (Fig. S1c), which drives a reduced moisture flux within the cloud and to the cloud base*
523 *(Fig. S1d). As the day progresses the continued reduction of w_e results in an increase in mean below–cloud RH*
524 *and a recovery, or increase, of the LWP. This explains why stronger perturbations to the entrainment rate on the*
525 *first day (such as when the layer is close to the cloud) results in a quicker recovery of the LWP (Fig. 7c, h, and m).”*

526

527 **520 the norain simulation is not a model setup modification, but a change in the modeling physics.**

528 Granted, although for the sake of simplicity we refer to those sensitivity experiments as experimenting with “model
529 setup”.

530

531 **522 the strengthening of the SDE is +1 W/m² (or +3) from -7 to -8 W/m² (or -9 to -12) why not -1 W/m² (and**
532 **-3)?**

533 We agree that the current text is confusing. We have rewritten the sentence to read:

534 *“Compared to the control setup the noRain setup is characterised by a consistent increase in the magnitude of the*
535 *SDE by 1 Wm⁻² when a cloud–aerosol gap is present and up to 3 Wm⁻² when there is no gap”*

536

537 **527 – 535 This discussion or interpretation of the results cannot be understood with the given information**
538 **on the 05cool simulations. Thus, this part should be omitted.**

539 As discussed in Section 3.4 the large-scale advective heat tendency is a large-scale forcing term that represents
540 a degree of variability in LES experiments. We therefore do not want to omit this result, and have instead rewritten
541 the paragraph to improve our interpretation of the results. The paragraph now reads:

542 *“When compared to the control setup, increasing the cooling rate of the large–scale advective heat tendency results*
543 *in stronger BL dynamics, enhanced cloud–top entrainment of warm dry air, and enhanced surface LHF (which acts*
544 *as a feedback to enhanced entrainment). As the processes maintaining the cloud layer become more important,*
545 *they become more sensitive to perturbations. Therefore, when the aerosol layer is present in the 05cool setup, the*

546 *responses of w_e , LHF, and below-cloud moisture flux are stronger than in the control setup and the simulations*
547 *are characterised by a quicker decrease in the TWP of the BL. However, this only becomes prominent on the third*
548 *day and results in little difference from the control setup over the first two days.”*

549

550 **537 and 547 Are the SST and wetFT simulations really with no-aerosol? This is probably a typo.**

551 This is not typo. In each set of sensitivity experiments a simulation was run with and without aerosols. This allows
552 us to investigate the response of each setup to the same aerosol perturbation. For each setup we briefly describe
553 what is changing in the ‘without aerosol’ simulations before discussing the response to the aerosol layers.

554 We have made this clearer in the revised manuscript by adding a sentence in Sect. 3.4 pointing out that a no-
555 aerosol simulation is run for each setup and referring to the no-aerosol simulations within our interpretation.

556

557 **549 allowing the BL to maintain below the cloud layer a greater RH?**

558 This has been changed to:

559 *“...allowing the BL to maintain a greater mean RH”*

560

561 **564-565 ... a redistribution of water from the cloud layer to the surface layer (Fig.9b). What do you mean**
562 **with redistribution? Does it mean that rain is responsible for the significant Qvap increase in the first 300**
563 **m? This is most unlikely. Water vapor is accumulated in the lowest levels due to surface evaporation in**
564 **the decoupled BL.**

565 Yes, the reduced coupling between surface and cloud layers results in an accumulation of water vapor towards the
566 surface, which can be viewed as a redistribution of the water. This does not occur due to precipitation processes.

567 The sentence has been amended to clarify our point:

568 *“This reduces the flux of water vapour from the surface layer to the cloud, resulting in an accumulation of water*
569 *vapour close to the surface (Fig. 9b).”*

570

571 **630 3b. The conclusion that RH increase as Q_{total} increase, implicates that the BL temperature remains**
572 **constant or decreases. This study, however, withholds this fundamental information.**

573 As per our previous discussion on the temperature response, this line has been amended to read:

574 *“The reduction in the entrainment of warm and dry air from the FT reduces the amount of mixing, reducing the sink*
575 *of \bar{q}_t in the cloud layer and allowing the BL to maintain a greater RH. The result is an increase in \bar{q}_t , a small*
576 *decrease in BL temperature, and an increase in RH.”*

577

578 **721 regional climate models as HadGEM certainly treat surface fluxes**

579 We have amended the sentence as follows:

580 *“The lack of BL adjustment may be due to processes that are not explicitly treated in HadGEM, such as BL*
581 *turbulence and subsequent missing feedbacks on surface fluxes...”*
582
583

584 **Diurnal cycle of the semi-direct effect from a persistent absorbing**
585 **aerosol layer over marine stratocumulus in large-eddy simulations**

586
587 Ross J. Herbert^{1,*}, Nicolas Bellouin¹, Ellie J. Highwood¹, Adrian A. Hill²

588 ¹Department of Meteorology, University of Reading, Reading, RG6 6BB, UK

589 ²Met Office, Fitzroy Road, Exeter, EX1 3PB, UK

590 *Now at Department of Physics, University of Oxford, Oxford, OX1 3PU, UK

591 *Correspondence to:* Ross Herbert (r.jross.herbert@readingphysics.ox.ac.uk)

592 The rapid adjustment, or semi-direct effect, of marine stratocumulus clouds to elevated layers of absorbing aerosols may
593 enhance or dampen the radiative effect of aerosol-radiation interactions. Here we use large eddy simulations to investigate the
594 sensitivity of stratocumulus clouds to the properties of an absorbing aerosol layer located above the inversion layer-, with a
595 focus on the location, timing, and strength of the radiative heat perturbation. The sign of the daily mean semi-direct effect
596 depends on the properties and duration of the aerosol layer, the properties of the boundary layer, and the model setup.
597 ~~Diurnal~~Our results suggest that the daily mean semi-direct effect is more elusive than previously assessed. We find that the
598 daily mean semi-direct effect is dominated by the distance between the cloud and absorbing aerosol layer. Within the first 24
599 hours the semi-direct effect is positive but remains under 2 Wm⁻² unless the aerosol layer is directly above the cloud. For
600 longer durations, the daily mean semi-direct effect is consistently negative but weakens by 30 %, 60 %, and 95 % when the
601 distance between cloud and aerosol layer is 100 m, 250 m, and 500 m, respectively. Both cloud response and semi-direct effect
602 increase for thinner and denser layers of absorbing aerosol. Considerable diurnal variations in the cloud response mean that an
603 instantaneous semi-direct effect is unrepresentative of the daily mean, and that observational studies may under- or over-
604 estimate semi-direct effects depending on the observed time of day. ~~The observed role of the distance between the cloud top~~
605 ~~and the absorbing layer in modulating the strength of the cloud and radiative response is reproduced by the large eddy~~
606 ~~simulations. Both cloud response and semi-direct effect increase for thinner, denser, layers of absorbing aerosol located nearer~~
607 ~~the cloud layer.~~The cloud response is particularly sensitive to the mixing state of the boundary layer: well-mixed boundary
608 layers generally result in a negative daily mean semi-direct effect, and poorly mixed boundary layers result in a positive daily
609 mean semi-direct effect. Properties of the boundary layer and model setup, particularly the sea surface temperature,
610 precipitation, and properties of the air entrained from the free troposphere, also impact the magnitude of the semi-direct effect
611 and the timescale of adjustment. These results suggest that the semi-direct effect simulated by coarse-resolution models may
612 be erroneous because the cloud response is sensitive to small-scale processes, especially the sources and sinks of buoyancy.

613 1 Introduction

614 Semi-permanent decks of marine stratocumulus clouds represent an important negative radiative effect within the Earth's
615 energy budget (Hartmann et al., 1992; Hartmann and Short, 1980; Wood, 2012). In addition, the sharp inversion layer and
616 small-scale turbulent processes that characterise the formation and maintenance of these clouds represent considerable
617 uncertainty in climate models, so stratocumulus clouds remain a key uncertainty in future climate projections (Bony and
618 Dufresne, 2005; Klein et al., 2017; Wood, 2012). Marine stratocumulus clouds are sensitive to sea surface temperature (SST)
619 and large-scale atmospheric properties both above the inversion, like subsidence rate and thermodynamic properties of the
620 overlying air mass, and below the inversion, like cloud condensation nuclei sinks and sources, that impact turbulent processes
621 and dynamics throughout the boundary layer (e.g., Bretherton et al., 2013; Feingold et al., 2010; Sandu et al., 2010). Therefore,
622 small changes to these properties could result in large changes to the fluxes of radiation in the atmosphere.

623

624 Perturbations to the aerosol distribution result in a radiative forcing through both aerosol-radiation and aerosol-cloud
625 interactions; this distinction separates the radiative forcing caused by aerosol scattering and absorption of longwave and
626 shortwave radiation from that caused by the availability of cloud condensation nuclei. Aerosol-cloud interactions lead to
627 changes in cloud albedo and subsequent rapid adjustments to the cloud properties that include changes to precipitation and
628 cloud evolution (Sherwood et al., 2015). Aerosol-radiation interactions result in instantaneous changes to the extinction profile
629 (also referred to as the direct radiative effect) and therefore heating profile, which lead to rapid adjustments in the physical and
630 radiative properties of the cloud (referred to in this paper as the semi-direct effect, SDE, for convenience). Quantifying rapid
631 adjustments is important as they may act to dampen or strengthen the instantaneous forcing. Aerosol-radiation interactions
632 represent an important uncertainty in the anthropogenic radiative forcing of the climate over the industrial era, especially from
633 absorbing aerosol species such as black carbon which may result in pronounced semi-direct effects (Boucher et al., 2013). In
634 a recent climate model intercomparison study Stjern et al. (2017) found that a ten-fold increase in black carbon emissions
635 resulted in a strong positive direct effect which was partially offset by a negative SDE. Although all models agree on the sign
636 (negative) they disagree on the size of that offset, from 12 to 63 % for the models studied by Stjern et al. (2017). High-
637 resolution models that can sufficiently represent the dominant processes within the boundary layer and cloud are a powerful
638 benchmark to test the realism of the response simulated by the climate-scale models.

639

640 During the African dry season, which lasts from August to October, plumes of strongly absorbing biomass burning aerosol
641 from central Africa are transported westward over the semi-permanent marine stratocumulus deck of the Southeast Atlantic
642 Ocean, where they eventually subside and mix into the boundary layer (Das et al., 2017). Observational and modelling studies
643 suggest that elevated absorbing layers result in thicker clouds and a negative SDE (Adebisi and Zuidema, 2018; Johnson et
644 al., 2004; Wilcox, 2010), and may impact the stratocumulus-to-cumulus transition process (Yamaguchi et al., 2015; Zhou et
645 al., 2017). Once mixed into the cloud layer the absorbing aerosol exerts aerosol-radiation interactions that enhance cloud

646 evaporation (Hill and Dobbie, 2008; Johnson et al., 2004) and aerosol–cloud interactions that impact microphysical and
647 dynamical processes (e.g., Feingold et al., 2010; Gordon et al., 2018; Hill et al., 2009). Observational studies have used satellite
648 retrievals from the NASA A–Train to investigate the interaction between clouds and absorbing aerosol over the Southeast
649 Atlantic. Wilcox (2010) used co–located CALIPSO, OMI, and AMSR–E retrievals and found that for all overcast scenes liquid
650 water path (LWP) increased for high aerosol loading. This response was attributed to absorbing aerosol layers above the cloud
651 top enhancing the heating rate and decreasing entrainment across the inversion. However, satellites do not provide direct
652 observations of entrainment and an alternative explanation could be that the aerosol layers travel in relatively moist layers
653 (Adebisi et al., 2015), increasing moisture transport across the inversion layer, even if entrainment remained unchanged. In a
654 study with a similar methodology, Costantino and Bréon (2013) separated the CALIPSO–derived aerosol layer heights into
655 cases when the smoke was close to (< 100 m) and well–separated (< 750 m) from the cloud top. The authors found that when
656 the aerosol layers are well separated from cloud top the LWP and cloud optical thickness showed no statistically significant
657 dependence on aerosol loading. These results are supported by Adebisi and Zuidema (2018) who used satellite observations
658 and reanalysis products to show evidence that the sensitivity of low–cloud cover to elevated aerosol layers increased for small
659 cloud–aerosol gaps. These observations suggest that the distance between the elevated aerosol layer and cloud layer plays an
660 important role in the strength of the SDE. Additionally, a recent satellite study of cloud–aerosol gaps by Rajapakshe et al.
661 (2017) suggests that the elevated aerosol layers may be closer to the cloud than previously thought, which demonstrates that
662 elevated layers may have an even more important impact on the clouds.

663

664 The observations hint at the potential importance of the extent of cloud–aerosol [gaps](#) for the SDE. However, this complexity
665 is not reflected in the frameworks presented in current reviews (Bond et al., 2013; Koch and Del Genio, 2010), and there is a
666 lack of high–resolution modelling studies investigating the SDE from elevated layers of absorbing aerosol. Johnson et al.
667 (2004) used large–eddy simulation (LES) to investigate the semi–direct of absorbing aerosols on non–precipitating marine
668 stratocumulus. In an experiment where a ~ 1 km thick layer of absorbing aerosol, with an aerosol optical depth (AOD) of 0.2
669 at 550 nm, was present above the marine boundary layer throughout a 48–hr simulation, the absorbing aerosol enhanced the
670 temperature inversion at the top of the boundary layer, weakening the entrainment rate across the inversion, and producing a
671 shallower, moister boundary layer and a higher LWP. The 48–hr mean SDE was estimated to be -9.5 Wm^{-2} , almost entirely
672 cancelling a direct effect of $+10.2$ Wm^{-2} . Yamaguchi et al. (2015) and Zhou et al. (2017) used LES models to investigate the
673 transition of marine stratocumulus to cumulus in the presence of a smoke layer. As the marine boundary layer deepened, the
674 cloud–aerosol gap decreased until the smoke layer made contact with the cloud layer. Both studies found little LWP response
675 when the smoke layer was separated by a no–aerosol gap. Yamaguchi et al. (2015) found that the elevated smoke layer reduced
676 boundary layer turbulence and cloud cover through a decrease in longwave cloud–top cooling. By isolating the aerosol heating
677 above and below the boundary layer top Zhou et al. (2017) found that when the layer was directly above the inversion layer
678 the elevated aerosol layer strengthened the inversion, inhibiting entrainment, and increased LWP and cloud cover, resulting in
679 a negative SDE. Global models have also been used to investigate the radiative impact of biomass burning aerosol in

680 stratocumulus regions (e.g., Lu et al., 2018; Penner et al., 2003; Sakaeda et al., 2011), however, Das et al. (2017) show that
681 these coarser resolution models may be unable to reproduce the observed vertical distribution of absorbing aerosol layers over
682 the southeast Atlantic, resulting in an under-representation of elevated aerosol layers and increased uncertainty in their
683 radiative impact.

684

685 In summary, observation and modelling studies suggest that the diurnal cycle and evolution of marine stratocumulus are
686 strongly impacted by the presence of absorbing aerosol layers at and above the top of the boundary layer. The SDE may act to
687 counteract or enhance the direct effect, resulting in either a small or large net radiative effect from aerosol-radiation
688 interactions. Yet the sensitivity of the SDE to the properties of the elevated aerosol layer has not been fully investigated. In
689 this study the UK Met Office Large Eddy Model (LEM) is used to investigate and quantify the impact that the properties of
690 ana persistent elevated absorbing aerosol layer have on the cloud and radiative response of marine stratocumulus, with a focus
691 on the role that the location, timing, and strength of the heat perturbation has on the underlying cloud and boundary layer.
692 Section 2 presents the LEM and its configuration and introduces a set of experiments designed to assess the SDE and its
693 sensitivity to the aerosol layer properties. Section 3 focuses on a single experiment to understand the processes that drive the
694 cloud response and SDE, then assesses the sensitivity of this response to the aerosol layer properties. Section 3 also investigates
695 the robustness of that assessment to the processes that affect the maintenance of the cloud, namely precipitation, sea surface
696 temperature, and boundary layer depth. Section 4 summarises the results, comparing to other modelling studies and
697 observations, and discussing the limitations of this study and identifying remaining questions.

698 2 Model description and setup

699 2.1 Description of model

700 The LEM (Gray et al., 2001) is a non-hydrostatic high-resolution numerical model that explicitly resolves the large-scale
701 turbulent motions responsible for the energy transport and flow. The LEM has a long track record of being used to study cloud-
702 precipitation-aerosol interactions in several cloud regimes (e.g., Efstathiou et al., 2016; Efstathiou and Beare, 2015; Hill et al.,
703 2009, 2014) and has been included in several LES inter-comparison studies (e.g., Ackerman et al., 2009; van der Dussen et
704 al., 2013; Ovchinnikov et al., 2014; de Roode et al., 2016). Sub-grid scale turbulence responsible for the dissipation of kinetic
705 energy is parameterised. Prognostic variables are the three-dimensional velocity fields (u, v, w), liquid-water potential
706 temperature (θ), and mass-mixing ratios of water vapour (q_v), liquid water (q_l), and rain (q_r). Liquid water mass is prognosed
707 at every grid point using a condensation-evaporation scheme in which excess supersaturation is converted to liquid water and
708 vice versa for sub-saturated air. Warm rain processes are represented by a single-moment microphysics scheme that includes
709 autoconversion and cloud droplet collection following Lee (1989), sedimentation of rain, and evaporation of rain into dry air.
710 The influence of aerosol on cloud droplet number concentration is not included in this study and cloud droplet number is fixed
711 to 240 cm^{-3} for microphysical processes. Surface fluxes of moisture and heat are calculated using Monin-Obukhov similarity

712 theory (Monin and Obukhov, 1954) with which predicts the surface frictional stresses and heat fluxes using the local gradients
713 between the surface and the overlying model level. For these experiments a prescribed constant sea surface temperature is
714 used. A damping layer that relaxes all prognostic variables to their horizontal mean is present above an altitude of 775 m
715 (~150 m above the cloud layer; see Sect. 2.2) with a height scale of 650 m and a timescale of 30 s. This prevents the reflection
716 of gravity waves at the rigid top boundary and prevents the production of trapped buoyancy waves above the inversion layer
717 (Ackerman et al., 2009). The subsidence rate w_s is represented by a height dependent function $w_s(z) = -Dz$ for which large-
718 scale divergence (D) is prescribed. The model is run with a variable time step with a maximum of 0.5 seconds. The LEM
719 radiation scheme, described by Edwards and Slingo (1996), is a two-stream solver with six shortwave spectral bands and eight
720 longwave bands that calculates the vertical distribution of radiative fluxes and heating rates. The scheme includes six aerosol
721 species with wavelength and humidity-dependent mass absorption coefficients, mass scattering coefficients, and asymmetry
722 factors. A single value for the mean cloud droplet effective radius of 10 μm is prescribed in the radiation scheme.

723 2.2 Model setup

724 All simulations are three dimensional-with periodic lateral boundary conditions. The model domain is 5200 m in the horizontal
725 with a horizontal grid resolution of 40 m, and 2600 m in the vertical with a variable vertical grid resolution with ~6 m resolution
726 at the cloud top and inversion and less than 10 m throughout the boundary layer (BL). The LEM is configured here to produce
727 a stratocumulus with a consistent diurnal cycle over an 8-day timescale. The initial profiles of θ_i and q_i were taken from
728 Johnson et al. (2004) and based on subtropical marine stratocumulus observations from the First International Satellite Cloud
729 Climatology Project Regional Experiment (FIRE) (Hignett, 1991) in the subtropical Pacific Ocean. A series of 10-day
730 simulations without absorbing aerosol were run with varying subsidence rates to obtain steady-state profiles of θ_i and q_i that
731 would produce a consistent stratocumulus layer with a maximum cloud top height of 600 m. The resulting initialisation profiles
732 are shown in Table 1; the BL is 0.6 g kg^{-1} drier than in Johnson et al. (2004) and Hill et al. (2008) due to the inclusion of
733 precipitation in our study and a cooler SST, which was necessary in order to attain a similar cloud LWP to these studies. The
734 large-scale divergence D is set to $5.5 \times 10^{-6} \text{ s}^{-1}$, giving a subsidence rate of $w_s = -3.3 \text{ mm s}^{-1}$ at the cloud top. D and w_s are
735 within the observed range for marine stratocumulus regions (Zhang et al., 2009) and of similar magnitude to other
736 stratocumulus LES studies (e.g., Johnson et al., 2004; De Roode et al., 2014). The initial profiles describe a well-mixed moist
737 BL capped by a sharp (10 K) inversion at 600 m with a warm and dry free troposphere (FT) above the inversion. To account
738 for a source of large-scale heat divergence a cooling rate of 0.1 K day^{-1} is applied. This value is lower than the 1.0 K day^{-1}
739 used by Johnson et al. (2004) and Hill et al. (2008) because the greater cooling rates result in an unstable cloud top height in
740 our simulations which is undesirable as we require a consistent cloud layer to isolate the cloud response due to the absorbing
741 aerosol. A prescribed surface pressure of 1012.5 hPa is used, and zonal and meridional geostrophic winds are 6.0 m s^{-1} and -
742 1.0 m s^{-1} , respectively. The radiation scheme is set up for consistency with the FIRE campaign with a time-varying solar zenith
743 angle for mid-July at the co-ordinates 33°N , 123°W . Radiation calculations are performed for all grid points within the domain
744 every 30 seconds. Surface roughness is fixed at $2 \times 10^{-4} \text{ m}$ and SST at 287.2 K.

745

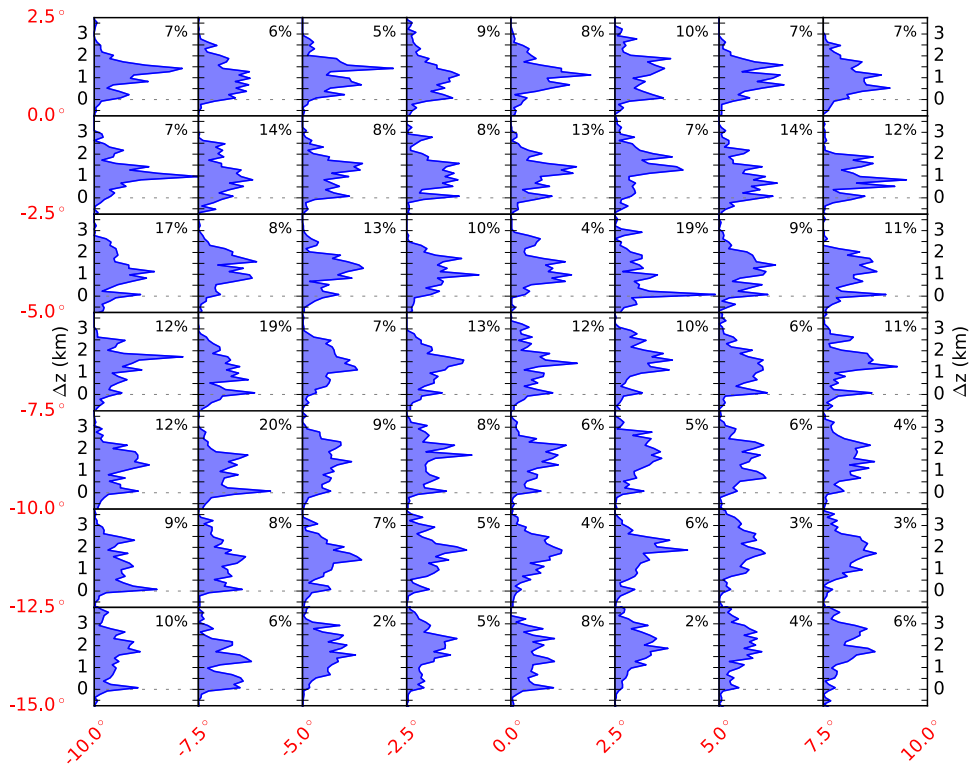
746 **Table 1. Initial profiles used in the control simulations**

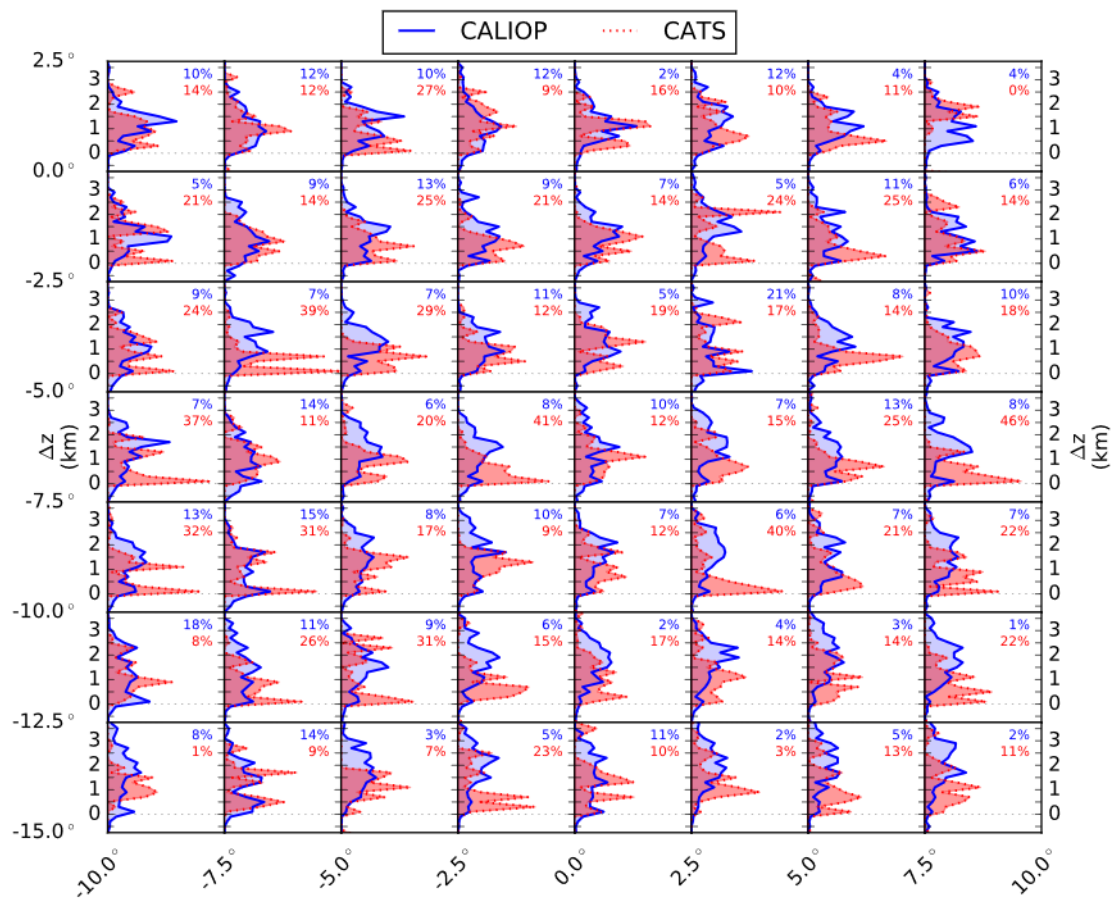
Altitude (m)	Liquid–water potential temperature (K)	Total water mixing ratio (g kg ⁻¹)
0	287.5	9.0
600	287.5	9.0
601	297.0	5.5
750	300.0	5.5
1000	301.7	5.5
1500	303.2	5.5
2600	304.0	5.5

747

748 **2.3 Setup of elevated–aerosol experiments**

749 To simulate the effect of an elevated absorbing–aerosol layer above the cloud top, a layer of dry aerosol is prescribed,
750 consisting of soot–like and water–soluble–like aerosol, representing predominantly absorbing and scattering species,
751 respectively. The interaction of longwave and shortwave radiation with the aerosol layer results in localised heating rates that
752 are coupled to the LEM. The prescribed aerosol layer properties include the height of layer base above the inversion layer
753 (referred to as the cloud–aerosol gap), geometric thickness, mean single–scattering albedo (SSA), and AOD. These properties
754 are set at the beginning of the experiment and applied during each call to the radiation scheme. Using the prescribed geometric
755 thickness of the aerosol layer, a balance between the mass–mixing–ratio of soot and water–soluble aerosol is used to achieve
756 the desired SSA and AOD throughout the simulation (see Appendix for more details on the method employed). In these
757 experiments SSA is 0.9, which is towards the higher end of the range of SSA for biomass burning aerosol (Peers et al., 2016)
758 and thus represents a relatively conservative value for the absorption of the aerosol layer.





760

761 **Figure 1. Normalised frequency of occurrence of gap distance between cloud layer top and aerosol base heights from CALIOP (blue**
 762 **solid line) and CATS (red dotted line) for single layer coincidences of aerosol and cloud in the months of July, August, and September**
 763 **(2007–2016 for CALIOP; 2015–2017 for CATS) over the southeast Atlantic (15°S to 2.5°N, 10°W to 10°E). Layer heights are binned**
 764 **from -1.5 to 5.5 km in 150/200 m increments and data in each grid has been normalised to the maximum frequency across the whole**
 765 **study area. The percentage of scenes where the aerosol layer base is below less than 360 m above the cloud top height is shown in the**
 766 **top right of each subplot for each dataset.**

767

768 Realistic cloud–aerosol gaps are needed for the elevated–aerosol experiments. They are taken from observations from the
 769 CALIPSO Cloud–Aerosol Lidar with Orthogonal Polarization (CALIOP) instrument (5-km resolution, 532 nm Aerosol Layer
 770 Product and Cloud Layer Product, v4.10, level 2 data) [and the NASA Cloud-Aerosol Transport System](#)
 771 [\(CATS\) lidar \(5 km resolution, V3-00, Mode 7.2, Level 2 Daytime Operational Layer Data Product, 1064 nm wavelength\)](#)
 772 over the Southeast Atlantic Ocean (15°S to 2.5°N, 10°W to 10°E). The distance Δz between the retrieved cloud top and the
 773 aerosol base heights is determined from scenes where vertical profiles only include a single layer of low cloud (cloud top
 774 below 2.5 km) and a single layer of aerosol. [Figure 1](#) shows the normalised frequency of occurrence of Δz in 2.5-

775 degree grids for all scenes within July, August, and September between 2007 and 2016 ~~for CALIOP data and between 2015~~
776 ~~and 2017 for CATS data. Both datasets display considerable variation in Δz at all locations, yet the CATS dataset has a higher~~
777 ~~percentage of scenes in close proximity (within 360 m) of the cloud top compared to CALIOP. This agrees well with the study~~
778 ~~of Rajapakshe et al. (2017). For the majority of scenes, the layer of aerosol tends to be above, or directly above, the cloud top~~
779 ~~layer. There is considerable variation in Δz at all locations; to the north of the study area the peak Δz is ~ 1 km, whereas to the~~
780 ~~south of the study area the peak Δz is closer to 2 km. In many regions there is a high frequency of the aerosol layer being in~~
781 ~~close proximity to the cloud top. have shown that in the southeast Atlantic the CALIOP product overestimates the aerosol~~
782 ~~layer base height and layers are likely much closer to the cloud layer than previously thought; they find that in 60% of their~~
783 ~~above-cloud aerosol cases the absorbing layer is less than 360 m above the cloud deck, therefore our Δz is likely~~
784 ~~overestimated.~~

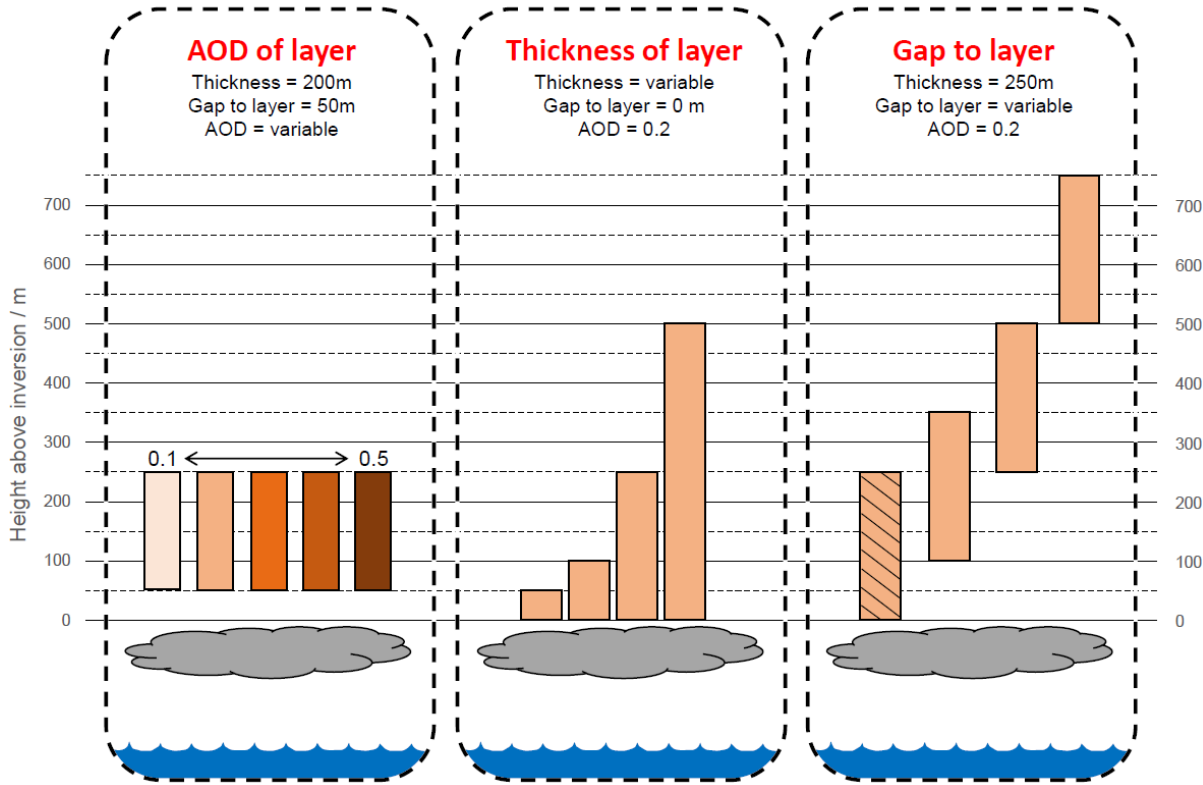
785

786 ~~The CALIOP~~ who found that the 532 nm wavelength used in the CALIOP retrieval often over-estimates the distance between
787 ~~cloud top and aerosol base, whereas the longer 1064 nm wavelength used by CATS provides a more reliable estimate. The~~
788 ~~CALIOP and CATS~~ analysis (Figure 1) suggests that elevated aerosol layers predominantly exist within 1500 m of
789 the cloud top with a common occurrence of layers in close proximity (~~≤ 150~~ less than 360 m) to the cloud, ~~and the study by~~
790 ~~suggests the aerosol layers are predominantly within 360 m of the cloud top.~~ In-line with this we focus on layers of absorbing
791 ~~layers aerosol~~ that range from directly above the cloud layer ($\Delta z = 0$ m) to elevated layers at $\Delta z = 500$ m, and we additionally
792 examine the role of the aerosol layer depth which, for a given AOD, will impact the vertical distribution and strength of the
793 localised heat perturbation.

794

795 A schematic of the experiments designed to investigate the sensitivity of the SDE and cloud diurnal cycle to key layer
796 properties, namely the AOD, geometric thickness, and the cloud-aerosol gap, is shown in Figure 2. The first set
797 investigates the sensitivity of the SDE to the strength of the aerosol layer absorption. Following AOD observations by Chand
798 et al. (2009), the AOD of the layer is varied from 0.1 to 0.5 while keeping the geometric thickness constant at 200 m and the
799 cloud-aerosol gap at 50 m. The second set of experiments investigates the sensitivity of the cloud response to the geometric
800 thickness of the aerosol layer at constant AOD. This type of experiment ~~is analogous aims to a satellite retrieval that estimates~~
801 ~~the AOD and aerosol layer top but does not detect~~ understand the importance of correctly retrieving the ~~lower full geometric~~
802 extent of the aerosol layer (altitudes of the layer top and base) from a satellite retrieval when the AOD is known; variables
803 ~~often provided in combined satellite products such as CCCM~~ (Kato et al., 2010, 2011). This is a known deficiency with
804 retrievals made using wavelengths that are strongly attenuated by biomass burning aerosol such as the 532 nm channel
805 currently used in the CALIPSO CALIOP aerosol products (Rajapakshe et al., 2017). For these experiments the geometric
806 thickness of the aerosol layer is increased from 50 to 500 m with no cloud-aerosol gap and are effectively experiments with
807 variable density of aerosol particles, since with a fixed AOD the aerosol layer mass-mixing ratio decreases with increasing
808 geometric thickness of the layer. The final set of experiments investigates the impact of the cloud-aerosol gap by placing the

809 aerosol layer **base** from 0 to 500 m above the inversion layer while keeping geometric thickness and AOD constant. A full list
 810 of experiments performed is presented in Table 2. We use one of the experiments, referred to as the base experiment, to provide
 811 an initial in-depth analysis of the cloud and radiative response. In the base experiment (hatched experiment in [Figure 2](#)[Figure](#)
 812 [2](#)) a 250 m thick absorbing aerosol layer with an AOD of 0.2 is placed directly above the inversion layer.
 813



814
 815 **Figure 2. Schematic showing the experiments performed for the aerosol-sensitivity simulations. The hatched experiment is named**
 816 **the base experiment and is used to provide initial analysis of the semi-direct effect in Sect. 3.2. AOD stands for aerosol optical depth**
 817 **and is given at a mid-band wavelength of 505 nm.**

818
 819 The SDE is calculated [following](#) Johnson et al. (2004), as a residual of the difference in top-of-atmosphere net radiation (F_{TOA})
 820 between the aerosol and no-aerosol simulations, minus the direct radiative effect (DRE):

$$821 \quad \text{SDE} = \left(\cancel{F_{TOA, \text{no-aerosol}}} - \cancel{F_{TOA, \text{aerosol}}} \right) - F_{TOA, \text{aerosol}} - F_{TOA, \text{no-aerosol}} - \text{DRE} \quad (1)$$

822
 823 where F_{TOA} is calculated using the upward (\uparrow) and downward (\downarrow) fluxes of longwave (LW) and shortwave (SW) radiation:
 824

$$F_{\text{TOA}} = F_{\text{TOA,SW}}^{\downarrow} - (F_{\text{TOA,SW}}^{\uparrow} + F_{\text{TOA,LW}}^{\uparrow}) \quad (2)$$

825

826 DRE is calculated as the difference between F_{TOA} and that obtained in a second, diagnostic, call to the radiation scheme with
 827 the same profiles of liquid water, water vapour, and atmospheric gases, but without aerosol. This second call is only performed
 828 for the simulations with aerosol present.

829

830 **Table 2. Breakdown of all experiments performed. AOD stands for aerosol optical depth and is given at a mid-band wavelength of**
 831 **505 nm.**

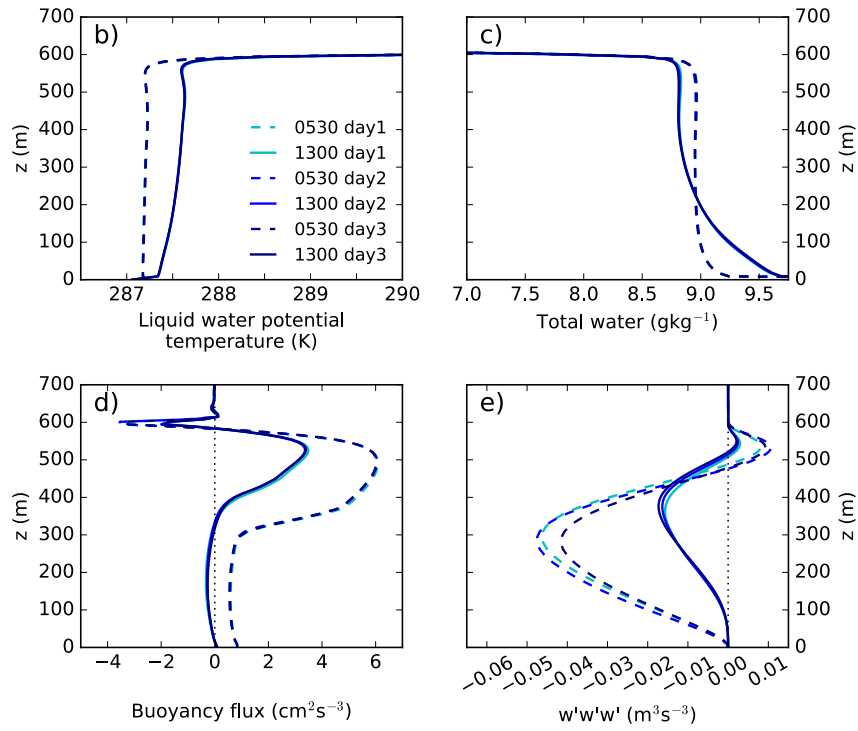
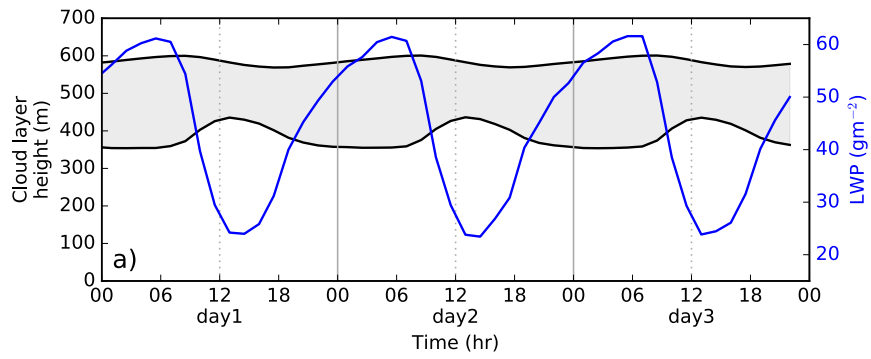
Type of experiment	Layer properties		
	Cloud–aerosol gap (m)	Layer thickness (m)	Layer AOD
Variable AOD	50	200	0.1
	50	200	0.2
	50	200	0.3
	50	200	0.4
	50	200	0.5
Variable thickness	0	50	0.2
	0	100	0.2
	0	250	0.2
	0	500	0.2
Variable gap	0*	250	0.2
	100	250	0.2
	250	250	0.2
	500	250	0.2

* Base experiment used for initial analysis

832 3 Results

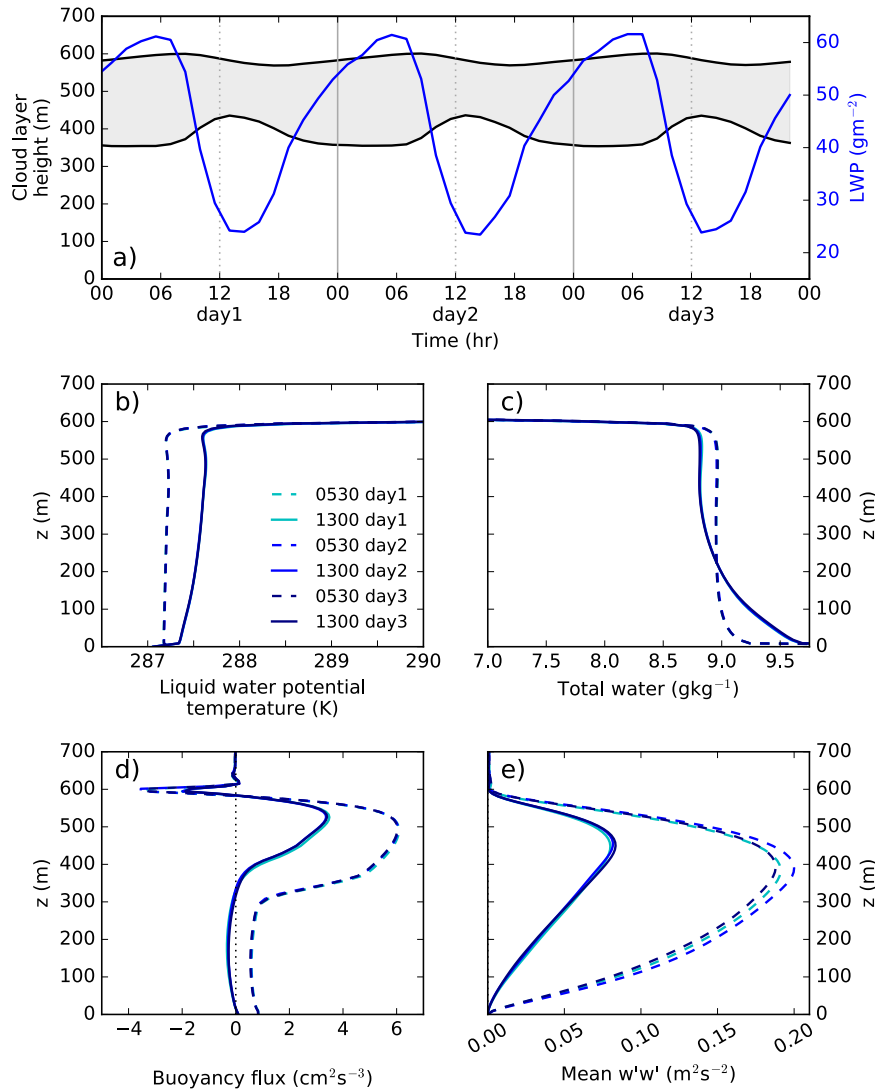
833 3.1 No-aerosol experiment

834 The no-aerosol experiment is initialised then run for fifteen days without the presence of an aerosol layer. The first five days
 835 are used as a spin-up period that allows the BL to reach a steady state; the following three days (days 6, 7, and 8 of the
 836 simulation) are shown in [Figure 3](#).



837

838



839

840 **Figure 3. Evolution of domain averaged cloud properties in the no-aerosol simulation including:** a) cloud top and base (black lines;
 841 left axis), and liquid water path (blue line; right axis); and vertical profiles taken at 0530 (dashed lines) and 1300 (solid lines) on each
 842 day for b) liquid water potential temperature, c) total water mass mixing ratio, d) buoyancy flux, and e) the **perturbation variance**
 843 **in mean-vertical velocity $w^2w^2w'w'$.**

844 The no-aerosol experiment produces a cloud-topped BL with strong diurnal variations. During the daytime, cloud top height
 845 decreases and cloud base height increases, thinning the cloud and producing a diurnal cycle of LWP that reaches a maximum
 846 of 60 g m⁻² at dawn and a minimum of 25 g m⁻² just after midday (Figure 3Figure 3a). The precipitation rate at the surface (not
 847 shown) ranges from a maximum of 0.2 mm day⁻¹ at night to a minimum of 0.01 mm day⁻¹ during the day. For a cloud with a
 848 LWP of 60 g m⁻² this is within the range of observations presented by Abel et al. (2010The diurnal cycle). The diurnal cycle
 849 of the cloud layer can be separated into a growth phase between 1400 and 0600, and a decay phase between 0700 and 1300.

850 The growth phase is driven by pronounced buoyancy production during the night (Figure 3d) from longwave cloud-
851 top cooling and evaporative cooling of entrained air, which drives strong eddies below cloud turbulent motion throughout the
852 BL (Figure 3e). During the daytime, solar heating reduces cloud-top negative buoyancy flux (Fig. 3d) through an
853 offset in the longwave cooling and reduces surface-driven positive buoyancy through weakened surface-to-atmosphere
854 gradients-turbulence throughout the BL (Fig. 3e). This weakens the BL circulation and prevents mixing throughout the BL and
855 promotes a decoupled state in which the flux of moisture from the surface to the cloud is insufficient to maintain the cloud
856 base height, as evident from the non-constant BL profiles of θ_1 (Figure 3b) and q_t (Figure 3c) at 1300 hours.
857 The weakened flux and solar heating of the cloud drives the lifting condensation level upwards and causes the cloud base to
858 increase with height, producing the decay phase. During the daytime weakened BL eddies are unable to ‘push’ against the
859 subsidence at the BL top, which decreases the BL depth and cloud top height. Due to the different processes that control the
860 cloud top and cloud base diurnal variations, the cloud top height minimum occurs about 2 hours after the cloud base reaches
861 its maximum. The cloud layer, LWP and thermodynamic profiles in Figure 3 (a – e) show very little change over the
862 three days of the simulation and present a stratocumulus deck with a consistent diurnal cycle in a steady state. This provides a
863 suitable simulation to use as control for the elevated-aerosol experiments.

864 3.2 Cloud response to elevated aerosol layer in the base experiment

865 We begin with the base experiment (hatched experiment in Figure 2) where a 250 m thick absorbing aerosol layer
866 with an AOD of 0.2 is placed directly above the inversion layer. Following a five-day spin-up period without aerosol, the
867 simulation runs for a further ten days with the aerosol layer present. The domain-averaged cloud response following the
868 introduction of aerosol is shown in Figure 4 and compared to the no-aerosol simulation.

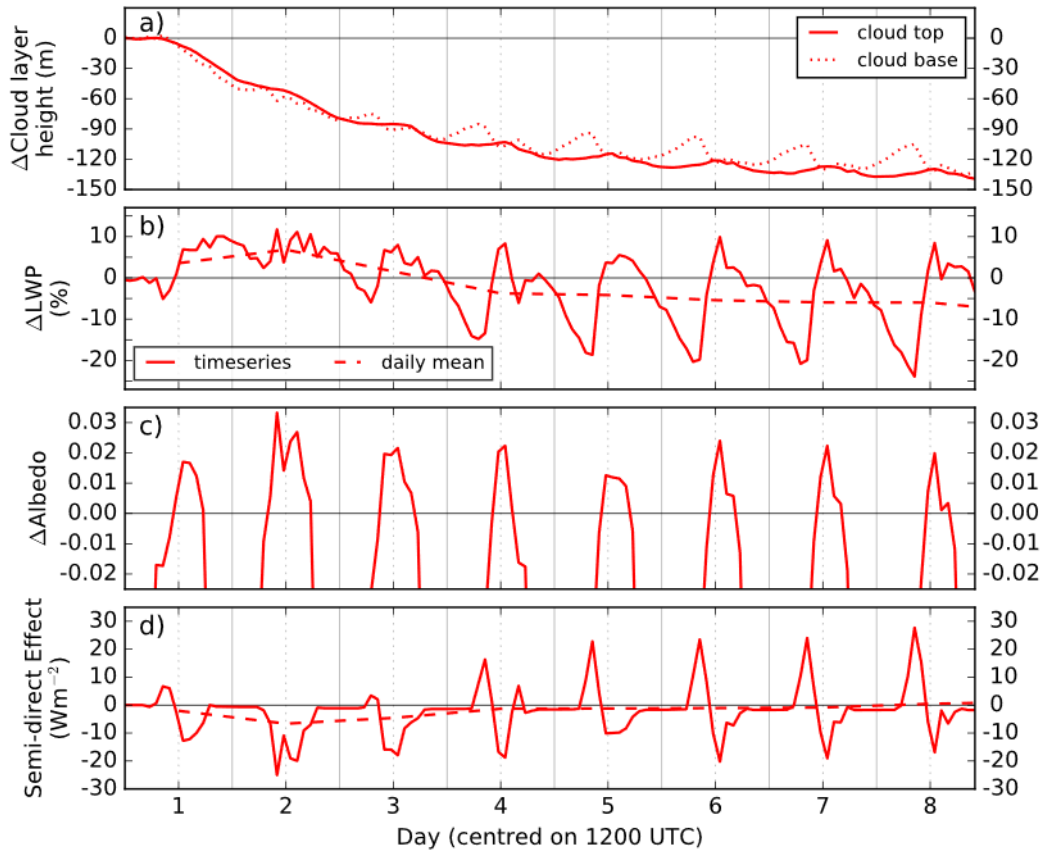
869
870 The simulations show that the absorbing aerosol drives changes in the diurnal cycle of cloud depth and LWP, predominantly
871 through changes in the cloud base height. The presence of the absorbing aerosol drives a decrease in cloud top height (Figure
872 4a) which occurs predominantly in the afternoon and evening and is indicative of a decrease in entrainment across the inversion
873 layer. During the initial two days the cloud base (Figure 4a) decreases in altitude ~10 m more than the cloud top resulting in a
874 thicker cloud, however from day three onwards there is less growth of the cloud throughout the evening and early morning,
875 followed by less thinning throughout the day. Compared to the cloud in the presence of no aerosol, the introduction of the
876 absorbing aerosol layer results in relatively less LWP (Figure 4b) during the growth phase of the cloud and more LWP during
877 the decay phase.

878
879 The SDE (Figure 4d) has a strong diurnal cycle that is directly driven by modifications to the cloud albedo diurnal cycle (Figure
880 4c) and shows considerable sensitivity to the LWP response during the cloud decay phase around midday. In the first three
881 days the albedo response is positive from mid-morning to the late afternoon. This drives an overall negative daily mean SDE.
882 The length of time with a positive albedo response gets shorter as the simulation progresses, driving an increasingly positive

883 SDE in the morning that cancels out, on a daily mean, the negative SDE in the afternoon. Consequently, the daily mean SDE
884 is negative for the initial three days but almost net zero SDE from the fourth day onwards.

885

886



887

888 **Figure 4. 10-day timeseries of domain-averaged cloud response to a layer of aerosol directly above the boundary layer inversion**
889 **with an aerosol optical depth of 0.2 and geometric thickness of 250 m. Plots show the response from Plots show the difference between**
890 **the no-aerosol simulation and the simulation with an elevated aerosol layer for a) cloud top height (solid line) and cloud base height**
891 **(dotted line), b) cloud liquid water path (LWP), c) albedo, and d) the semi-direct effect. Solid lines in b), c), and d) show the timeseries**
892 **of the response and dashed lines in b) and d) show the daily mean.**

893

894 The cloud response and SDE are therefore markedly different in the initial phase compared to the steady-state that is reached
895 after 6 or 7 days following the introduction of the absorbing aerosol layer. In that steady-state phase the BL depth has decreased
896 by ~130 m (~20%) and the diurnal cycle response in cloud thickness has stabilised. This suggests there are timescales in the
897 response to the introduction of the aerosol layer: a short-term response that can be interpreted as a rapid adjustment of the

898 humidity profile, and longer-term response that can be interpreted as a new equilibrium state for the BL sources of moisture,
899 turbulence, and heat.

900

901 This study focuses on the initial response because it is more relevant for real-world understanding as the aerosol perturbation
902 is unlikely to remain constant for several days, and the lifetime of stratocumulus decks is generally on the order of a few days
903 only. However, the steady-state response provides insight into the key drivers behind the BL modifications.

904 3.2.1 Initial response in the base experiment

905 The domain-averaged timeseries of the response in the first three days following the introduction of the aerosol layer (days 6,
906 7, and 8 of the simulation) are shown in Figure 5. The initial response of the cloud to the elevated aerosol layer is driven by

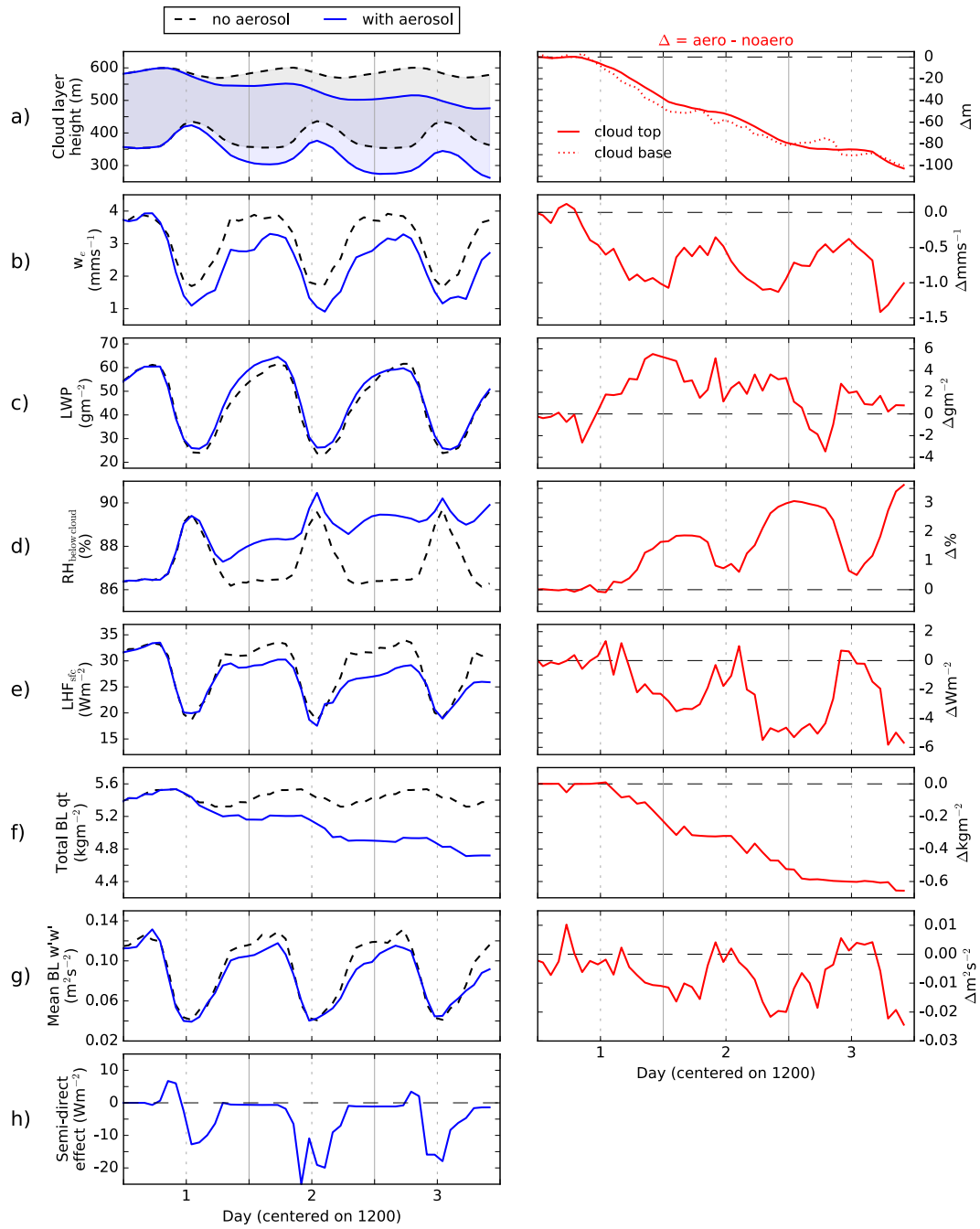
907 the weakening of the entrainment rate ($w_e = dz_{\text{cloudtop}}/dt - w_s$) and subsequent increase in the mean RH
908 below cloud which acts to produce a thicker cloud in the first two days. Solar radiation heats the elevated absorbing aerosol
909 layer above the inversion layer. Strengthening of the temperature inversion at the top of the BL drives a weakened w_e (Figure
910 5b) which causes the BL depth to decrease (Figure 5a). Simultaneously, there is an increase in mean RH below cloud (Figure
911 5d), which allows the cloud base height to decrease (Figure 5a) and the LWP to increase (Figure 5c); this response continues
912 for the first two days, after which the LWP starts to display a diurnal response with a decrease in LWP during the night and an
913 increase in the afternoon. The increase in RH occurs due to the weakened w_e which reduces the amount of warm dry FT air
914 that is mixed into the BL and allows the ~~cloud layer to maintain a higher RH.~~ sub-cloud layer to maintain a higher RH. The
915 relatively small decrease in potential temperature of ~ 0.1 K (Fig. 5g) suggests that the RH response is driven by an increase
916 in available water vapour. There is little response of the cloud before sunrise, which suggests a weak insulating effect of the
917 aerosol layer on longwave fluxes at the cloud top. This is supported by a lack of systematically weakened cloud-top longwave
918 cooling (Fig. S1 in the supporting information), which would be expected for an increased downwelling longwave flux from
919 the aerosol layer.

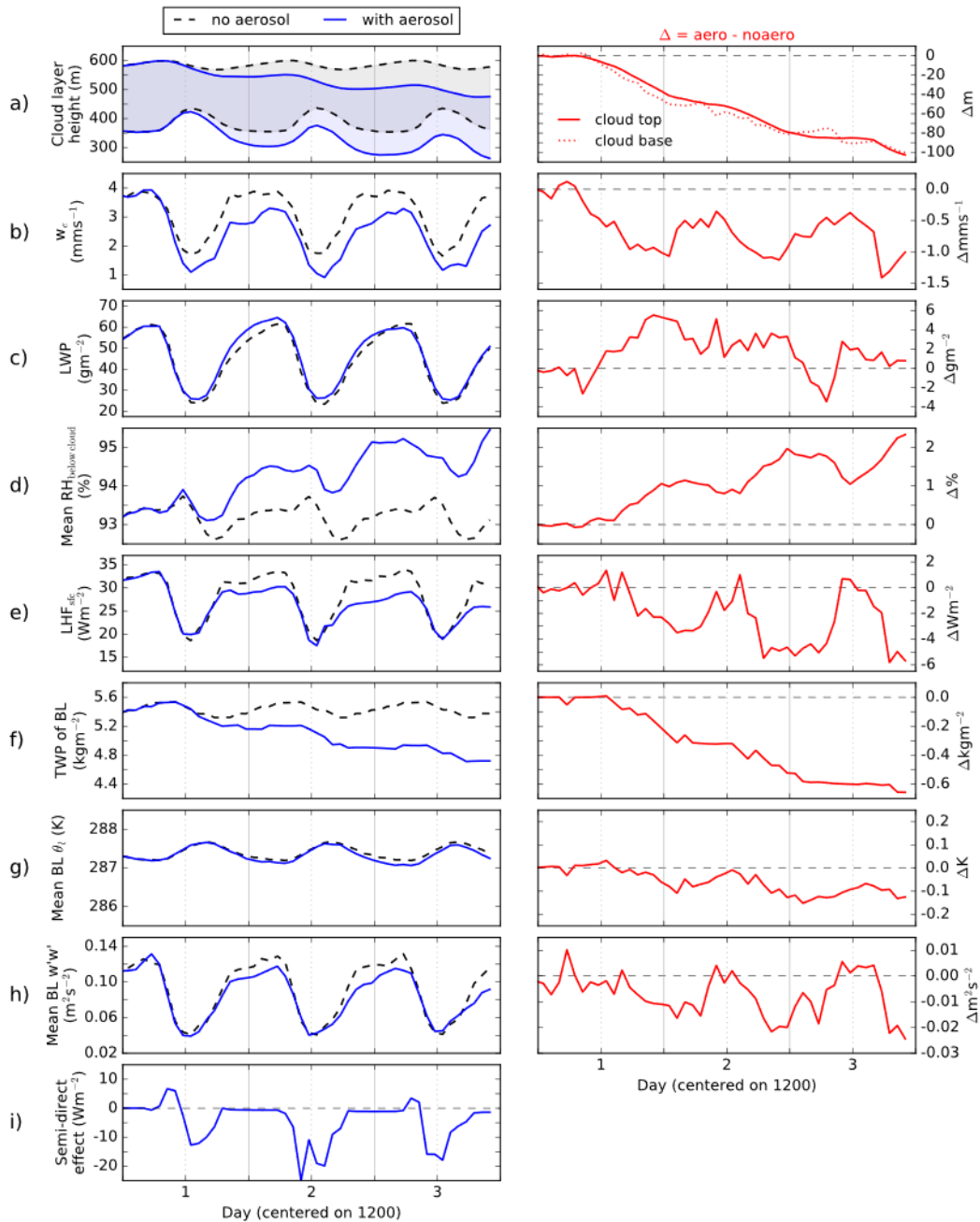
920

921 The thinner cloud (lower LWP; Fig. 5a) on the morning of the third day is driven by changes to the supply of moisture to the
922 cloud layer. The enhanced RH below cloud (~~caused by an increase in water vapour~~) and weakened vertical motions (Figure
923 5gh) drive a strong reduction in surface evaporation as demonstrated by the decrease in latent heat flux (LHF; Figure 5e),
924 especially during the night. By the end of day three the LHF at the surface has reduced by 20% and the total ~~column~~-water
925 ~~content~~ path (TWP) of the BL (Figure 5f) has reduced by 10%. During the night when the BL is well mixed this reduction in
926 ~~total water content~~ TWP prevents the cloud from developing to the same extent as in the no-aerosol simulation, resulting in a
927 thinner cloud when the sun rises. This process is amplified by the reduced BL dynamics which will weaken the flux of moisture
928 from the sub-cloud region to the cloud.

929

930 The thicker cloud ([enhanced LWP; Fig. 5a](#)) on the afternoon of the third day is driven by relatively stronger coupling with the
931 surface moisture fluxes at midday, which produces a slightly thicker cloud and a negative SDE (Figure [5hi](#)). Under no-aerosol
932 conditions, shortwave absorption by the cloud stabilises the cloud layer during the day, which results in a degree of decoupling
933 between the surface layer and cloud base ([Figure 3Figure-3](#)). When an elevated absorbing aerosol layer is present, the decrease
934 in cloud layer height, following the BL depth decrease, allows better coupling to the surface; ([see Fig. S2 in the supporting](#)
935 [information](#)), which becomes increasingly important around midday when BL dynamics are weakest (Figure [5gh](#)). The
936 enhanced source of moisture to cloud base, along with weakened entrainment of dry FT air, prevents the cloud from thinning
937 to the same extent. Although the change in LWP is only 2–3 g m⁻², this amounts to a 10% increase, which helps drive a strong
938 negative SDE at midday and early afternoon.





940

941 Figure 5. 3-day timeseries showing the initial domain averaged cloud response to a layer of absorbing aerosol in the base
 942 experiment (0 m cloud-aerosol gap, 250 m thick layer, and AOD of 0.2). In the first column the black dashed lines refer to the
 943 control experiment (no-aerosol) and solid blue lines to the experiments with the aerosol layer present. The second column shows
 944 the cloud response (red solid line). The plots show a) the altitude of the cloud base and top, b) the entrainment rate w_e , c) the liquid
 945 water path (LWP), d) the mean relative humidity (RH) below-between the ocean surface and the cloud base, e) the surface-latent
 946 heat flux (LHF_s) from the surface, f) the total mass of water in-path (TWP) of the boundary layer (BL)-column, g) the mean

947 ~~squared liquid-water potential temperature (θ) of the BL, h) the mean BL vertical velocity perturbation variance ($w'w'$), and h)~~
948 ~~the semi-direct effect.~~

949

950 The analysis of the initial cloud response shows that the first two days are characterised by a general thickening of the cloud
951 driven by the reduction in w_e across the temperature inversion and subsequent enhanced RH profile below cloud: via an increase
952 in water vapour. The weakened w_e , BL dynamics, and moisture flux from the surface begin to dry the BL resulting in less
953 cloud growth overnight, whilst the lower cloud base enhances coupling to the surface moisture fluxes during the middle of the
954 day, and less cloud decay.

955

956 3.2.2 Steady-state response in the base experiment

957 The final three days of the 15-day base experiment provide a mean diurnal cycle of the cloud response. Although aerosol
958 layers do not persist above stratocumulus decks for so long in reality, the steady-state response provides insight into the key
959 drivers behind the BL modifications. The steady-state response of the cloud to the elevated aerosol layer, shown in Figure 6,
960 shows strong similarities to the third day of the initial response: the growth phase of the cloud (Figure 6b) is weakened,
961 producing a thinner cloud in the morning, and the decay phase of the cloud (Figure 6b) is weakened, producing a thicker cloud
962 in the early afternoon. This modification to the diurnal cycle of the cloud is driven by an increased coupling between surface
963 moisture flux and cloud base during the daytime (see Fig. S2 in the supporting information) and an overall decrease in ~~total~~
964 ~~water content~~ TWP of the BL and weakened dynamics overnight. The decrease in cloud layer height allows better mixing
965 beneath the cloud base, which enhances the evaporation of moisture from the surface between 0900 and 1500 (Figure 6d); this
966 is evident from the ~~lack of a weekend~~ diurnal cycle in mean RH below-cloud RH (Figure 6c), which usually occurs due to
967 poor mixing, and the strengthened BL dynamics at midday (Figure 6f–g). The small response in mean BL potential
968 temperature of -0.2 K (Fig. 6f) strengthens the hypothesis that the RH response below cloud is driven by changes in available
969 water vapour, rather than the decrease in temperature, although it is worth noting that this decrease in temperature will act to
970 slightly increase the RH.

971

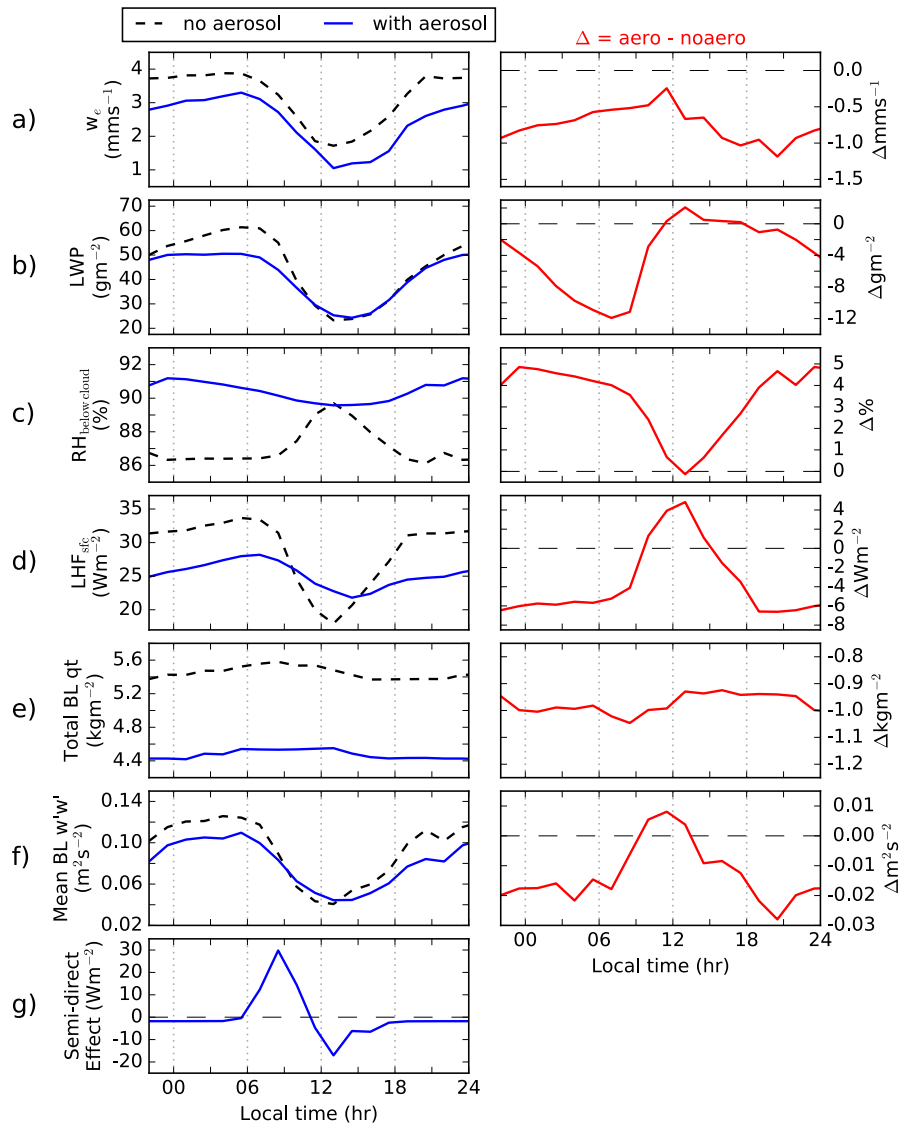
972 The weakened cloud growth phase overnight occurs due to a 15% reduction in ~~total water content~~ TWP of the BL (Figure 6e)
973 and a reduction in mean BL vertical motions overnight of $\sim 20\%$, indicated by the mean ~~perturbation to BL~~ vertical velocity ~~in~~
974 ~~the BL variance~~ ($w'w'$) in Figure 6fg. The reduction in w_e (Figure 6a) and subsequent changes to below-cloud water vapour
975 set up a positive feedback mechanism with BL dynamics: vertical motions in the BL are considerably weakened throughout
976 the night and slightly strengthened at midday. Although there is a decrease in LWP there is no systematic impact to the cloud-
977 top longwave cooling due to its weak sensitivity to LWP above 50 g m^{-2} (van der Dussen et al., 2013; Garrett and Zhao, 2006).
978 The weakened BL circulation is therefore due to a reduction in entrainment. The mixing of dry air into the cloud layer results
979 in evaporation and associated a cooling of entrained air, which generates buoyancy; a reduction in entrainment therefore

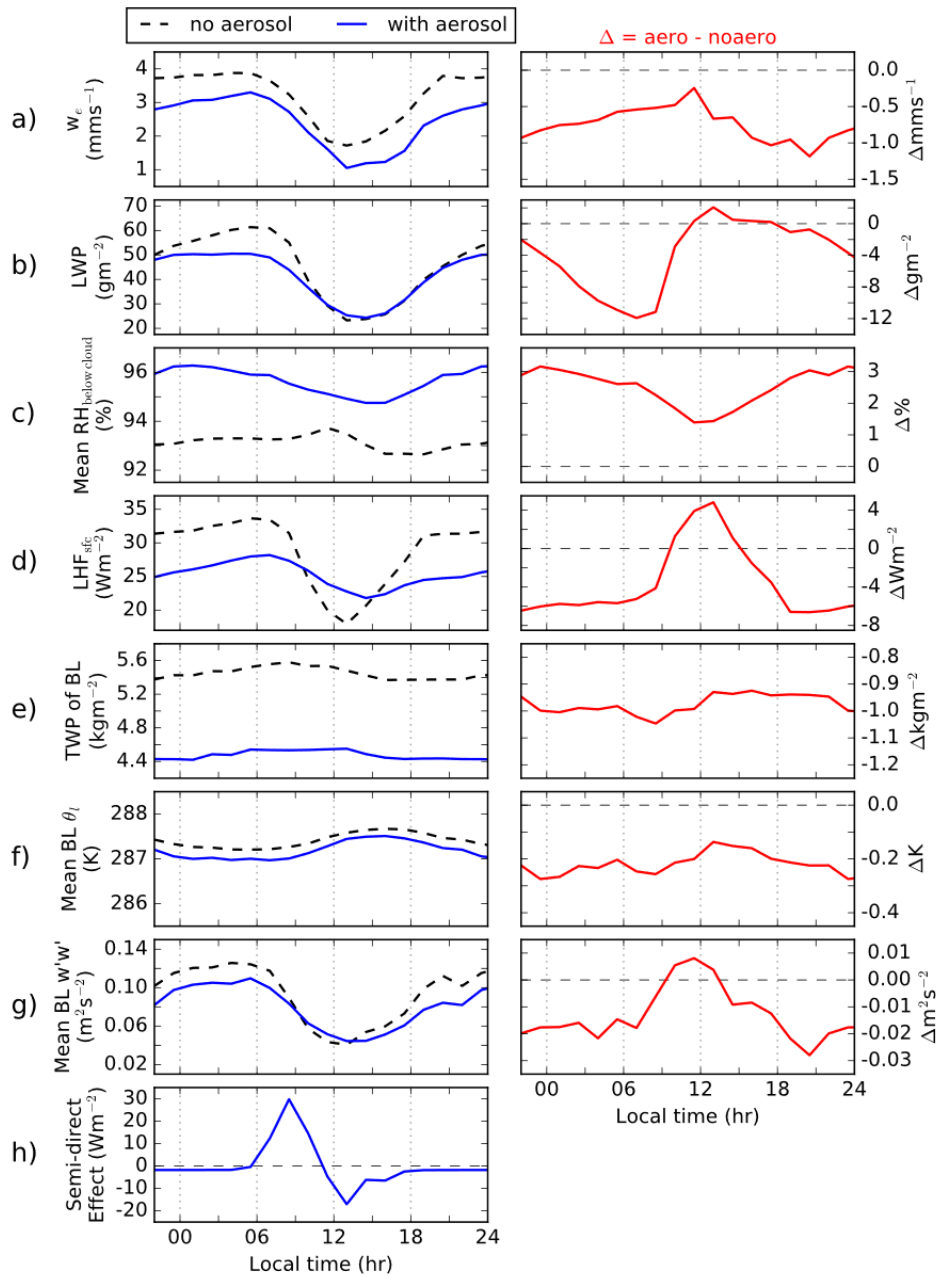
980 weakens cloud–top buoyancy production. These combined changes result in reduced vertical motions within the BL, which
981 reduce surface evaporation, cloud LWP, and buoyancy production from condensation at cloud base, which allow the reduced
982 vertical motions to persist. A partial offset to this process occurs during midday when stronger coupling to the surface results
983 in enhanced transport of water vapour to the cloud base.

984

985 The steady–state response establishes itself by the third day of the simulation. The daily mean steady–state SDE (Figure 6gh)
986 results from a balance between the degree to which the BL ~~total column water content~~TWP has decreased, producing a positive
987 SDE in the morning, and the degree to which the midday coupling is enhanced, producing a negative SDE in the afternoon. In
988 both cases modifications to BL depth, and thus w_e , play a significant role in cloud response and SDE.

989





991

992 Figure 6. Domain averaged cloud response to a layer of absorbing aerosol directly above the inversion in the base experiment (0 m
 993 cloud–aerosol gap, 250-m thick layer, and AOD of 0.2) for the mean diurnal cycle using the final three days of the 15–day simulation.
 994 In the first column the black dashed lines refer to the control experiment (no–aerosol) and solid blue lines to the experiments with
 995 the aerosol layer present. The second column shows the cloud response (red solid line). The plots show a) the entrainment rate w_e ,
 996 b) the liquid water path (LWP), c) the mean relative humidity (RH) below between ocean surface and cloud base, d) the latent heat
 997 flux (LHF) from the surface, e) the total mass water path (TWP) of water (vapour + liquid) in the boundary layer (BL) column, f)
 998 the mean squared liquid–water potential temperature (θ_l) of the BL, g) the mean BL vertical velocity perturbation variance ($w'w'$),
 999 and gh) the semi–direct effect.

1000

1001 3.3 Sensitivity of initial response to aerosol layer properties

1002 Figure 7 shows timeseries for the aerosol layer–sensitivity experiments. In this analysis the inversion strength $\Delta\theta_1$ is determined
1003 between altitudes z_{upper} and z_{lower} ~~defined as:~~

$$1004 \begin{cases} z_{\text{lower}} = z \text{ at } 0.025 \cdot z_{\text{max}} \text{ below } z_{\text{max}} \\ z_{\text{upper}} = z \text{ at } 0.25 \cdot z_{\text{max}} \text{ above } z_{\text{max}} \end{cases} \quad (3)$$

1005

1006 ~~where z_{max} . The value of z_{upper} is the topmost altitude at which where the maximum absolute gradient in θ_1 occurs. The upper~~
1007 ~~value $\left|\frac{d\theta_1}{dz}\right|$ is 25% of its maximum, and z_{lower} is the lowermost altitude where $\left|\frac{d\theta_1}{dz}\right|$ is 2.5% of its maximum. The upper threshold~~
1008 ~~is determined at a higher percentage of $\left|\frac{d\theta_1}{dz}\right|$ than the lower threshold to limit spurious values occurring from aerosol layers~~
1009 ~~close to the inversion layer that impact θ_1 .~~

1010 3.3.1 Cloud response

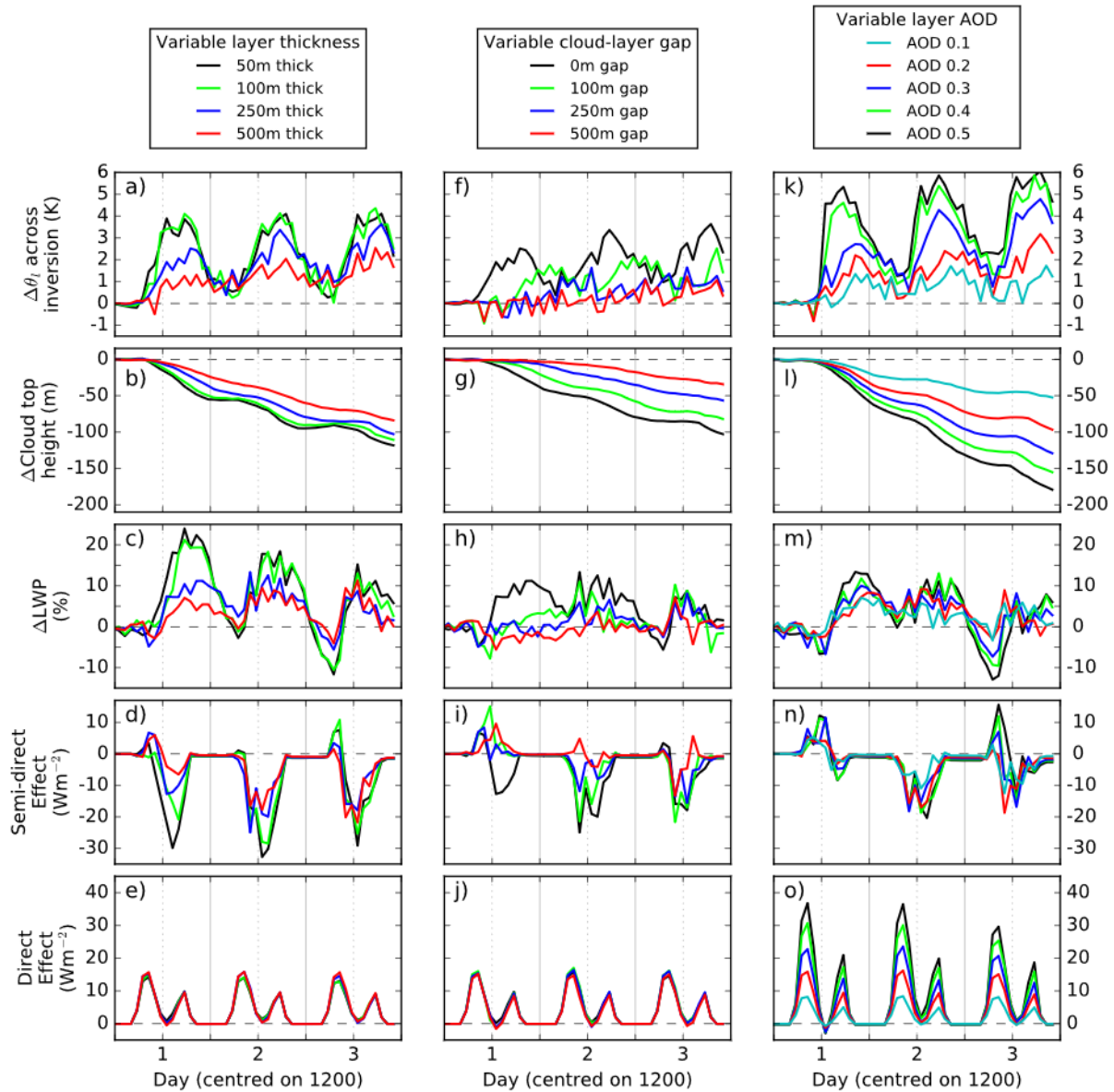
1011 The majority of experiments show a positive spike in SDE (Figure 7d, i and n) just ~~after~~before midday on the first day. This
1012 occurs due to the lag–time in response between the direct impact onto the cloud top height, which is driven by from changes to
1013 w_e , and the cloud base, which is driven by changes–increase in sub–cloud RH. This lag occurs due to weaker coupling of the
1014 cloud and sub–cloud layers and therefore poorer BL mixing around midday (see). This smallFigure S1 in the supporting
1015 information focuses on the response in the initial 24 hours. The positive SDE is driven by the decrease in LWP and subsequent
1016 positive SDE is consistent caused by an increase in cloud base height (Fig. 5a and Fig. S1a) without a corresponding change in
1017 cloud top height. The decrease in w_e weakens buoyancy production throughout the rangecloud layer (Fig. S1c), which drives
1018 a reduced moisture flux within the cloud and to the cloud base (Fig. S1d). As the day progresses the continued reduction of w_e
1019 results in an increase in mean below–cloud RH and a recovery, or increase, of experiments but mitigated in some cases due to
1020 rapid impactsthe LWP. This explains why stronger perturbations to the entrainment rate on the LWP (i.e., the 50–first day (such
1021 as when the layer is close to the cloud) results in a quicker recovery of the LWP (Fig. 7c, h, and m thickness experiment) that
1022 occur before BL coupling weakens.) This result suggests the specific timing of the incoming aerosol plume may play a role
1023 in the cloud response and SDE on the first day.

1024

1025 Geometrically thinner aerosol layers equate, for a given AOD, to a greater aerosol mass mixing ratio and therefore stronger
1026 heating. This results in a stronger inversion layer (Figure 7a) and stronger modification to the LWP response (Figure 7c) and
1027 SDE (Figure 7d), especially on the first day. This produces a stronger inversion layer, weaker w_e , and a decrease in BL depth
1028 (Figure 7b). For the two thinnest layers the cloud top height decreases at a faster rate during the day than at night, which

|029 correlates with the peak heat perturbation. For thicker layers the heat perturbation extends further into the night; this
|030 corresponds with the delay in time for the heating towards the top of the layer to reach the inversion layer and drives a steadier
|031 reduction in BL depth when compared to the thinner layers. By the third day the BL has started to adjust and less dependence
|032 on aerosol layer thickness is apparent, however the thinner layers cause the BL to dry out at a quicker rate, thus producing a
|033 stronger positive SDE on the morning of the third day.

|034



037

038 **Figure 7.** 3-day timeseries showing the sensitivity of the initial cloud response **(difference between the no-aerosol simulation and the**
 039 **simulation with an elevated aerosol layer)** to the properties of the elevated absorbing aerosol layer. The three columns correspond
 040 to experiments where systematic changes have been made to the aerosol layer thickness (a – e), cloud-aerosol gap (f – j), and aerosol
 041 layer AOD (k – o).

042

043 Increasing the cloud–aerosol gap leads to a weaker and increasingly delayed ~~maximum~~ cloud top height (Figure 7g) and LWP
044 response (Figure 7h) driven by changes in peak strengthening of the inversion (Figure 7f); this is most pronounced in the first
045 two days. Only aerosol layers directly above the inversion trigger a considerable cloud response on the first day because of the
046 relatively rapid strengthening of the inversion layer and weakening of w_e which forces the cloud top downwards more rapidly
047 than the RH profile can adjust, resulting in a deeper cloud base. On the second day a cloud response is seen with gaps up to
048 100 m and by the third day all gaps lead to a response in cloud LWP. The delay in response is driven by the delay in the
049 inversion layer strengthening. In the free troposphere the advection of the heat perturbation is driven by subsidence, therefore,
050 greater cloud–aerosol gaps require more time for the heat perturbation to reach the cloud top. Simultaneously longwave cooling
051 acts to weaken the heat perturbation throughout its advection, which drives a relatively weaker strengthening of the temperature
052 inversion as the cloud–aerosol gap increases.

053
054 The initial cloud top response (Figure 7l) displays a strong dependence on the AOD of the aerosol layer throughout the three
055 days with greater AOD resulting in a greater response. As with geometric layer thickness, larger AODs absorb more radiation
056 and drive a stronger heat perturbation and inversion strength (Figure 7k). So larger AODs result in a thicker cloud and a more
057 negative SDE. On the third day layers with the largest AODs, which have had the greatest impact on cloud top height and w_e ,
058 exhibit a considerably thinner cloud, driving an increasingly positive SDE in the morning.

059
060 In summary, the layer–sensitivity experiments show that on the first day the initial response is for the cloud top to drop quicker
061 than the cloud base, resulting in a thinner cloud and a positive SDE in the morning, the magnitude of which is primarily driven
062 by the proximity of the aerosol layer with the cloud top. With no gap between the inversion at cloud top and aerosol layer, the
063 afternoon of the first day is characterised by a thicker cloud and negative SDE which increases in magnitude for stronger heat
064 perturbations. The second day is generally characterised by an increase in the LWP at midday which drives a negative SDE
065 and is dependent on the location and properties of the aerosol layer. By the third day a consistent pattern occurs: the cloud is
066 consistently thinner in the morning and thicker at midday, the magnitude of which is dependent on the strength of the
067 perturbation.

068 3.3.2 Radiative response

069 Figure 8 shows timeseries of the daily mean radiative effects for the layer–sensitivity experiments. The immediate radiative
070 response following the introduction of the absorbing aerosol layer is primarily dependent on the distance between the inversion
071 layer and aerosol layer base. When there is no cloud–aerosol gap the increase in LWP results in a negative SDE; thinner layers
072 and larger AODs increase the inversion layer strengthening and drive a stronger negative SDE on the first day. When any
073 cloud–aerosol gap is present there is little LWP response on the first day due to the delayed inversion layer strengthening,
074 however, all experiments with a gap present are characterised by a small positive SDE. For the experiments with a 50-m gap

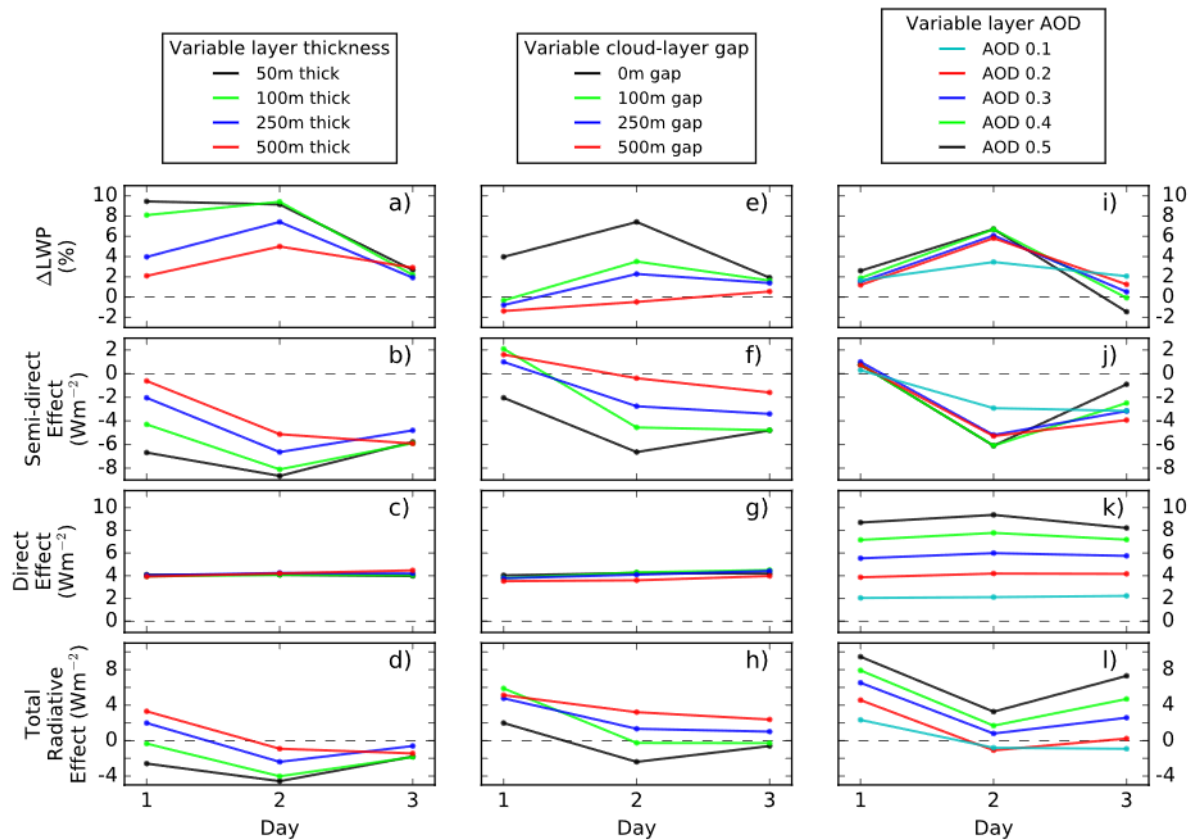
075 (variable AOD experiments) the delay is short enough that there is an increase in LWP in the evening of the first day (Figure
 076 8i).

077

078 On the second and third day the SDE is negative for all experiments; the magnitude of the SDE increases for thinner layers,
 079 closer to the inversion layer. When a cloud–aerosol gap is present the AOD tends to have little impact on the magnitude of the
 080 SDE. The rate at which the BL moisture content decreases, itself a factor of how strongly w_e is perturbed, results in variations
 081 in which day the peak SDE occurs. In experiments with gaps smaller than 100 m the maximum SDE is reached on the second
 082 day, whereas for gaps larger than or equal to 100 m the maximum occurs on the third day. In all experiments the third day is
 083 characterised by a decrease in the daily mean LWP response which is primarily driven by less cloud growth overnight and in
 084 the morning (see Figure 7c, h and m) and becomes more pronounced as the temperature inversion strengthens. The thinner
 085 cloud in the morning helps to shift the daily mean SDE towards zero.

086

087



088

089 **Figure 8. Daily mean radiative impact to the elevated aerosol layer properties over the initial three days following the introduction**
 090 **of the aerosol layer for systematic changes to a) – d) aerosol layer thickness, e) – h) cloud–aerosol gap, and i) – l) aerosol optical**
 091 **depth of layer.**

1092

1093 The properties of the aerosol layer have a considerable impact on the total radiative effect, calculated as the sum of the DRE
 1094 and SDE (Figure 8d, h, and l). Generally, the SDE acts to counteract the positive DRE and in some cases results in an overall
 1095 negative total radiative effect. In all experiments the total radiative effect is sensitive to the layer properties, whereas DRE is
 1096 only sensitive to the layer AOD. In many instances the SDE is greater in magnitude than the DRE, with the second day
 1097 constituting the period of time with the greatest impact. The relative insensitivity of the SDE to changes in AOD suggest that
 1098 layers with a moderate AOD (~ 0.2) may have the strongest overall radiative impact due to the relatively low DRE; however,
 1099 the behaviour may change for increasing gaps.

1100

1101 The results of the experiments are summarised in Table 3 with the daily mean SDE alongside the means for the periods before
 1102 and after midday. The daily mean SDE is only consistently negative throughout the three days when there is no cloud–aerosol
 1103 gap. This result is consistent with Johnson et al. (2004) who similarly found a negative SDE for a ~ 1000 m layer of absorbing
 1104 aerosol (AOD of 0.2, SSA of 0.88) directly above the inversion layer. Johnson et al. (2004) calculated a mean SDE of -9.5 Wm^{-2}
 1105 and a mean DRE of 10 Wm^{-2} . These magnitudes are greater than in this study but similarly show the SDE is of approximately
 1106 equal magnitude to the DRE and of opposite signs. Our results also show that geometrically thin, but optically thick, aerosol
 1107 layers will have a stronger forcing than a thicker layer with the same AOD due to a stronger localised heat perturbation; this
 1108 effect is most prominent on the first day. When a gap to the aerosol layer base is present, as is predominantly observed (Fig.
 1109 1), our results show that the short–term SDE is likely to be weakly positive but then becomes negative once the BL has been
 1110 mixed, which usually occurs during the first night when BL mixing occurs, highlighting a sensitivity to the specific arrival
 1111 timing of the incoming plume. On the second and third day the magnitude of the SDE then depends on the AOD, cloud–aerosol
 1112 gap, and aerosol layer thickness.

1113

1114 **Table 3. Mean semi–direct effect (in Wm^{-2}) for each of the aerosol experiments shown in Figure 2 and Table 2. Mean**
 1115 **values are presented for each day (Daily), between 0000 and 1200 hours (am), and between 1200 and 2400 (pm). For the daily**
 1116 **mean, increasingly negative values are shaded in blue and increasingly positive in red.**

Type of experiment	gap	dz	AOD	Day 1			Day 2			Day 3		
				Daily	am	pm	Daily	am	pm	Daily	am	pm
Variable gap	0	250	0.2	-2	1	-5	-7	-6	-7	-5	-4	-6
	100	250	0.2	2	4	0.4	-5	-5	-4	-5	-5	-5
	250	250	0.2	1	2	0.3	-3	-3	-3	-3	-3	-4
	500	250	0.2	2	1	2	-0.4	1	-1	-2	-3	-0.5
Variable thickness	0	50	0.2	-7	-2	-12	-9	-5	-13	-6	-2	-10
	0	100	0.2	-4	-1	-8	-8	-5	-11	-6	-2	-10
	0	250	0.2	-2	1	-5	-7	-6	-7	-5	-4	-6

	0	500	0.2	-1	2	-3	-5	-4	-6	-6	-5	-7
	50	200	0.1	<u>0.3</u>	2	-1	-3	-3	-3	-3	-2	-4
	50	200	0.2	1	2	<u>-0.1</u>	-5	-5	-6	-4	-4	-4
Variable	50	200	0.3	1	2	<u>-0.1</u>	-5	-5	-5	-3	-1	-5
AOD	50	200	0.4	1	2	-1	-6	-4	-8	-2	<u>-0.4</u>	-5
	50	200	0.5	1	3	-1	-6	-4	-8	-1	3	-5

1117

1118 Table 3 highlights the diurnal variations in the SDE. The SDE is generally more negative after midday but that contrast varies
 1119 with aerosol layer properties. Geometrically thin, optically thick layers, directly above the inversion layer display the strongest
 1120 contrast with the daily mean SDE dominated by the mean after midday. When a gap is present there is less contrast and both
 1121 time periods are generally representative of the daily mean, until the BL begins to dry out significantly in the high AOD
 1122 experiments. These results demonstrate that there are often strong diurnal variations in the SDE which are sensitive to the
 1123 aerosol layer properties and suggest that observations of the SDE made within a small window of time, e.g., those from polar
 1124 orbiting satellites, may be unrepresentative of the daily mean SDE.

1125 3.4 Sensitivity to boundary layer and cloud properties

1126 This section investigates the robustness of the results and conclusions from Sect. 3.3. The parameter space considered in this
 1127 section includes previous LEM studies, such as Hill and Dobbie (2008) and Johnson et al. (2004), and the range of
 1128 environmental forcings observed within marine stratocumulus regions.

1129

1130 The first set of sensitivities focus on the model setup and includes no precipitation from the cloud (*noRain*) and an enhanced
 1131 large-scale advective heat tendency of -0.5 Kday^{-1} (*05cool*).

- 1132 • In the *noRain* setup the production of precipitation is switched off. Stratocumulus frequently produce precipitation in
 1133 the form of drizzle (Leon et al., 2009) yet studies often simplify simulations by focusing on non-precipitating
 1134 stratocumulus (e.g., Hill and Dobbie, 2008; Johnson et al., 2004). Precipitation redistributes moisture from the cloud
 1135 layer to the sub-cloud layer, promoting BL stability and acting to reduce BL dynamics and cloud LWP (Ackerman
 1136 et al., 2009).
- 1137 • In the *05cool* sensitivity, the magnitude of the large-scale advective heat tendency is increased from -0.1
 1138 to -0.5 Kday^{-1} . That parameter accounts for the equatorward transport of the large-scale air mass and is negative in
 1139 subtropical marine regions. This value can be estimated using large-scale reanalyses (e.g., Johnson et al., 2004) or
 1140 used as a balancing term to prevent subsidence heating (e.g., Duynkerke et al., 2004) and represents a degree of
 1141 variability in LES setups.

1142

1143 The second set of sensitivities focuses on properties of the BL that may impact the diurnal cycle and maintenance of the cloud.

- In the *SST-1K* and *SST+1K* setups, SST is decreased and increased by 1K, respectively, while keeping the BL depth at 600 m. Stratocumulus decks in the Atlantic and Pacific Oceans are observed over a wide range of sea surface temperatures (Sandu and Stevens, 2011; Wood, 2012). As the SST increases the differential temperature across the surface–air boundary increases, resulting in more pronounced surface moisture and sensible heat fluxes.
- The *wetFT* setup increases the mass mixing ratio of water vapour in the FT by $+0.4 \text{ g kg}^{-1}$ to assess the impact of the water vapour content of the entrained air on the SDE. Trajectory analyses from the Pacific and Atlantic Oceans by Sandu et al. (2010) show that the mass mixing ratio of water vapour in the FT varies spatially and temporally, ranging from 1.0 to 7.5 g kg^{-1} at 700 hPa; this result is supported by in–situ data summarised by Albrecht et al. (1995).
- The *800-m* and *1000-m* setups increase the height of the temperature inversion by 200 and 400 m, respectively, by changing the large–scale divergence rate and initial profiles of θ_t and q_t , while keeping SST constant at 287.2 K. Observations show that cloud top heights in regions of semi–permanent stratocumulus coverage (southeast Atlantic, southeast Pacific, and northeast Pacific) typically range from ~ 500 to ~ 1500 m (Muhlbauer et al., 2014; Painemal et al., 2014; Wyant et al., 2010) with variations driven by SST and subsidence.

To isolate the cloud response due to the aerosol layer, the cloud–sensitivity experiments are initialised using profiles that produce an approximately constant stratocumulus cloud layer at the top of the BL following the method described in Sect. 2.2. Table 4 shows the resulting initial profiles and large–scale divergence rates for each setup. The same set of experiments from Sect. 3.3 are performed for each setup, along with a simulation without aerosol to calculate the BL response to the aerosol perturbation. The daily mean SDE on day 2 following the introduction of the absorbing aerosol layer (day 7 of the simulation) is shown in Table 5 for each setup and aerosol experiment. For the *control* setup the SDE values are the same as shown in Figure 8.

Table 4. Initial profiles of liquid–water potential temperature (θ_t in K) and total liquid mass–mixing ratio (q_t in g kg^{-1}) against altitude (z in m) for each cloud–sensitivity setup. Values in parentheses indicate the large–scale divergence rate (D in s^{-1}) used for each setup. All setups result in a stable stratocumulus cloud deck at the top of the boundary layer.

z	<i>noRain</i> (5.4×10^{-6})		<i>05cool</i> (6.2×10^{-6})		<i>SST-1K</i> (4.75×10^{-6})		<i>SST+1K</i> (5.75×10^{-6})		<i>wetFT</i> (5.25×10^{-6})		<i>800m</i> (4.0×10^{-6})			<i>1000m</i> (2.75×10^{-6})		
	θ_t	q_t	θ_t	q_t	θ_t	q_t	θ_t	q_t	θ_t	q_t	z	θ_t	q_t	z	θ_t	q_t
0	287.5	9.0	287.3	9.0	286.5	8.6	288.3	9.4	287.3	9.0	0	287.3	9.0	0	287.3	9.0
600	287.5	9.0	287.3	9.0	286.5	8.6	288.3	9.4	287.3	9.0	800	287.3	9.0	1000	287.3	9.0
601	297.0	5.5	296.0	5.5	296.0	5.5	297.2	5.5	297.0	5.9	801	297.0	5.9	1001	297.0	5.9
750	300.0	5.5	299.0	5.5	300.0	5.5	300.0	5.5	299.5	5.9	900	299.5	5.9	1100	299.5	5.9
1000	301.7	5.5	300.3	5.5	301.7	5.5	301.7	5.5	301.5	5.9	1200	301.5	5.9	1300	301.5	5.9
1500	303.2	5.5	301.5	5.5	303.2	5.5	303.2	5.5	302.6	5.9	1700	302.6	5.9	1900	302.6	5.9
2600	304.0	5.5	302.8	5.5	304.0	5.5	304.0	5.5	303.8	5.9	2600	303.8	5.9	2600	303.8	5.9

170 3.4.1 Sensitivity to model setup

171 ~~The~~ Comparing the no-aerosol simulations, the removal of precipitation results in stronger BL dynamics and a greater peak in
 172 LWP (+15 g m⁻²). ~~Compared to) than~~ the *control* setup ~~the~~. The *noRain* setup is characterised by a consistent
 173 ~~strengthening~~ increase in the magnitude of the SDE at ~~+by~~ 1 Wm⁻² when a cloud-aerosol gap is present and up to +3 Wm⁻²
 174 when there is no gap. In the *control* setup the presence of the aerosol layer increases cloud LWP, which is partially offset by
 175 an increase in precipitation. In the *noRain* setup that partial offset is not allowed, resulting in relatively enhanced LWP response
 176 and SDE.

177

178 ~~Increasing~~ When compared to the *control* setup, increasing the cooling rate of the large-scale advective heat tendency
 179 ~~produces results in~~ stronger buoyancy production and BL dynamics, ~~which are balanced by stronger subsidence ($D = 6.2 \times 10^{-6}$ s⁻¹) in order to maintain a 600 m BL depth. An enhanced cloud-top entrainment of warm dry air is balanced by, and enhanced~~
 180 ~~flux of vapour from below cloud and surface LHF. Relative to the *control* setup (which acts as a feedback to enhanced~~
 181 ~~entrainment). As the processes maintaining the cloud layer become more important, they become more sensitive to~~
 182 ~~perturbations. Therefore, when~~ the aerosol layer ~~has a more pronounced impact on the cloud dynamics and results in a greater~~
 183 ~~decrease in w_e ; this is likely due to the enhanced role that evaporation of entrained air has on buoyancy production is present~~
 184 ~~in the *05cool* setup. Below cloud the two setups have a consistent dynamical response, however, the responses of w_e , LHF,~~
 185 ~~and below-cloud moisture flux are stronger than~~ in the *05cool/control* setup ~~and the cloud maintenance is more dependent on~~
 186 ~~the below-cloud flux of water vapour. This causes simulations are characterised by~~ a quicker decrease in BL water content
 187 ~~which the TWP of the BL. However, this only~~ becomes ~~more pronounced throughout the simulation and manifests as a more~~
 188 ~~pronounced period of positive SDE and a less negative mean SDE prominent~~ on the third day, ~~which in some experiments and~~
 189 ~~results in a positive daily mean SDE (not shown); little difference from the *control* setup over the first two days.~~

191 3.4.2 Sensitivity to BL properties

192 In the no-aerosol simulations warmer SST drives an enhanced ~~advection of water vapour below-cloud, and moisture flux but~~
 193 a lower LWP due to an increase in BL temperature. The warmer BL also leads to stronger in-cloud buoyancy production.
 194 When the aerosol layer is present the LWP response increases with SST, driving a stronger negative SDE in all experiments.
 195 The cloud response is particularly sensitive to SST when the aerosol layer is near the cloud top. As discussed in Sect. 3.2, the
 196 initial response from the weakened w_e , and subsequently enhanced RH, occurs quicker than the moisture source from the
 197 surface can readjust to. The reduction in ~~entrainment rate~~ w_e and BL depth are equivalent for all SST, but the greater flux of
 198 moisture from warmer SST results in a greater increase in mean q_1 and RH perturbation, leading to a lower cloud base, thicker
 199 cloud, and tending to push the SDE towards a more negative daily mean. The sensitivity of the radiative response is driven

|200 both by the SST and the perturbation to w_e , therefore stronger heat perturbations closer to the cloud top result in a more
|201 pronounced sensitivity to SST.

|202

|203 The no-aerosol simulation for the *wetFT* setup is characterised by an LWP +5 g m⁻² greater than the *control* setup, with slightly
|204 weaker surface evaporation. This increase in LWP is caused by entrainment of slightly moister FT air in the *wetFT* setup,
|205 allowing the BL to maintain a greater mean RH. The mixing of entrained air has a smaller impact on the cloud humidity, which
|206 then does not need to be balanced as strongly from a source at the surface. When the aerosol layer is present the weakened w_e
|207 therefore has a smaller impact on the RH response of the BL, which results in a smaller SDE. This setup shows that the degree
|208 by which the entrained air impacts the cloud plays an important role in the strength of the SDE: very dry FT air will play a
|209 more important role in reducing RH, so that a perturbation to w_e will have a greater impact on the cloud response.

|210

211 Table 5. Daily mean semi-direct radiative effect for the second day following the introduction of the absorbing aerosol layer for
 212 control and cloud-sensitivity setups. All values are in daily mean Wm^{-2} with increasingly negative values shaded in blue and
 213 increasingly positive values shaded in red. Layer properties include the cloud-aerosol gap ('gap', in metres), the geometric thickness
 214 of the layer ('dz', in metres), and the aerosol optical depth (AOD) of the layer given at a mid-band wavelength of 505 nm.

Type of experiment	gap	dz	AOD	control	noRain	05cool	SST-1K	SST+1K	wetFT	800-m	1000-m
Variable gap	0	250	0.2	-7	-8	-5	-5	-8	-6	4	17
	100	250	0.2	-5	-6	-5	-3	-7	-3	6	10
	250	250	0.2	-3	-4	-4	-1	-5	-2	6	6
	500	250	0.2	0	-1	-2	1	0	0	4	2
Variable thickness	0	50	0.2	-9	-12	-7	-7	-13	-8	0	18
	0	100	0.2	-8	-10	-7	-5	-11	-7	2	20
	0	250	0.2	-7	-8	-5	-5	-8	-6	4	17
	0	500	0.2	-5	-7	-5	-2	-8	-5	5	11
Variable AOD	50	200	0.1	-3	-5	-3	-1	-3	-3	6	7
	50	200	0.2	-5	-7	-4	-3	-6	-5	5	15
	50	200	0.3	-5	-9	-4	-4	-8	-6	5	22
	50	200	0.4	-6	-9	-5	-4	-10	-5	6	25
	50	200	0.5	-6	-7	-5	-4	-10	-5	5	26

215

216 3.4.3 Sensitivity to BL depth

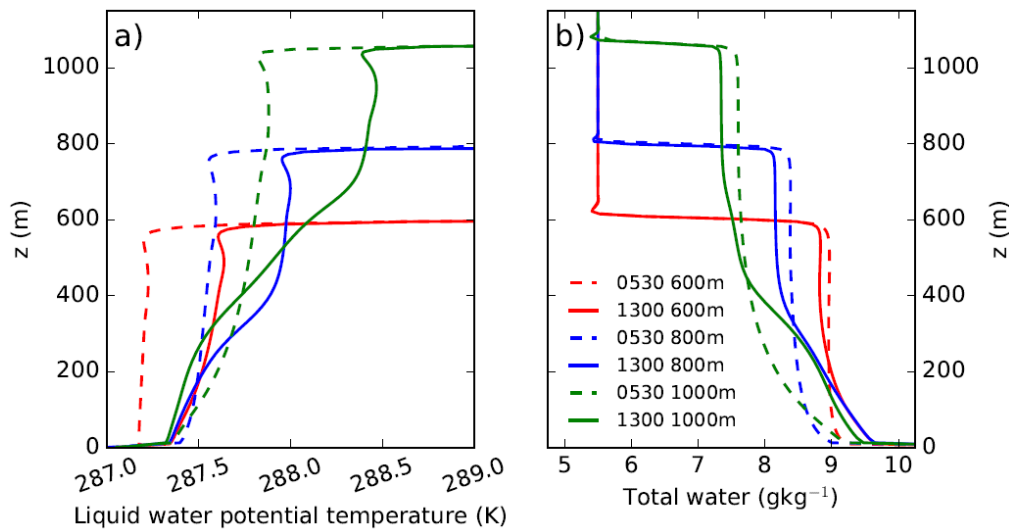
217 As the BL depth increases its temperature increases and the ~~total water content~~TWP of the BL decreases. ~~Figure 9~~Figure-9
 218 shows the profiles of θ_t and q_t for the three setups (*control*, *800-m*, *1000-m*) during the time of strongest (0530 hours) and
 219 weakest (1300 hours) BL dynamics. During the period with weakest dynamics the degree of coupling, or mixing, between the
 220 sub-cloud and cloud layers is weakened. This reduces the flux of water vapour from the surface layer to the cloud, and
 221 resultsresulting in a redistributionan accumulation of water from the cloud layer vapour close to the surface layer (Figure
 222 9Figure-9b). That redistribution becomes more pronounced as the BL depth increases, increasing BL decoupling.

223

224 Increasing the BL depth has a dramatic effect on the sign and magnitude of the SDE shown in Table 5. The SDE switches sign
 225 from negative for a 600-m deep BL in the *control* setup to positive in the *800-m* and *1000-m* setups. The SDE in the *800-m*
 226 setup is roughly of equal magnitude to the *control* but the *1000-m* setup is considerably greater in magnitude, peaking at
 227 $+26 \text{ Wm}^{-2}$. Responses for the base experiment shown in ~~Figure 10~~Figure-10 help to understand why the BL depth has such a
 228 strong impact on the SDE. In all setups the cloud top height decreases by $\sim 100 \text{ m}$ over the three days (~~Figure 10~~Figure-10a, g,
 229 and m), driven by similar changes in w_e (~~Figure 10~~Figure-10e, k, and q), however the response in cloud base height depends
 230 on the simulation and accounts for the variation in LWP response (~~Figure 10~~Figure-10b, h, and n). In the *1000-m* setup (~~Figure~~
 231 ~~10~~Figure-10m) the cloud base decreases less than the cloud top throughout the timeseries, driving a consistently reduced LWP.

232

233



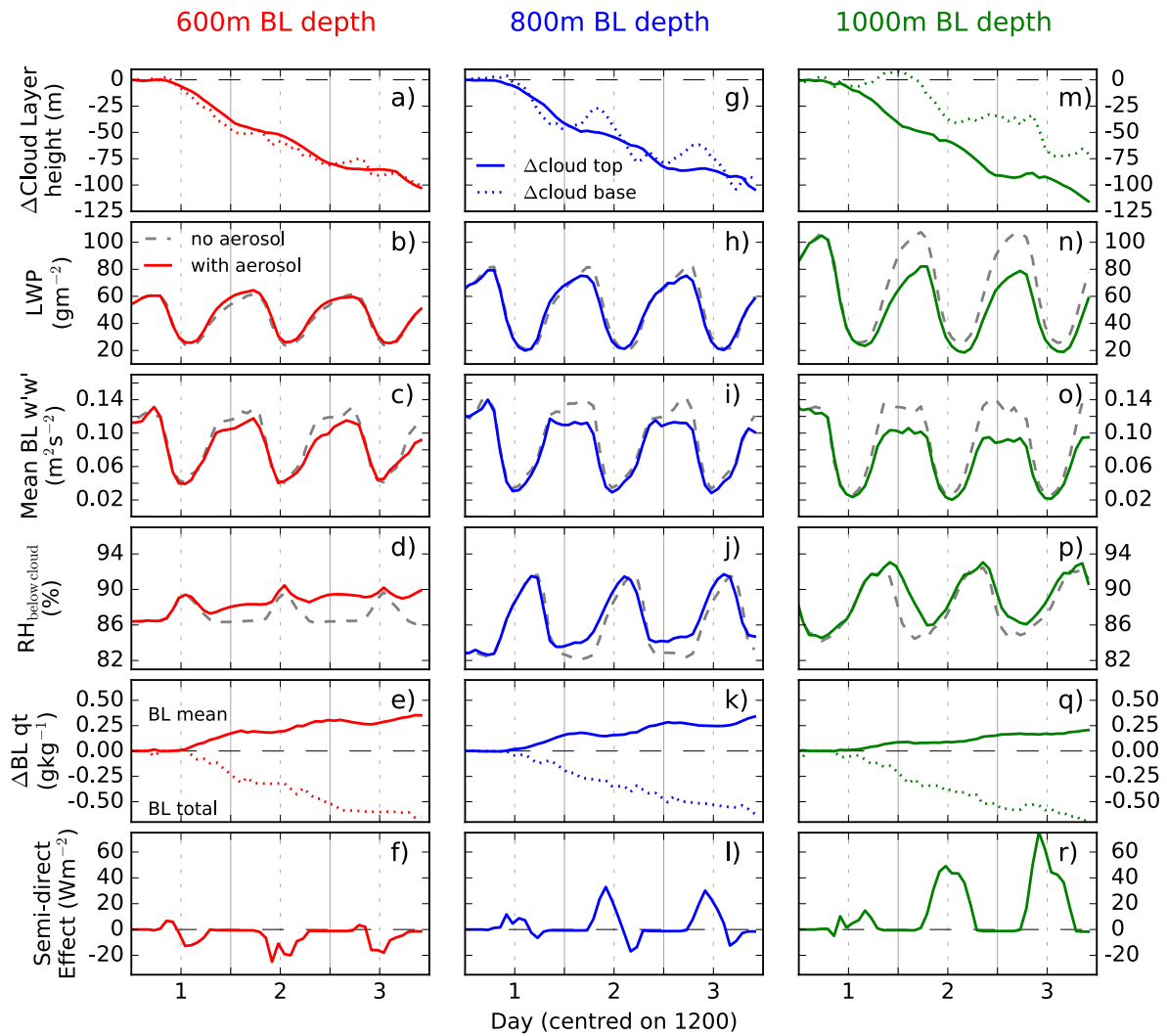
234

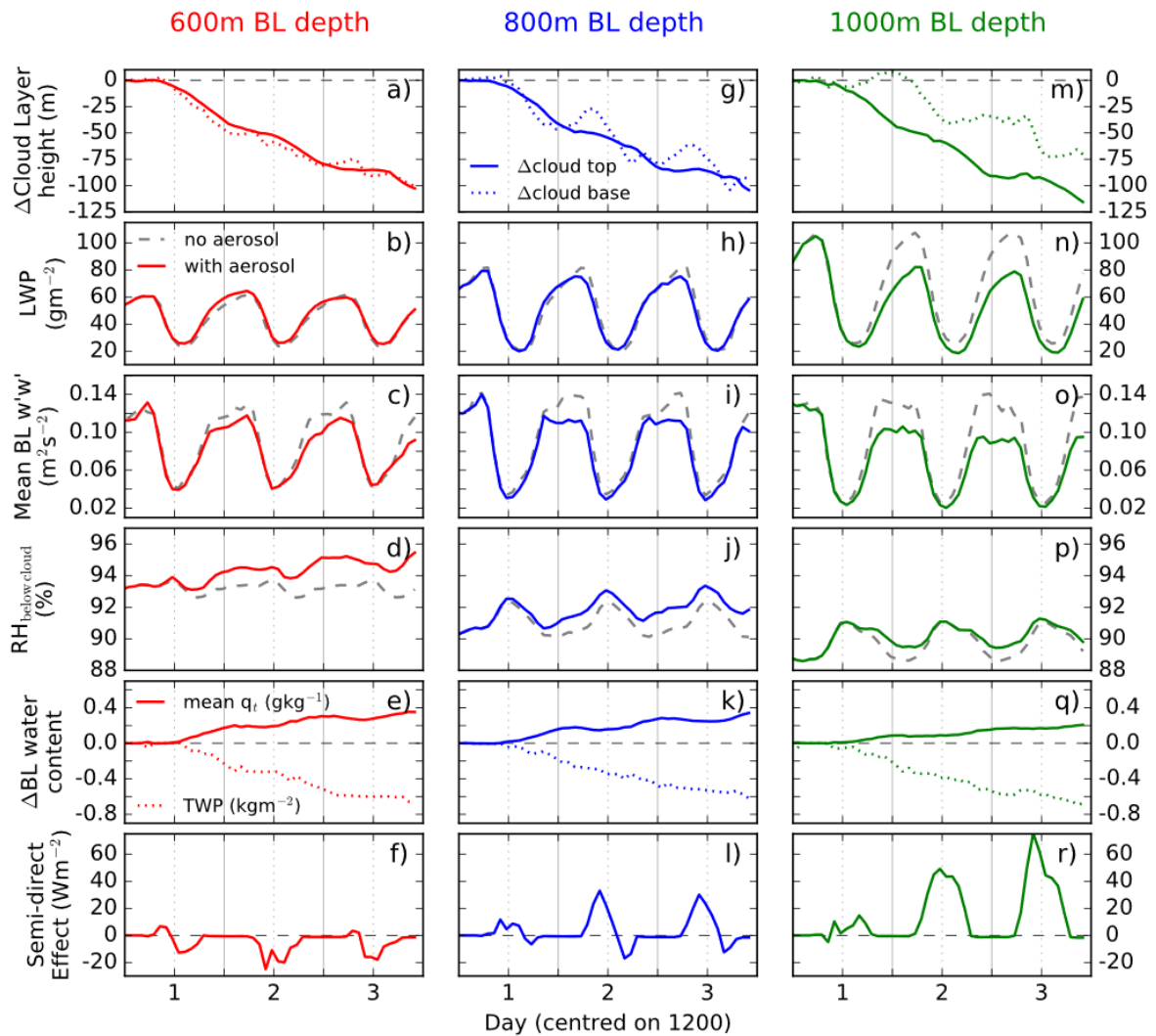
235 **Figure 9. Vertical profiles of a) liquid water potential temperature and b) total water mass mixing ratio taken at 0530 (dashed lines)**
 236 **and 1300 (solid lines) on day 1 (after spin-up) for the no-aerosol simulations.**

237

238 As shown in [Figure 9](#) the degree of decoupling between the sub-cloud and cloud layers increases with BL depth. The
 239 diurnal cycle of the sub-cloud RH for the three setups ([Figure 10](#) [Figure 10d](#), [j](#), and [p](#)) shows that longer periods of decoupling
 240 occur as the BL depth increases (~~peaks in elevated and prolonged mean~~ sub-cloud RH ~~corresponds~~ corresponds to a poorly
 241 mixed BL). In both the *control* and *800-m* setups the BL is reasonably well mixed throughout the day. The presence of the
 242 aerosol layer enhances the midday coupling and weakens the cloud decay phase, producing a thicker cloud in the afternoon.
 243 However, for the *1000-m* setup the lowering of the cloud layer is not sufficient to overcome the decoupling that occurs,
 244 therefore there is no additional flux of moisture at midday and the cloud does not thicken, producing a positive SDE in the
 245 afternoon. As the BL deepens overnight, the dynamics become increasingly sensitive to the elevated absorbing aerosol layer
 246 ([Figure 10](#) [Figure 10c](#), [i](#), and [o](#)). The result is a more pronounced decrease in the cloud growth phase overnight and a thinner
 247 cloud in the morning. The *800-m* and *1000-m* setups produce a strong positive SDE in the morning from day 2 onwards ([Figure](#)
 248 [10](#) [Figure 10l](#) and [r](#)), which dominates the daily mean SDE (Table 5). As described in Sect. 3.2.2, reductions in w_e and below-
 249 cloud moisture fluxes set up a feedback mechanism that decreases the BL dynamics. As the BL deepens this mechanism occurs
 250 more rapidly and may be further enhanced by reduced cloud-top longwave cooling that occurs when the LWP is sufficiently
 251 reduced. The reduction by $\sim 30 \text{ g m}^{-2}$ of the LWP in the *1000-m* setup is a large enough perturbation to reduce the longwave
 252 cloud-top cooling by $\sim 40\%$ and decrease buoyancy production.

253





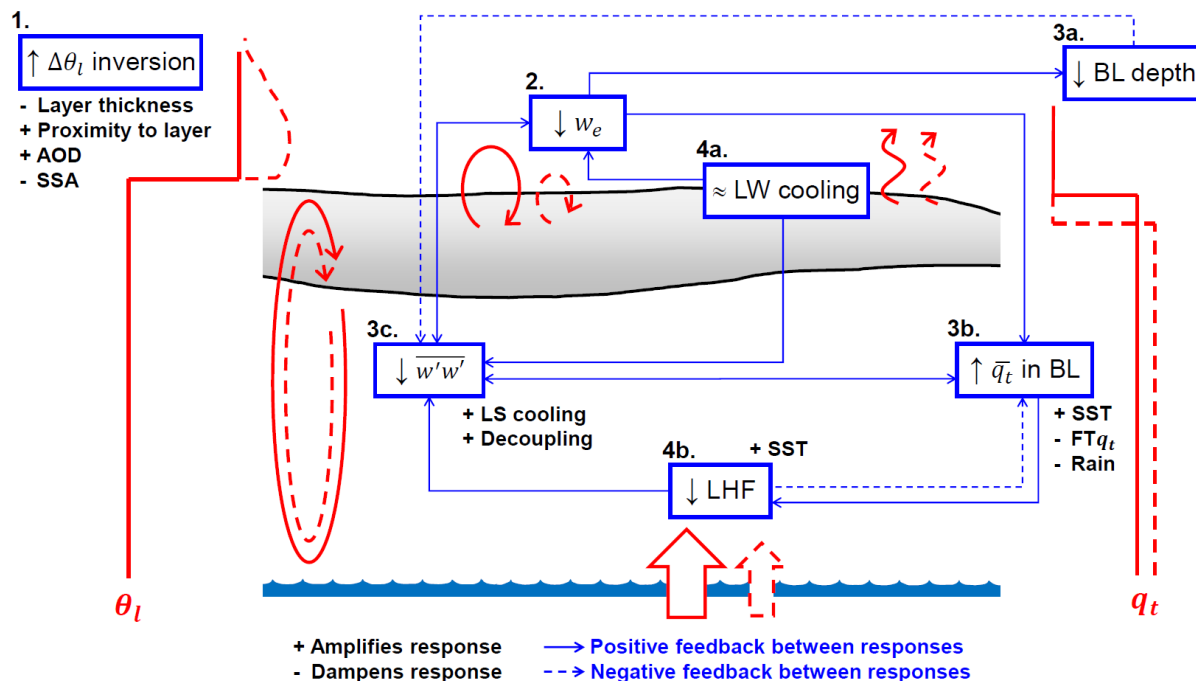
256

257 **Figure 10.** 3-day timeseries showing the initial response of the cloud to a 250 m thick layer of aerosol directly above the inversion
 258 with an aerosol optical depth of 0.2 from the a) – f) control setup with a boundary layer depth of 600 m, g) – l) 800-m setup, and m)
 259 – r) 1000-m setup. From top to bottom row, panels show the altitude of the cloud base and top, the liquid water path (LWP), the
 260 mean boundary layer (BL) vertical velocity variance ($w'w'$), the mean relative humidity (RH) between the ocean surface and the
 261 cloud base, changes to the BL water content as the mean total water content q , and the total water path (TWP), and the semi-direct
 262 effect.

263 These results explain the different aerosol–layer sensitivities shown in Table 5. In all setups the enhanced temperature inversion
 264 weakens w_e and the mixing of warm, dry FT air into the cloud layer and enhances midday coupling. For the *control* setup there
 265 is little impact on BL dynamics, so the cloud becomes thicker due to enhanced sources of moisture; as the temperature inversion
 266 strengthens this response increases. As the BL deepens the BL dynamics are increasingly weakened, driving a reduction in
 267 sub–cloud sources of moisture and a thinner cloud; as the temperature inversion strengthens this response also increases. The

1268 1000-m setup represents an extreme case of this scenario, whereas in the 800-m setup the enhanced coupling is sufficient to
 1269 produce an increase in sub-cloud moisture flux during the afternoon, which acts to partially mitigate the cloud thinning.

1270 **4 Discussion and conclusions**



1271
 1272 **Figure 11.** Summary of how the semi-direct effect manifests in a cross section of a stratocumulus-topped boundary layer. Solid red
 1273 lines refer to the no-aerosol simulation and dashed red lines to the elevated absorbing aerosol-layer simulations. Key responses to
 1274 the boundary layer profiles are depicted in the blue boxes and include the strength of the inversion layer ($\Delta\theta_I$ inversion), entrainment
 1275 rate (w_e), boundary layer depth (BL depth), cloud-top longwave cooling (LW cooling), mean vertical motions in the boundary layer
 1276 ($\overline{w'w'}$), mean total water content of the BL ($\overline{q_t}$), and the latent heat flux at the ocean surface (LHF). Solid (dashed) arrows between
 1277 boxes represent positive (negative) feedbacks between responses. For each response we include properties of the aerosol layer,
 1278 boundary layer, or model setup that amplify (denoted by +) or dampen (denoted by -) the response; this includes the aerosol layer
 1279 thickness (Layer thickness), cloud-aerosol gap (Proximity to layer), the aerosol optical depth of the layer (AOD), the single scattering
 1280 albedo of the aerosol layer (SSA), the sea surface temperature (SST), the water content of the free troposphere (FT q_t), precipitation
 1281 (Rain), large-scale advective heat tendency (LS cooling), and the degree of boundary layer decoupling (Decoupling).

1282
 1283 **Figure 11** summarises the findings of this study. The SDE manifests itself as a modification to the processes that
 1284 maintain the supply of moisture to the cloud layer and are ultimately driven by the strengthened inversion layer and weakened
 1285 entrainment rate caused by an absorbing aerosol layer above the inversion. The initial sequence of responses to an elevated
 1286 layer of absorbing aerosol is summarised below, with numbers referring to each response labelled in **Figure 11**:

- 1287 1. The absorbing aerosol layer produces a heat perturbation that results in a strengthened temperature inversion.

- 288 2. Buoyant parcels of air in the BL require more energy in order to push through the strengthened temperature inversion.
289 This weakens the entrainment rate (w_e) across the inversion layer.
- 290 3a. Weakened entrainment results in a decrease in the cloud top altitude and BL depth.
- 291 3b. The reduction in the entrainment of warm and dry air from the FT reduces the amount of mixing, reducing the sink
292 of q_t in the cloud layer and allowing the BL to maintain a greater RH. The result is an increase in \bar{q}_t ~~and RH.~~ a small
293 decrease in BL temperature, and an increase in RH.
- 294 3c. Weakened entrainment reduces the production of buoyancy from evaporative cooling of entrained air, causing a
295 decrease in BL dynamics ($\overline{w'w'}$), especially overnight.
- 296 4a. Cloud-top longwave cooling remains largely unchanged due to the weak sensitivity to LWPs larger than 50 g m^{-2}
297 overnight and the relatively small changes in LWP during the daytime. The insulating effect of the aerosol layer only
298 weakly influences the net longwave fluxes and divergence above the cloud.
- 299 4b. Increased \bar{q}_t in the BL and weakened BL dynamics reduces the evaporation rate of water from the surface, as
300 evidenced by the reduction in latent heat flux (LHF).

301

302 According to the model sensitivity simulations presented, SDE is ~~increased~~ amplified through the following mechanisms:

- 303 – Geometrically thinner aerosol layers of high aerosol density and low SSA, which produce a stronger localised heat
304 perturbation.
- 305 – Aerosol layers close to the inversion, while larger cloud-aerosol gaps result in a delayed and weaker cloud response.
- 306 – Warmer SSTs, which enhance the flux of moisture to the BL. As a secondary response, the increased SST also drives
307 a stronger reduction in LHF and causes the BL to adjust at a quicker rate.

308 Conversely, SDE is reduced by:

- 309 – Precipitation that, as a sink of cloud liquid water, dampens the cloud response. It follows that any feedbacks that
310 result in an increase in precipitation further weakens the SDE.
- 311 – Increases to the large-scale advective heat tendency (stronger cooling), which are balanced by enhanced buoyancy
312 production from w_e and a more rapid BL adjustment.
- 313 – An increase in the moisture content of the FT, which increases the role that entrainment plays in the supply of moisture
314 to the BL.

315 Finally, an increase in the degree of decoupling in the BL increases the sensitivity of the BL dynamics to changes in w_e , driving
316 towards a positive daily mean SDE. Extreme cases result in a strong positive SDE from day two after applying the aerosol
317 perturbation ~~onwards~~.

318

319 Several feedbacks between responses occur as the BL adjusts to the perturbations. The key feedbacks occur in the sub-cloud
320 layer and can work together to greatly reduce the supply of moisture to the cloud layer. Processes that act to decrease $\overline{w'w'}$

1321 also further decrease w_e and the LHF; these changes weaken the response of \bar{q}_t in the BL so that there is a weaker flux of q_v
1322 to the cloud layer. Reduced w_e and a reduction in condensation at the base of the cloud layer weakens buoyancy production in
1323 the cloud layer which acts to further decrease $\overline{w'w'}$ and w_e . These feedbacks are most pronounced during the cloud growth
1324 phase overnight when the diurnal cycles of w_e , $\overline{w'w'}$, and LHF peak, resulting in a weakened cloud growth phase and a thinner
1325 cloud overnight and into the morning when the aerosol layer is present, thus producing a positive SDE. Longwave cloud-top
1326 cooling is only weakly sensitive to changes in LWP above 50 gm^{-2} and therefore we do not see changes in the buoyancy
1327 production from this process unless the LWP is significantly impacted, which occurs when the BL is decoupled. In this case
1328 the reduced LWP further weakens the buoyancy production in the cloud layer, and consequently w_e and BL dynamics.

1329

1330 A second adjustment feedback on the cloud maintenance occurs through the reduced depth of the BL which acts to promote
1331 coupling of the cloud and sub-cloud layers. In this case the feedback mechanism outlined previously acts in reverse so that
1332 $\overline{w'w'}$, LHF, and the supply of q_v to the cloud layer increase. This weaker feedback mechanism likely occurs throughout the
1333 diurnal cycle but only becomes important at midday when BL dynamics and sub-cloud moisture fluxes are at their weakest
1334 and most sensitive to small changes. This adjustment results in reduced cloud decay throughout the afternoon and a thicker
1335 cloud, and thus negative SDE, when the elevated layer of absorbing aerosol is present. The strength of this feedback mechanism
1336 decreases as the degree of BL decoupling increases until the mechanism ceases to have any impact on the BL; in our study
1337 this occurs when the BL is 1000 m deep.

1338

1339 The sign and magnitude of the SDE from elevated layers of absorbing aerosol is sensitive to the layer properties and BL
1340 properties, especially the diurnal variations in coupling between the cloud and sub-cloud layers. For coupled BLs, the SDE on
1341 the first day after adding the absorbing aerosol layer is slightly positive unless the aerosol layer is close to the inversion layer.
1342 On the second and third day the SDE is strongly negative and peaks on the second day. Generally, for coupled BLs the SDE
1343 is of opposite sign to the DRE and often greater in magnitude, resulting in a small or negative total radiative effect for aerosol-
1344 radiation interactions from elevated absorbing aerosol layers. For BLs that show characteristics of being decoupled for most
1345 of the diurnal cycle the SDE is positive for all three days and increases in magnitude throughout; as the BL becomes more
1346 decoupled the magnitude of the SDE increases. For decoupled BLs the SDE acts to enhance the DRE, resulting in a larger total
1347 radiative effect.

1348

1349 The increased LWP and negative SDE in the well-mixed coupled BL experiments is consistent with satellite observations over
1350 the southeast Atlantic from Adebisi and Zuidema (2018) and Wilcox (2012). However, our LEM simulations suggest a positive
1351 SDE in decoupled BL regions, such as near the stratocumulus-to-cumulus transition region. In reality, the BL may not be as
1352 decoupled as in the simulations. The deepening BL is usually accompanied by an increasing SST (Sandu and Stevens, 2011)
1353 which was not represented in our simulations; the increase in SST would provide a considerably larger flux of moisture from

354 the surface and enhance the production of buoyancy at the surface which may act to weaken the sensitivity of the BL to changes
355 in dynamics. ~~Contrary to the results presented here, The aerosol-layer sensitivity experiments in section 3.3 suggest that the~~
356 ~~daily mean SDE strongly weakens as the distance of the gap between the cloud top and aerosol layer increases. Table 3 shows~~
357 ~~that on the second day of the simulation no gap results in a daily mean SDE of -7 Wm^{-2} compared to -0.4 Wm^{-2} for a 500 m~~
358 ~~gap. Additionally, even for a large perturbation (AOD of 0.5) the daily mean SDE in the initial 24 hours of the 50 m gap~~
359 ~~experiment is only 1 Wm^{-2} . These results are in general agreement with~~ the stratocumulus–to–cumulus transition LES studies
360 by Yamaguchi et al. (2015) and Zhou et al. (2017) ~~which~~ suggest that only those elevated smoke layers that are very close, or
361 in direct contact with, the cloud layer impact the cloud properties. ~~However, in these studies the prescribed subsidence rate~~
362 ~~above the cloud layer was -1.5 to -2 mms^{-1} , which is lower than used in our study (-5 mms^{-1} at an equivalent altitude) and~~
363 ~~would delay the response from the heat perturbation. This difference in subsidence rate represents an important sensitivity to~~
364 ~~the impact that elevated layers may have on the cloud, both in terms of LES and in the real world. It~~ Combined with the satellite
365 observations in Fig. 1 these results suggest the overall SDE from elevated layers of aerosol over the Southeast Atlantic is weak.
366 However, it is worth noting that Yamaguchi et al. (2015) and Zhou et al. (2017) used the same case study (Sandu and Stevens,
367 2011) yet found opposing results on whether the absorbing aerosol layer inhibits or hastens the transition to cumulus.
368 Yamaguchi et al. (2015) state that throughout their simulations the BL is decoupled below 800 m, whereas in Zhou et al. (2017)
369 vertical mixing within the BL continues until the inversion height exceeds ~ 1.4 km (Zhou et al., 2017; Fig. 1b). Our results
370 highlight that the cloud response is sensitive to the diurnal variations in BL mixing, which may explain these opposing results.
371 Additionally, inconsistent responses between LES models can also arise through differences in the representation of processes,
372 including unresolved sub-grid scale turbulence (Stevens et al., 2005) and microphysics (van der Dussen et al., 2013). Our
373 results show that the heat perturbation above the cloud layer impacts all aspects of the BL profile, therefore it would be
374 beneficial to repeat this study using other LES models to test our conclusions.

375

376 Satellite products provide an excellent opportunity to observe aerosol–cloud and aerosol–radiation interactions in remote
377 locations such as the southeast Atlantic Ocean, however most instruments are on polar orbiting satellites that only provide
378 observations from a limited window within the diurnal cycle of the clouds. Our simulations suggest the cloud response to
379 elevated absorbing aerosol layers and the SDE display important diurnal variations so a single observation is unlikely to be
380 representative of the daily mean response. Important changes to the cloud properties occur overnight and play a considerable
381 role in the SDE of the morning period, yet little is known about the impact from absorbing aerosol layers overnight. Future
382 studies should use geostationary satellite observations to investigate the full diurnal cycle of the SDE.

383

384 For a well–mixed coupled BL, the initial cloud and radiative response depend on small–scale processes, such as entrainment
385 and turbulence, which must to be parameterised in climate models. Gordon et al. (2018) used a nested regional model within
386 the Hadley Centre Global Environment Model (HadGEM) to investigate the impact of an incoming elevated plume of smoke
387 in the southeast Atlantic. They found that the elevated aerosol layer reduced cloud top height and enhanced LWP through a

1388 reduction in w_e driven by localised heating at or just above the cloud layer of ~ 6 K. The importance of the weakened w_e aligns
1389 well with the LES results of the present study, but the magnitude of the cloud and radiative response are much greater in
1390 HadGEM, with an LWP increase of 90%, an increase in cloud fraction of 19% and a mean SDE of -30 Wm^{-2} . Gordon et al.
1391 (2018) do not find a consistent longer-term (~ 3 days) reduction in LWP following BL adjustments. In the LES simulations
1392 presented here, cloud fraction remained $\sim 100\%$, which may explain the smaller SDE than Gordon et al. (2018). Additionally,
1393 concurrent aerosol-cloud interactions may modify the underlying cloud properties, which may act to amplify the SDE. The
1394 lack of BL adjustment may be due to processes that are not explicitly treated in HadGEM, such as BL turbulence and
1395 subsequent missing feedbacks on surface fluxes, or due to aerosol-cloud interactions not represented in the LES. Alternatively,
1396 differences may be due to different simulated cases. The trajectory analysis of Gordon et al. (2018) suggests that their BL air
1397 mass traverses the study region more quickly than the absorbing aerosol layer, which may prevent the BL adjustments from
1398 occurring.

1399

1400 In our simulations the SST and subsidence rate are held constant for the whole duration whereas real stratocumulus decks tend
1401 to experience an increasing SST and decreasing subsidence rate. An increasing SST increases surface latent heat fluxes, cloud
1402 liquid water content, and the strength of BL eddies, and acts to deepen the BL through increased entrainment and enhance
1403 decoupling of the sub-cloud layer (Bretherton and Wyant, 1997). As the cloud is advected over the warmer sea surface the
1404 enhanced flux of moisture would act to increase the magnitude of the SDE and prevent the BL from drying out as quickly.
1405 Simultaneously, the enhanced decoupling of the sub-cloud layer may result in BL dynamical feedbacks that result in a
1406 reduction in LWP (see Figure 10~~Figure 10~~). Our model uses a Eulerian framework where the absorbing aerosol layer remains
1407 at a constant height above the cloud whereas the heat perturbation is allowed to subside into the cloud. In reality the aerosol
1408 layer may also subside. The sensitivity experiments in section 3.3 show that as the aerosol layer approaches the cloud layer
1409 the SDE increases, therefore if we were to represent aerosol layer subsidence we would expect an enhanced cloud response
1410 and SDE.

1411

1412 Changes to the aerosol distribution within the cloud or in the cloud droplet distribution have not been considered in this study.
1413 A weakened w_e increases condensate in the cloud and likely results in an increase in cloud droplet effective radius (r_e). This
1414 would promote warm rain process and enhance precipitation, thus reducing the LWP and amplifying the reduction in BL
1415 dynamics. These combined effects could lead to a decrease in LWP and shift the SDE towards a positive sign at a quicker rate
1416 than suggested by the LES. For the cases where the aerosol layer is directly above the smokecloud layer an enhanced flux of
1417 CCN into the BL would be expected and would act to reduce r_e , suppress precipitation, and act to enhance buoyancy production.
1418 However, in-situ observations routinely find that the layers of smoke over the Southeast Atlantic are embedded in moist layers
1419 (Adebisi et al., 2015), which could increase the flux of water from the free-troposphere and act to mitigate the changes that
1420 occurs alongside an increased CCN. The introduction of the absorbing aerosol into the cloud layer would additionally enhance
1421 cloud evaporation and act to thin the cloud layer (Hill and Dobbie, 2008; Johnson et al., 2004). Thus, although the experiments

422 where the aerosol layer is directly above the inversion result in the most strongly negative SDE, the response would be at least
 423 partially mitigated if the aerosol distribution was represented explicitly: decreasing further the role that SDE plays in the total
 424 radiative effect of elevated layers of absorbing aerosol. Extending the present study using a binned microphysics scheme would
 425 include the additional response of the droplet size distribution and using an aerosol scheme would include the additional
 426 impacts the weakened w_e has on the availability of CCN and subsequent cloud response.

427 5 Appendix

428 This appendix describes how the AOD and SSA is prescribed in elevated aerosol layer experiments, along with the geometric
 429 thickness of the aerosol layer and the distance between the inversion layer and the aerosol base. In each call to the radiation
 430 scheme the desired AOD and SSA are used to determine the mass mixing ratio of two aerosol species, water-soluble like (WS)
 431 and biomass-burning like (BB).

432

433 For a single wavelength, the AOD between the altitudes z_0 and z , corresponding to the base and top of the aerosol layer
 434 respectively, is calculated as:

$$435 \text{AOD} = \sum_{i=z_0}^z \sum_{j=WS, BB} (K_{scat_j} + K_{abs_j}) \cdot q_{i,j} \cdot \rho_i \cdot dz_i \quad (\text{A1})$$

436

437 where K_{scat} and K_{abs} are the specific scattering and absorption coefficients, respectively, for the aerosol species j , in units
 438 $\text{m}^2 \text{kg}^{-1}$, with mass mixing ratio q in $\text{kg kg}_{\text{dry}}^{-1}$, at each model level i of geometric thickness dz in m, and density of dry air ρ in
 439 kg m^{-3} . If the mass mixing ratio of each species is assumed equal and constant with height ($q_{WS} = q_{BB}$ and $q_i = q$), Eq. A1
 440 becomes:

441

$$442 q \cdot \sum_{i=z_0}^z \rho_i \cdot dz_i = \frac{\text{AOD}}{\sum_{j=WS, BB} K_{scat_j} + K_{abs_j}} \quad (\text{A2})$$

443

444 We incorporate a factor X_{SSA} into Eq. A2 that can be used to describe the relative ratio of WS mass to BB mass so that Eq. A2
 445 becomes:

446

$$447 q \cdot \sum_{i=z_0}^z \rho_i \cdot dz_i = \frac{\text{AOD}}{(K_{scat_{WS}} + K_{abs_{WS}}) + X_{SSA} \cdot (K_{scat_{BB}} + K_{abs_{BB}})} \quad (\text{A3})$$

448

449 Equation A3 can be re-arranged to give q for a given AOD:

450

$$q = \frac{\text{AOD}_{\text{constant}}}{\sum_{i=z_0}^z \rho_i \cdot dz_i} \quad (\text{A4})$$

1447 where

$$\text{AOD}_{\text{constant}} = \frac{\text{AOD}}{(K_{\text{scat}_{WS}} + K_{\text{abs}_{WS}}) + X_{SSA} \cdot (K_{\text{scat}_{BB}} + K_{\text{abs}_{BB}})} \quad (\text{A5})$$

1448

1449 Therefore for the two aerosol species:

$$q_j = \begin{cases} q, & j = WS \\ X_{SSA} \cdot q, & j = BB \end{cases} \quad (\text{A6})$$

1450

1451 The overall SSA is calculated as:

1452

$$\text{SSA} = \frac{K_{\text{scat}_{WS}} + X_{SSA} \cdot K_{\text{scat}_{BB}}}{K_{\text{scat}_{WS}} + X_{SSA} \cdot K_{\text{scat}_{BB}} + K_{\text{abs}_{WS}} + X_{SSA} \cdot K_{\text{abs}_{BB}}} \quad (\text{A7})$$

1453

1454 Equation A7 can be re-arranged to solve for X_{SSA}

1455

$$X_{SSA} = \frac{K_{\text{scat}_{WS}} - \text{SSA} \cdot (K_{\text{scat}_{WS}} + K_{\text{abs}_{WS}})}{\text{SSA} \cdot (K_{\text{scat}_{BB}} + K_{\text{abs}_{BB}}) - K_{\text{scat}_{BB}}} \quad (\text{A8})$$

1456

1457 At the beginning of the simulation X_{SSA} and $\text{AOD}_{\text{constant}}$ are calculated using Equations A8 and A5, respectively, using the
 1458 shortwave extinction coefficients of the aerosols for the wavelength band 320 – 690 nm and the prescribed AOD and SSA. At
 1459 each horizontal grid point q is then calculated using Eq. A4 for the elevated aerosol layer where z_0 is the base of the aerosol
 1460 layer, and z is the top of the aerosol layer. The mass mixing ratio of each species is calculated using Eq. A6 and finally the
 1461 mass mixing ratio profiles of WS and BB applied to the radiation scheme.

1462 6 Author contribution

1463 RJH, NB, EJH, and AAH designed the methodology and experiments. AAH provided model expertise and assistance. RJH
 1464 setup, performed, and post-processed the simulations. RJH, NB, EJH, and AAH analysed the results. RJH provided all
 1465 visualisations and wrote the initial manuscript draft. NB, EJH, and AAH provided revisions and commentary on the
 1466 manuscript.

1467 7 Competing interests

1468 The authors declare that they have no conflict of interest.

1469 8 Acknowledgments

1470 This research was funded by the UK Natural Environment Research Council (NERC) CLOUDS and Aerosol Radiative Impacts
1471 and Forcing: Year 2016 (CLARIFY-2016) project NE/L013479/1. We acknowledge use of the Monsoon system, a
1472 collaborative facility supplied under the Joint Weather and Climate Research Programme, a strategic partnership between the
1473 Met Office and the Natural Environment Research Council. The CALIOP data were obtained from the NASA Langley
1474 Research Center Atmospheric Science Data Center.

1475 9 References

1476 Abel, S. J., Walters, D. N. and Allen, G.: Evaluation of stratocumulus cloud prediction in the Met Office
1477 forecast model during VOCALS-REx, *Atmos. Chem. Phys.*, 10(21), 10541–10559, doi:10.5194/acp-10-
1478 10541-2010, 2010.

1479 Ackerman, A. S., vanZanten, M. C., Stevens, B., Savic-Jovicic, V., Bretherton, C. S., Chlond, A., Golaz,
1480 J.-C., Jiang, H., Khairoutdinov, M., Krueger, S. K., Lewellen, D. C., Lock, A., Moeng, C.-H., Nakamura,
1481 K., Petters, M. D., Snider, J. R., Weinbrecht, S. and Zulauf, M.: Large-Eddy Simulations of a Drizzling,
1482 Stratocumulus-Topped Marine Boundary Layer, *Mon. Weather Rev.*, 137(3), 1083–1110,
1483 doi:10.1175/2008MWR2582.1, 2009.

1484 Adebiyi, A. A. and Zuidema, P.: Low cloud cover sensitivity to biomass-burning aerosols and meteorology
1485 over the Southeast Atlantic, *J. Clim.*, 31(11), 4329–4346, doi:10.1175/JCLI-D-17-0406.1, 2018.

1486 Adebiyi, A. A., Zuidema, P. and Abel, S. J.: The convolution of dynamics and moisture with the presence
1487 of shortwave absorbing aerosols over the southeast Atlantic, *J. Clim.*, 28(5), 1997–2024,
1488 doi:10.1175/JCLI-D-14-00352.1, 2015.

1489 Albrecht, B. A., Jensen, M. P. and Syrett, W. J.: Marine boundary layer structure and fractional
1490 cloudiness, *J. Geophys. Res.*, 100222(20), 209–14, doi:10.1029/95JD00827, 1995.

1491 Bond, T. C., Doherty, S. J., Fahey, D. W., Forster, P. M., Berntsen, T., DeAngelo, B. J., Flanner, M. G.,
1492 Ghan, S., Kärcher, B., Koch, D., Kinne, S., Kondo, Y., Quinn, P. K., Sarofim, M. C., Schultz, M. G.,
1493 Schulz, M., Venkataraman, C., Zhang, H., Zhang, S., Bellouin, N., Guttikunda, S. K., Hopke, P. K.,
1494 Jacobson, M. Z., Kaiser, J. W., Klimont, Z., Lohmann, U., Schwarz, J. P., Shindell, D., Storelvmo, T.,
1495 Warren, S. G. and Zender, C. S.: Bounding the role of black carbon in the climate system: A scientific
1496 assessment, *J. Geophys. Res. Atmos.*, 118(11), 5380–5552, doi:10.1002/jgrd.50171, 2013.

1497 Bony, S. and Dufresne, J. L.: Marine boundary layer clouds at the heart of tropical cloud feedback
1498 uncertainties in climate models, *Geophys. Res. Lett.*, 32(20), 1–4, doi:10.1029/2005GL023851, 2005.

1499 Boucher, O., Randall, D., Artaxo, P., Bretherton, C., Feingold, G., Forster, P., Kerminen, V.-M., Kondo,

1500 Y., Liao, H., Lohmann, U., Rasch, P., Satheesh, S. K., Sherwood, S., Stevens, B. and Zhang, X.-Y.:
1501 IPCC AR5 Clouds and Aerosols, in *Climate Change 2013 - The Physical Science Basis*, pp. 571–658,
1502 Cambridge University Press, Cambridge, United Kingdom and New York, NY, USA., 2013.

1503 Bretherton, C. S. and Wyant, M. C.: Moisture Transport, Lower-Tropospheric Stability, and Decoupling
1504 of Cloud-Topped Boundary Layers, *J. Atmos. Sci.*, 54(1), 148–167, doi:10.1175/1520-
1505 0469(1997)054<0148:MTL TSA>2.0.CO;2, 1997.

1506 Bretherton, C. S., Blossey, P. N. and Jones, C. R.: Mechanisms of marine low cloud sensitivity to
1507 idealized climate perturbations: A single-LES exploration extending the CGILS cases, *J. Adv. Model.*
1508 *Earth Syst.*, 5(2), 316–337, doi:10.1002/jame.20019, 2013.

1509 Chand, D., Wood, R., Anderson, T. L., Satheesh, S. K. and Charlson, R. J.: Satellite-derived direct
1510 radiative effect of aerosols dependent on cloud cover, *Nat. Geosci.*, 2(3), 181–184,
1511 doi:10.1038/ngeo437, 2009.

1512 Cook, J. and Highwood, E. J.: Climate response to tropospheric absorbing aerosols in an intermediate
1513 general-circulation model, *Q. J. R. Meteorol. Soc.*, 130(596), 175–191, doi:10.1256/qj.03.64, 2004.

1514 Costantino, L. and Bréon, F. M.: Aerosol indirect effect on warm clouds over South-East Atlantic, from
1515 co-located MODIS and CALIPSO observations, *Atmos. Chem. Phys.*, 13(1), 69–88, doi:10.5194/acp-13-
1516 69-2013, 2013.

1517 Das, S., Harshvardhan, H., Bian, H., Chin, M., Curci, G., Protonotariou, A. P., Mielonen, T., Zhang, K.,
1518 Wang, H. and Liu, X.: Biomass burning aerosol transport and vertical distribution over the South African-
1519 Atlantic region, *J. Geophys. Res.*, 122(12), 6391–6415, doi:10.1002/2016JD026421, 2017.

1520 van der Dussen, J. J., de Roode, S. R., Ackerman, A. S., Blossey, P. N., Bretherton, C. S., Kurowski, M.
1521 J., Lock, A. P., Neggers, R. A. J., Sandu, I. and Siebesma, A. P.: The GASS/EUCLIPSE model
1522 intercomparison of the stratocumulus transition as observed during ASTEX: LES results, *J. Adv. Model.*
1523 *Earth Syst.*, 5(3), 483–499, doi:10.1002/jame.20033, 2013.

1524 Edwards, J. M. and Slingo, A.: Studies with a flexible new radiation code. I: Choosing a configuration for
1525 a large-scale model, *Q. J. R. Meteorol. Soc.*, 122(531), 689–719, doi:10.1256/smsqj.53106, 1996.

1526 Efstathiou, G. A. and Beare, R. J.: Quantifying and improving sub-grid diffusion in the boundary-layer
1527 grey zone, *Q. J. R. Meteorol. Soc.*, 141(693), 3006–3017, doi:10.1002/qj.2585, 2015.

1528 Efstathiou, G. A., Beare, R. J., Osborne, S. and Lock, A. P.: Grey zone simulations of the morning
1529 convective boundary layer development, *J. Geophys. Res. Atmos.*, 121(9), 4769–4782,
1530 doi:10.1002/2016JD024860, 2016.

1531 Feingold, G., Koren, I., Wang, H., Xue, H. and Brewer, W. A.: Precipitation-generated oscillations in open
1532 cellular cloud fields, *Nature*, 466(7308), 849–852, doi:10.1038/nature09314, 2010.

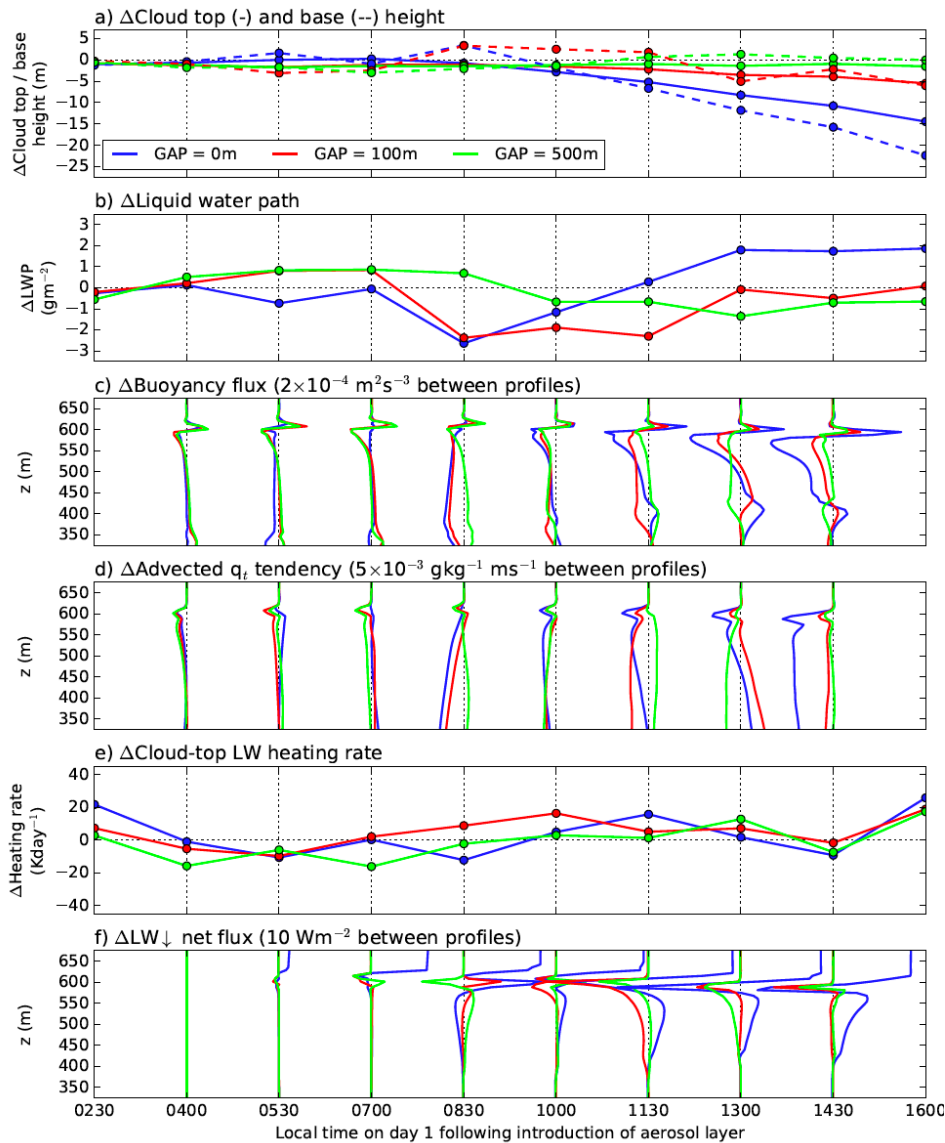
1533 Garrett, T. J. and Zhao, C.: Increased Arctic cloud longwave emissivity associated with pollution from
1534 mid-latitudes, *Nature*, 440(7085), 787–789, doi:10.1038/nature04636, 2006.

1535 Gordon, H., Field, P. R., Abel, S. J., Dalvi, M., Grosvenor, D. P., Hill, A. A., Johnson, B. T., Miltenberger,
1536 A. K., Yoshioka, M. and Carslaw, K. S.: Large simulated radiative effects of smoke in the south-east
1537 Atlantic, *Atmos. Chem. Phys.*, 18(20), 15261–15289, doi:10.5194/acp-18-15261-2018, 2018.

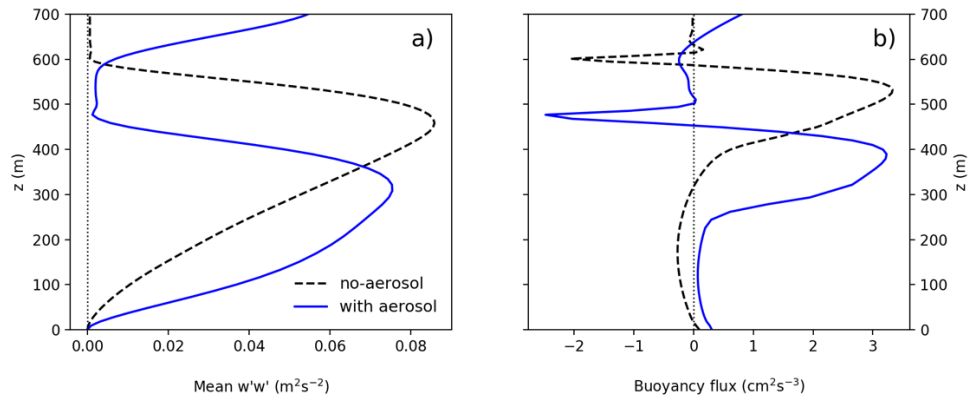
- 1538 Gray, M. E. B., Brown, A. R., Lock, A. P. and Petch, J.: Version 2.3 Of The Met Office Large Eddy Model:
1539 Part III. Software Documentation, Met Office, Bracknell, UK., 2001.
- 1540 Hartmann, D. L. and Short, D. A.: On the Use of Earth Radiation Budget Statistics for Studies of Clouds
1541 and Climate, *J. Atmos. Sci.*, 37(6), 1233–1250, doi:10.1175/1520-
1542 0469(1980)037<1233:OTUOER>2.0.CO;2, 1980.
- 1543 Hartmann, D. L., Ockert-Bell, M. E. and Michelsen, M. L.: Hartmann_EtAl_1992_EnergyBalance, *J.*
1544 *Clim.*, 5(November), 1281–1304, doi:Doi 10.1175/1520-0442(1992)005<1281:Teocto>2.0.Co;2, 1992.
- 1545 Hignett, P.: Observations of Diurnal Variation in a Cloud-capped Marine Boundary Layer, *J. Atmos. Sci.*,
1546 48(12), 1474–1482, doi:10.1175/1520-0469(1991)048<1474:OODVIA>2.0.CO;2, 1991.
- 1547 Hill, A. A. and Dobbie, S.: The impact of aerosols on non-precipitating marine stratocumulus. II: The
1548 semi-direct effect, *Q. J. R. Meteorol. Soc.*, 134(634 A), 1155–1165, doi:10.1002/qj.277, 2008.
- 1549 Hill, A. A., Dobbie, S. and Yin, Y.: The impact of aerosols on non-precipitating marine stratocumulus. I:
1550 Model description and prediction of the indirect effect, *Q. J. R. Meteorol. Soc.*, 134(634 A), 1143–1154,
1551 doi:10.1002/qj.278, 2008.
- 1552 Hill, A. A., Feingold, G. and Jiang, H.: The Influence of Entrainment and Mixing Assumption on Aerosol–
1553 Cloud Interactions in Marine Stratocumulus, *J. Atmos. Sci.*, 66(5), 1450–1464,
1554 doi:10.1175/2008JAS2909.1, 2009.
- 1555 Hill, A. A., Field, P. R., Furtado, K., Korolev, A. and Shipway, B. J.: Mixed-phase clouds in a turbulent
1556 environment. Part 1: Large-eddy simulation experiments, *Q. J. R. Meteorol. Soc.*, 140(680), 855–869,
1557 doi:10.1002/qj.2177, 2014.
- 1558 Johnson, B. T., Shine, K. P. and Forster, P. M.: The semi-direct aerosol effect: Impact of absorbing
1559 aerosols on marine stratocumulus, *Q. J. R. Meteorol. Soc.*, 130(599 PART B), 1407–1422,
1560 doi:10.1256/qj.03.61, 2004.
- 1561 Kato, S., Sun-Mack, S., Miller, W. F., Rose, F. G., Chen, Y., Minnis, P. and Wielicki, B. A.: Relationships
1562 among cloud occurrence frequency, overlap, and effective thickness derived from CALIPSO and
1563 CloudSat merged cloud vertical profiles, *J. Geophys. Res.*, 115, D00H28, doi:10.1029/2009JD012277,
1564 2010.
- 1565 Kato, S., Rose, F. G., Sun-Mack, S., Miller, W. F., Chen, Y., Rutan, D. A., Stephens, G. L., Loeb, N. G.,
1566 Minnis, P., Wielicki, B. A., Winker, D. M., Charlock, T. P., Stackhouse, P. W., Xu, K.-M. and Collins, W.
1567 D.: Improvements of top-of-atmosphere and surface irradiance computations with CALIPSO-, CloudSat-
1568 , and MODIS-derived cloud and aerosol properties, *J. Geophys. Res.*, 116(D19), D19209,
1569 doi:10.1029/2011JD016050, 2011.
- 1570 Klein, S. A., Hall, A., Norris, J. R. and Pincus, R.: Low-Cloud Feedbacks from Cloud-Controlling Factors:
1571 A Review, *Surv. Geophys.*, 38(6), 1307–1329, doi:10.1007/s10712-017-9433-3, 2017.
- 1572 Koch, D. and Del Genio, A. D.: Black carbon semi-direct effects on cloud cover: review and synthesis,
1573 *Atmos. Chem. Phys.*, 10(16), 7685–7696, doi:10.5194/acp-10-7685-2010, 2010.
- 1574 Lee, I. Y.: Evaluation of cloud microphysics parameterizations for mesoscale simulations, *Atmos. Res.*,
1575 24(1–4), 209–220, doi:https://doi.org/10.1016/0169-8095(89)90046-X, 1989.

- 1576 Leon, D. C., Wang, Z. and Liu, D.: Climatology of drizzle in marine boundary layer clouds based on 1
1577 year of data from CloudSat and Cloud-Aerosol Lidar and Infrared Pathfinder Satellite Observations
1578 (CALIPSO), *J. Geophys. Res. Atmos.*, 114(8), D00A14, doi:10.1029/2008JD009835, 2009.
- 1579 Lu, Z., Liu, X., Zhang, Z., Zhao, C., Meyer, K., Rajapakshe, C., Wu, C., Yang, Z. and Penner, J. E.:
1580 Biomass smoke from southern Africa can significantly enhance the brightness of stratocumulus over the
1581 southeastern Atlantic Ocean, *Proc. Natl. Acad. Sci.*, 115(12), 2924–2929,
1582 doi:10.1073/pnas.1713703115, 2018.
- 1583 Monin, A. S. and Obukhov, A. M.: Basic laws of turbulent mixing in the surface layer of the atmosphere,
1584 *Geophys. Dir. AF Cambridge Res. Cent.*, 24(151), 163–187, doi:10.1016/j.jallcom.2004.05.088, 1954.
- 1585 Muhlbauer, A., McCoy, I. L. and Wood, R.: Climatology of stratocumulus cloud morphologies:
1586 Microphysical properties and radiative effects, *Atmos. Chem. Phys.*, 14(13), 6695–6716,
1587 doi:10.5194/acp-14-6695-2014, 2014.
- 1588 Ovchinnikov, M., Ackerman, A. S., Avramov, A., Cheng, A., Fan, J., Fridlind, A. M., Ghan, S., Harrington,
1589 J., Hoose, C., Korolev, A., McFarquhar, G. M., Morrison, H., Paukert, M., Savre, J., Shipway, B. J.,
1590 Shupe, M. D., Solomon, A. and Sulia, K.: Intercomparison of large-eddy simulations of Arctic mixed-
1591 phase clouds: Importance of ice size distribution assumptions, *J. Adv. Model. Earth Syst.*, 6(1), 223–
1592 248, doi:10.1002/2013MS000282, 2014.
- 1593 Painemal, D., Kato, S. and Minnis, P.: Boundary layer regulation in the southeast Atlantic cloud
1594 microphysics during the biomass burning season as seen by the A-train satellite constellation, *J.*
1595 *Geophys. Res.*, 119(19), 11,288–11,302, doi:10.1002/2014JD022182, 2014.
- 1596 Peers, F., Bellouin, N., Waquet, F., Ducos, F., Goloub, P., Mollard, J., Myhre, G., Skeie, R. B., Takemura,
1597 T., Tanré, D., Thieuleux, F. and Zhang, K.: Comparison of aerosol optical properties above clouds
1598 between POLDER and AeroCom models over the South East Atlantic Ocean during the fire season,
1599 *Geophys. Res. Lett.*, 43(8), 3991–4000, doi:10.1002/2016GL068222, 2016.
- 1600 Penner, J. E., Zhang, S. Y. and Chuang, C. C.: Soot and smoke aerosol may not warm climate, *J.*
1601 *Geophys. Res. Atmos.*, 108(D21), doi:10.1029/2003JD003409, 2003.
- 1602 Rajapakshe, C., Zhang, Z., Yorks, J. E., Yu, H., Tan, Q., Meyer, K., Platnick, S. and Winker, D. M.:
1603 Seasonally transported aerosol layers over southeast Atlantic are closer to underlying clouds than
1604 previously reported, *Geophys. Res. Lett.*, 44(11), 5818–5825, doi:10.1002/2017GL073559, 2017.
- 1605 de Roode, S. R., Sandu, I., van der Dussen, J. J., Ackerman, A. S., Blossey, P., Jarecka, D., Lock, A.,
1606 Siebesma, A. P. and Stevens, B.: Large-Eddy Simulations of EUCLIPSE–GASS Lagrangian
1607 Stratocumulus-to-Cumulus Transitions: Mean State, Turbulence, and Decoupling, *J. Atmos. Sci.*, 73(6),
1608 2485–2508, doi:10.1175/JAS-D-15-0215.1, 2016.
- 1609 De Roode, S. R., Siebesma, A. P., Gesso, S. D., Jonker, H. J. J., Schalkwijk, J. and Sival, J.: A mixed-
1610 layer model study of the stratocumulus response to changes in large-scale conditions, *J. Adv. Model.*
1611 *Earth Syst.*, 6(4), 1256–1270, doi:10.1002/2014MS000347, 2014.
- 1612 Sakaeda, N., Wood, R. and Rasch, P. J.: Direct and semidirect aerosol effects of southern African
1613 biomass burning aerosol, *J. Geophys. Res.*, 116(D12), D12205, doi:10.1029/2010JD015540, 2011.

- 1614 Sandu, I. and Stevens, B.: On the Factors Modulating the Stratocumulus to Cumulus Transitions, *J.*
1615 *Atmos. Sci.*, 68(9), 1865–1881, doi:10.1175/2011JAS3614.1, 2011.
- 1616 Sandu, I., Stevens, B. and Pincus, R.: On the transitions in marine boundary layer cloudiness, *Atmos.*
1617 *Chem. Phys.*, 10(5), 2377–2391, doi:10.5194/acp-10-2377-2010, 2010.
- 1618 Sherwood, S. C., Bony, S., Boucher, O., Bretherton, C., Forster, P. M., Gregory, J. M., Stevens, B.,
1619 Sherwood, S. C., Bony, S., Boucher, O., Bretherton, C., Forster, P. M., Gregory, J. M. and Stevens, B.:
1620 Adjustments in the Forcing-Feedback Framework for Understanding Climate Change, *Bull. Am.*
1621 *Meteorol. Soc.*, 96(2), 217–228, doi:10.1175/BAMS-D-13-00167.1, 2015.
- 1622 Stevens, B., Moeng, C.-H., Ackerman, A. S., Bretherton, C. S., Chlond, A., de Roode, S., Edwards, J.,
1623 Golaz, J.-C., Jiang, H., Khairoutdinov, M., Kirkpatrick, M. P., Lewellen, D. C., Lock, A., Müller, F.,
1624 Stevens, D. E., Whelan, E. and Zhu, P.: Evaluation of Large-Eddy Simulations via Observations of
1625 Nocturnal Marine Stratocumulus, *Mon. Weather Rev.*, 133(6), 1443–1462, doi:10.1175/MWR2930.1,
1626 2005.
- 1627 Stjern, C. W., Samset, B. H., Myhre, G., Forster, P. M., Hodnebrog, Ø., Andrews, T., Boucher, O.,
1628 Faluvegi, G., Iversen, T., Kasoar, M., Kharin, V., Kirkevåg, A., Lamarque, J. F., Olivie, D., Richardson,
1629 T., Shawki, D., Shindell, D., Smith, C. J., Takemura, T. and Voulgarakis, A.: Rapid Adjustments Cause
1630 Weak Surface Temperature Response to Increased Black Carbon Concentrations, *J. Geophys. Res.*
1631 *Atmos.*, 122(21), 11,462–11,481, doi:10.1002/2017JD027326, 2017.
- 1632 Wilcox, E. M.: Stratocumulus cloud thickening beneath layers of absorbing smoke aerosol, *Atmos.*
1633 *Chem. Phys.*, 10(23), 11769–11777, doi:10.5194/acp-10-11769-2010, 2010.
- 1634 Wilcox, E. M.: Direct and semi-direct radiative forcing of smoke aerosols over clouds, *Atmos. Chem.*
1635 *Phys.*, 12(1), 139–149, doi:10.5194/acp-12-139-2012, 2012.
- 1636 Wood, R.: Stratocumulus Clouds, *Mon. Weather Rev.*, 140(8), 2373–2423, doi:10.1175/MWR-D-11-
1637 00121.1, 2012.
- 1638 Wyant, M. C., Wood, R., Bretherton, C. S., Mechoso, C. R., Bacmeister, J., Balmaseda, M. A., Barrett,
1639 B., Codron, F., Earnshaw, P., Fast, J., Hannay, C., Kaiser, J. W., Kitagawa, H., Klein, S. A., Köhler, M.,
1640 Manganello, J., Pan, H. L., Sun, F., Wang, S. and Wang, Y.: The PreVOCA experiment: Modeling the
1641 lower troposphere in the Southeast Pacific, *Atmos. Chem. Phys.*, 10(10), 4757–4774, doi:10.5194/acp-
1642 10-4757-2010, 2010.
- 1643 Yamaguchi, T., Feingold, G., Kazil, J. and McComiskey, A.: Stratocumulus to cumulus transition in the
1644 presence of elevated smoke layers, *Geophys. Res. Lett.*, 42(23), 10478–10485,
1645 doi:10.1002/2015GL066544, 2015.
- 1646 Zhang, Y., Stevens, B., Medeiros, B. and Ghil, M.: Low-cloud fraction, lower-tropospheric stability, and
1647 large-scale divergence, *J. Clim.*, 22(18), 4827–4844, doi:10.1175/2009JCLI2891.1, 2009.
- 1648 Zhou, X., Ackerman, A. S., Fridlind, A. M., Wood, R. and Kollias, P.: Impacts of solar-absorbing aerosol
1649 layers on the transition of stratocumulus to trade cumulus clouds, *Atmos. Chem. Phys.*, 17(20), 12725–
1650 12742, doi:10.5194/acp-17-12725-2017, 2017.



655 Figure S1. Response to the presence of an aerosol layer above the cloud (gap of 0 m in blue, 100 m in red, and 500 m in green) of a)
 656 the cloud top (solid line) and cloud base (dashed line) heights, b) the cloud liquid water path (LWP), c) profiles of the mean
 657 buoyancy flux, d) profiles of the mean advected total water content tendency, e) cloud-top longwave cooling, and f) profiles of
 658 mean longwave net flux (positive values indicate increased downward flux). The geometric thickness of the aerosol layer is 250 m
 659 and its optical depth is 0.2. Data is shown for the first day following the introduction of the aerosol layer. Mean instantaneous
 660 profiles (shown in panels c, d, and f) for each time are centred on a value of zero, depicted by the vertical dotted lines. Each profile
 661 is separated on the x-axis by a constant magnitude shown above each corresponding plot.



663

664

665

666

Figure S2. Domain-mean vertical profiles of a) variance in vertical velocity perturbation $w'w'$, and b) buoyancy flux on day 13 of the simulation at 1300 local time for the no-aerosol simulation (black dashed line) and following the introduction of a layer of absorbing aerosol (blue solid line) in the base experiment (0 m cloud–aerosol gap, 250 m thick layer, and AOD of 0.2).